Computerized Tomography Images and Leonardo Da Vinci

The center image on the next page is a famous sketch of a man by *Leonardo Da Vinci* (1452–1519). While other great men and women that humanity produced in arts and science generally excelled in only one specific area of art or science, Leonardo da Vinci was a man of enormous talents covering most areas of human endeavor, whether in arts or science; a truly versatile renaissance man. He was active as sculptor, painter, musician, architect, engineer, inventor, and researcher of human body. Many of Leonardo Da Vinci's drawings of the human body helped doctors understand better the layout of muscle and bone structures within the human body.

The left and right images on the next page are examples of *computerized tomography* (CT) images of the human body, representing the most important development resulting from *Wilhelm Roentgen's* discovery of x rays in 1895. A CT scanner is a machine that uses an x-ray beam rotating about a specific area of a patient to collect x-ray attenuation data for patient's tissues. It then manipulates these data with special mathematical algorithms to display a series of transverse slices through the patient. The transverse CT data can be reconstructed so as to obtain sagittal sections (shown in the right image on the next page) and coronal sections (shown in the left image on the next page) through the patient's organs or to obtain digitally reconstructed radiographs. The excellent resolution obtained with a modern CT scanner provides an extremely versatile "non-invasive" diagnostic tool. CT scanners have been in clinical and industrial use since the early 1970s and evolved through five generations, each generation becoming increasingly more sophisticated and faster.

Three types of detectors are used in CT scanners: (1) scintillation detectors (sodium iodide or calcium fluoride) in conjunction with a photomultiplier tube; (2) gas filled (xenon or krypton) ionization chamber; and (3) semiconductor detectors (cesium iodide) in conjunction with a p–n junction photodiode.

Three-dimensional images can be obtained through three techniques: (1) multiple 2D acquisitions (based on a series of sequential scans); (2) spiral (helical) CT (the x-ray source rotates continuously around the patient while simultaneously the patient is translated through the gantry); and (3) cone-beam CT (a 2D detector array is used in order to measure the entire volume-of-interest during one single orbit of the x-ray source.

Allan Cormack (1924–1998), a South African-American physicist, developed the theoretical foundations that made computerized tomography possible and published his work during 1963–64. His work generated little interest until *Godfrey Hounsfield* (1919–2004), a British electrical engineer, developed a practical model of a CT scanner in the early 1970s. Hounsfield and Cormack received the 1979 Nobel Prize in Psychology and Medicine for their independent invention of the CT scanner.

7 Interactions of Photons with Matter

In this chapter we discuss the various types of photon interactions with absorbing media. Photons are indirectly ionizing radiation and they deposit energy in the absorbing medium through a two-step process: (1) energy transfer to an energetic light charged particle (electron or positron) and (2) energy deposition in medium by the charged particle. Some of the interactions are only of theoretical interest and help in the understanding of the general photon interaction phenomena, others are of great importance in medical physics since they play a fundamental role in imaging, radiotherapy as well as radiation dosimetry. Depending on their energy and the atomic number of the absorber, photons may interact with an absorber atom as a whole, with the nucleus of an absorber atom or with an orbital electron of the absorber atom. The probability of a particular interaction to occur depends on the photon energy as well as on the density and atomic number of the absorber, and is generally expressed in the form of an interaction cross section.

In this chapter we first discuss in detail the individual photon interactions of importance to medical physics and then concentrate on the general aspects of photon interactions with absorbers including the mass energy transfer coefficients and mass energy absorption coefficients for use in radiation dosimetry. Also discussed are the various effects that follow the individual photon interactions.

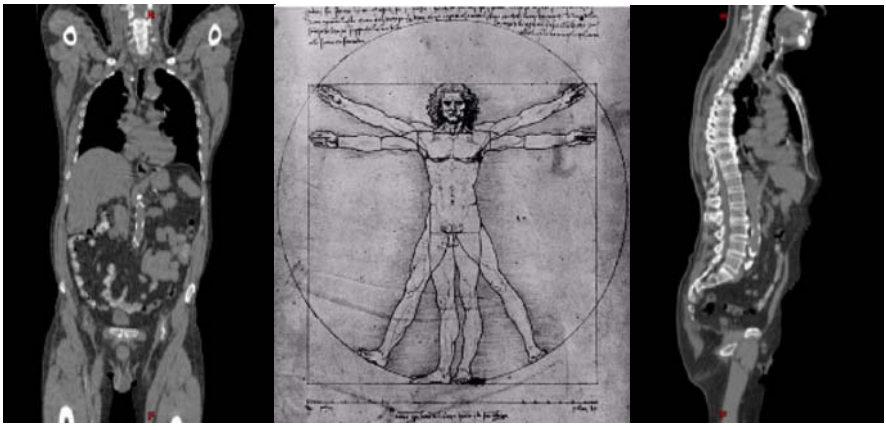

7.1 General Aspects of Photon Interactions with Absorbers

In penetrating an absorbing medium, photons may experience various interactions with the atoms of the medium. These interactions with atoms may involve either the *nuclei* of the absorbing medium or the *orbital electrons* of the absorbing medium.

The interactions with nuclei may be direct *photon-nucleus* interactions (*photodisintegration*) or interactions between the photon and the electrostatic field of the nucleus (*pair production*).

The *photon-orbital electron* interactions are characterized as interactions between the photon and either (i) a loosely bound electron (*Thomson scattering, Compton effect, triplet production*) or (ii) a tightly bound electron (*photoelectric effect*).

- A *loosely bound electron* is an electron whose binding energy E_B is small in comparison with the photon energy $h\nu$, i.e., $E_B \ll h\nu$. An interaction between a photon and a loosely bound electron is considered to be an interaction between a photon and a free (unbound) electron.
- A *tightly bound electron* is an electron whose binding energy E_B is comparable to, larger than, or slightly smaller than the photon energy $h\nu$. For a photon interaction to occur with a tightly bound electron, the binding energy E_B of the electron must be of the order of, but slightly smaller, than the photon energy, i.e., $E_B \lesssim h\nu$. An interaction between a photon and a tightly bound electron is considered an interaction between a photon and the atom as a whole.

As far as the photon fate after the interaction with an atom is concerned there are two possible outcomes:

1. *Photon disappears* (i.e., is absorbed completely) and a portion of its energy is transferred to light charged particles (electrons and positrons).
2. *Photon is scattered* and two outcomes are possible:
   a) The resulting photon has the same energy as the incident photon and no light charged particle is released in the interaction.
   b) The resulting scattered photon has a lower energy than the incident photon and the energy excess is transferred to a light charged particle (electron).

The light charged particles produced in the absorbing medium through photon interactions will:

1. either deposit their energy to the medium through Coulomb interactions with orbital electrons of the absorbing medium (collision loss also referred to as ionization loss), as discussed in detail in Sect. 5.3.

2. or radiate their kinetic energy away through Coulomb interactions with the nuclei of the absorbing medium (radiative loss), as discussed in detail in Sect. 5.2.

7.2 Thomson Scattering

The scattering of low energy photons ($h\nu \ll m_e c^2$) by loosely bound, i.e., essentially free electrons is described adequately by non-relativistic classical theory of *Joseph J. Thomson*.

Thomson assumed that the incident photon beam sets a quasi-free electron of the atom into a forced resonant oscillation. He then used classical theory to calculate the cross section for the re-emission of the electromagnetic (EM) radiation as a result of induced dipole oscillation of the electrons. This type of photon elastic scattering is now called *Thomson scattering*.

The electric fields $\mathscr{E}_{\text{in}}$ for the harmonic incident radiation and $\mathscr{E}_{\text{out}}$ for the emitted scattered electromagnetic waves [far field, see (3.5)] are given, respectively, by

$$\mathscr{E}_{\text{in}} = \mathscr{E}_{\text{o}} \sin \omega t \tag{7.1}$$

and

$$\mathscr{E}_{\text{out}} = \frac{e}{4\pi\varepsilon_{\text{o}}} \frac{\ddot{x} \sin \Theta}{c^2 r} , \tag{7.2}$$

where

$\mathscr{E}_{\text{o}}$ is the amplitude of the incident harmonic oscillation,
Θ is the angle between the direction of emission $\vec{r}$ and the polarization vector of the incident wave $\vec{\mathscr{E}}_{\text{in}}$,
$\ddot{x}$ is the acceleration of the electron.

The equation of motion for the accelerated electron vibrating about its equilibrium position is

$$m_e \ddot{x} = e\vec{\mathscr{E}} = e\vec{\mathscr{E}}_{\text{o}} \sin \omega t . \tag{7.3}$$

Inserting $\ddot{x}$ from the equation of motion for the accelerated electron into (7.2), we get the following expression for $\mathscr{E}_{\text{out}}$:

$$\mathscr{E}_{\text{out}} = \frac{e^2}{4\pi\varepsilon_{\text{o}}} \frac{\mathscr{E}_{\text{o}}}{m_e c^2} \frac{\sin \omega t \, \sin \Theta}{r} = r_e \mathscr{E}_{\text{o}} \frac{\sin \omega t \, \sin \Theta}{r} , \tag{7.4}$$

where r_e is the so-called classical radius of the electron ($r_e = 2.818$ fm).

The electronic differential cross section $d_e\sigma_{Th}$ for re-emission of radiation into a solid angle $d\Omega$ is by definition given as follows:

$$d_e\sigma_{Th} = \frac{\bar{S}_{out}}{\bar{S}_{in}} dA = \frac{\bar{S}_{out}}{\bar{S}_{in}} r^2 d\Omega \quad \text{or} \quad \frac{d_e\sigma_{Th}}{d\Omega} = r^2 \frac{\bar{S}_{out}}{\bar{S}_{in}} \,. \tag{7.5}$$

The incident and emitted wave intensities are expressed as follows by the time averages of the corresponding Poynting vectors $\bar{S}_{out}$ and $\bar{S}_{in}$, respectively [see (3.9)]:

$$\bar{S}_{in} = \varepsilon_o c \overline{\mathscr{E}_{in}^2} = \varepsilon_o c \mathscr{E}_o^2 \overline{\sin^2 \omega t} = \frac{1}{2} \varepsilon_o c \mathscr{E}_o^2 \tag{7.6}$$

and

$$\bar{S}_{out} = \varepsilon_o c \overline{\mathscr{E}_{out}^2} = \varepsilon_o c \frac{r_e^2 \mathscr{E}_o^2 \overline{\sin^2 \omega t}\, \overline{\sin^2 \Theta}}{r^2} = \frac{\varepsilon_o c r_e^2 \mathscr{E}_o^2}{2} \frac{\overline{\sin^2 \Theta}}{r^2} \,, \tag{7.7}$$

recognizing that $\overline{\sin^2 \omega t} = \frac{1}{2}$.

Inserting $\bar{S}_{in}$ and $\bar{S}_{out}$ into (7.5) we get the following expression for $d_e\sigma_{Th}/d\Omega$

$$\frac{d_e\sigma_{Th}}{d\Omega} = r_e^2 \overline{\sin^2 \Theta} \,. \tag{7.8}$$

The average value of $\sin^2 \Theta$ for unpolarized radiation may be evaluated using the following relationships:

$$\cos\Theta = \frac{a}{r}; \qquad \sin\theta = \frac{b}{r}; \qquad \text{and} \qquad \cos\psi = \frac{a}{b} \,, \tag{7.9}$$

where the angles θ, Θ and ψ as well as the parameters a and b are defined in Fig. 7.1.

Combining the expressions given in (7.9) we obtain

$$\cos\Theta = \sin\theta \, \cos\psi \,, \tag{7.10}$$

where

θ is the scattering angle defined as the angle between the incident photon and the scattered photon, as shown in Fig. 7.1,

ψ is the polarization angle.

$\overline{\sin^2 \Theta}$ is now determined by integration over the polarization angle ψ from 0 to 2π

$$\begin{aligned} \overline{\sin^2 \Theta} &= \int_0^{2\pi} \sin^2 \Theta \, d\psi \Big/ \int_0^{2\pi} \mathrm{d}\psi = \frac{1}{2\pi} \int_0^{2\pi} (1 - \cos^2 \Theta) d\psi \\ &= 1 - \frac{\sin^2 \theta}{2\pi} \int_0^{2\pi} \cos^2 \psi \, d\psi \\ &= 1 - \frac{1}{2} \sin^2 \theta = \frac{1}{2}(1 + \cos^2 \theta). \end{aligned} \tag{7.11}$$

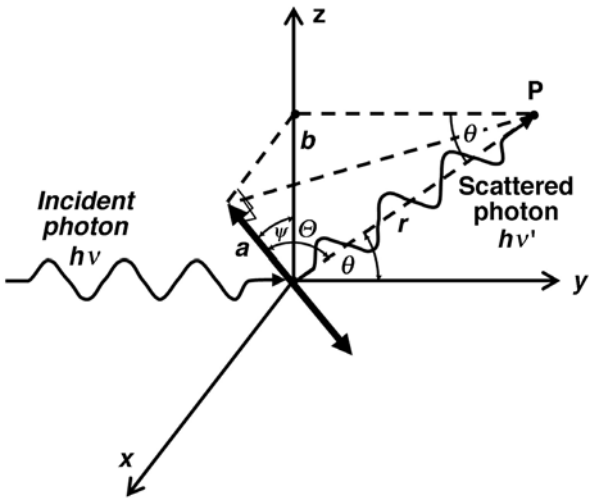

Fig. 7.1. Schematic diagram of Thomson scattering where the incident photon with energy $h\nu$ is scattered and emitted with a scattering angle θ. Note that angles θ and Θ are not coplanar (i.e., they are not in the same plane)

The differential electronic cross section per unit solid angle for Thomson scattering $d_{\mathrm{e}}\sigma_{\mathrm{Th}}/d\Omega$ is from (7.8) and (7.11) expressed as follows:

$$\frac{d_{\mathrm{e}}\sigma_{\mathrm{Th}}}{\mathrm{d}\Omega} = \frac{r_{\mathrm{e}}^2}{2}(1+\cos^2\theta) \tag{7.12}$$

and drawn in Figs. 7.2 and 7.3 against the scattering angle θ in the range from 0 to π. The graph in Fig. 7.2 is plotted in the Cartesian coordinate system; that in Fig. 7.3 shows the same data in the polar coordinate system. Both graphs show that $d_{\mathrm{e}}\sigma_{\mathrm{Th}}/d\Omega$ ranges from 39.7 mb/electron.sterad at $\theta = \pi/2$ to 79.4 mb/electron.sterad for $\theta = 0^{\mathrm{o}}$ and $\theta = \pi$.

The differential electronic cross section per unit angle for Thomson scattering $d_{\mathrm{e}}\sigma_{\mathrm{Th}}/d\theta$ gives the fraction of the incident energy that is scattered into a cone contained between θ and $\theta + d\theta$. The function, plotted in Fig. 7.4 against the scattering angle θ, is expressed as follows, noting that $d\Omega = 2\pi \sin\theta\, d\theta$:

$$\frac{d_{\mathrm{e}}\sigma_{\mathrm{Th}}}{d\theta} = \frac{d_{\mathrm{e}}\sigma_{\mathrm{Th}}}{d\Omega}\frac{d\Omega}{d\theta} = 2\pi\sin\theta\frac{d_{\mathrm{e}}\sigma_{\mathrm{Th}}}{d\Omega} = \pi r_{\mathrm{e}}^2\sin\theta(1+\cos^2\theta)\ . \tag{7.13}$$

As shown in Fig. 7.4, $d_{\mathrm{e}}\sigma_{\mathrm{Th}}/d\theta$ is zero at $\theta = 0$ and $\theta = 180°$, reaches maxima at $\theta = 55°$ and $\theta = 125°$ and attains a non-zero minimum at $\theta = 90°$. The two maxima and the non-zero minimum are determined after setting $d^2\sigma_{\mathrm{Th}}/d\theta^2 = 0$ and solving the result for θ.

The total electronic cross section ${}_{\mathrm{e}}\sigma_{\mathrm{Th}}$ for Thomson scattering is obtained by determining the area under the $d_{\mathrm{e}}\sigma_{\mathrm{Th}}/d\theta$ curve of Fig. 7.4 or by integrating

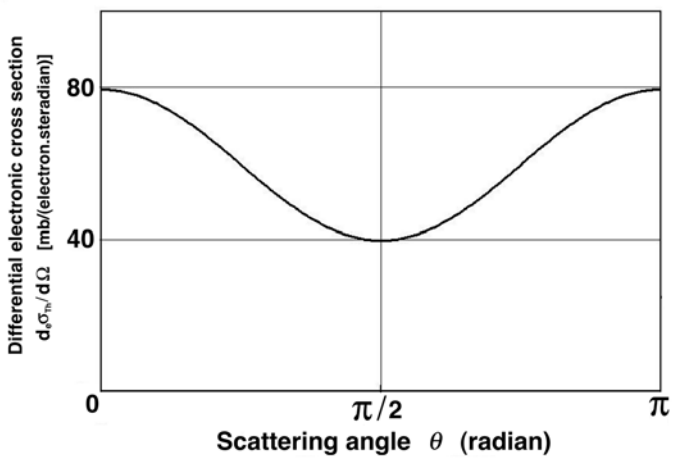

Fig. 7.2. Differential electronic cross section $d_e\sigma_{Th}/d\Omega$ per unit solid angle plotted against the scattering angle θ for Thomson scattering, as given by (7.12)

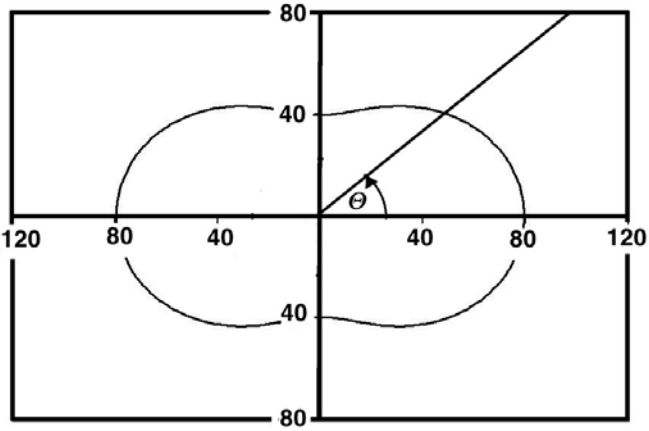

Fig. 7.3. Differential Thomson electronic cross section $d_e\sigma_{Th}/d\Omega$ per unit solid angle plotted against the scattering angle θ in polar coordinate system. The units shown are mb/electron.steradian

(7.13) over all scattering angles θ from 0 to π to obtain

$$
\begin{aligned}
{}_e\sigma_{Th} &= \int \frac{d_e\sigma_{Th}}{d\Omega} d\Omega = \frac{r_e^2}{2} \int_0^\pi (1+\cos^2\theta) 2\pi \sin\theta \, d\theta \\
&= \frac{8\pi}{3} r_e^2 = 0.665 \text{ b} \, . \qquad (7.14)
\end{aligned}
$$

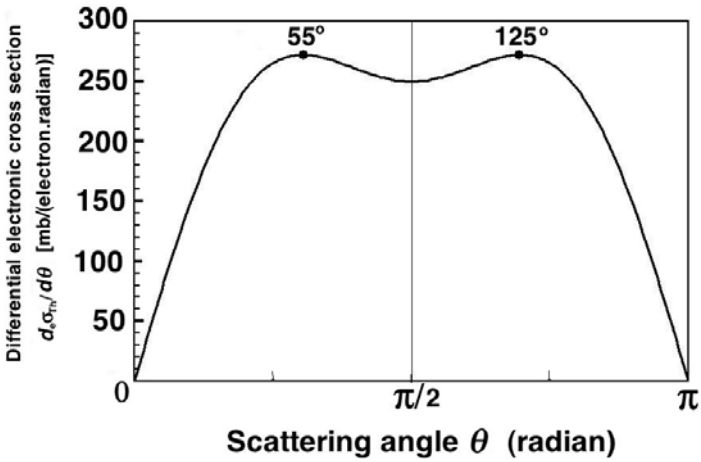

Fig. 7.4. Differential electronic cross section $d_{\mathrm{e}}\sigma_{\mathrm{Th}}/d\theta$ per unit angle θ plotted against the scattering angle θ

This is a noteworthy result in that it contains no energy-dependent terms and predicts no change in energy upon re-emission of the electromagnetic radiation. The cross section ${}_{\mathrm{e}}\sigma_{\mathrm{Th}}$ is called the Thomson classical cross section for a free electron and has the same value (0.665 b) for all incident photon energies.

The atomic cross section ${}_{\mathrm{a}}\sigma_{\mathrm{Th}}$ is in terms of the electronic cross section ${}_{\mathrm{e}}\sigma_{\mathrm{Th}}$ given as follows:

$$ {}_{\mathrm{a}}\sigma_{\mathrm{Th}} = Z\, {}_{\mathrm{e}}\sigma_{\mathrm{Th}} \,, \tag{7.15} $$

showing a linear dependence upon atomic number Z, as elucidated for low atomic number elements by *Charles Glover Barkla*, an English physicist who received the Nobel Prize in Physics for his discovery of characteristic x rays.

For photon energies $h\nu$ exceeding the electron binding energy but small in comparison with $m_{\mathrm{e}}c^2$, i.e., $E_{\mathrm{B}} \ll h\nu \ll m_{\mathrm{e}}c^2$, the atomic cross section measured at small θ approaches the Thomson's value of (7.15). At larger θ and larger photon energies ($h\nu \rightarrow m_{\mathrm{e}}c^2$), however, Thomson's classical theory breaks down and the intensity of coherently scattered radiation on free electrons diminishes in favor of incoherently Compton-scattered radiation.

7.3 Compton Scattering (Compton Effect)

An interaction of a photon of energy $h\nu$ with a loosely bound orbital electron of an absorber is called Compton effect (Compton scattering) in honor of *Arthur Compton* who made the first measurements of photon-"*free electron*" scattering in 1922.

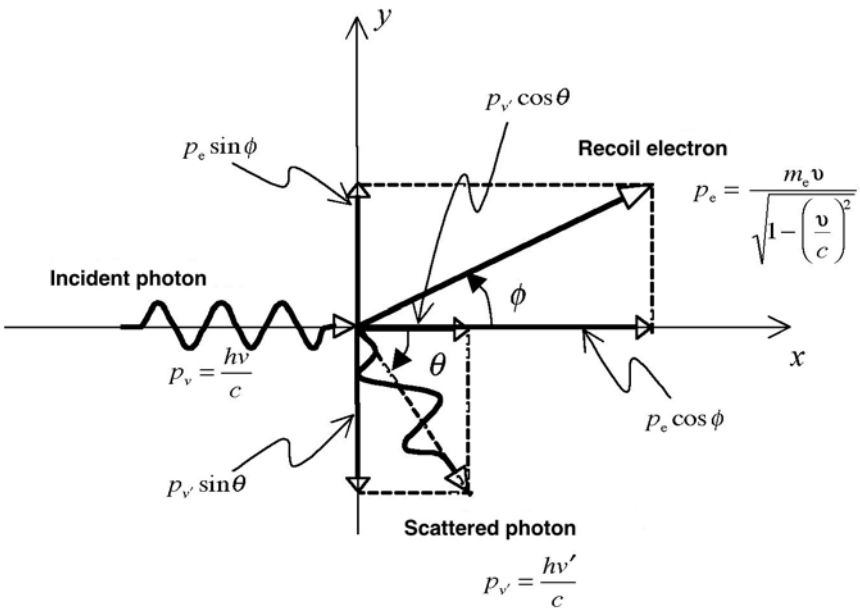

Fig. 7.5. Schematic diagram of the Compton effect. An incident photon with energy $h\nu$ interacts with a stationary and free electron. A photon with energy $h\nu'$ is produced and scattered with a scattering angle $\theta = 60°$. The difference between the incident photon energy $h\nu$ and the scattered photon energy $h\nu'$ is given as kinetic energy to the recoil electron

In theoretical studies of the Compton effect an assumption is made that the photon interacts with a free and stationary electron. A photon, referred to as scattered photon with energy $h\nu'$ that is smaller than the incident photon energy $h\nu$, is produced and an electron, referred to as the Compton (recoil) electron, is ejected from the atom with kinetic energy E_K.

A typical Compton effect interaction is shown schematically in Fig. 7.5 for a 1 MeV photon scattered on a "free" (loosely bound) electron with a scattering angle $\theta = 60°$. The scattering angle θ is the angle between the incident photon direction and the scattered photon direction and can range from $\theta = 0°$ (forward scattering) through 90° (side scattering) to $\theta = 180°$ (back scattering). The recoil electron angle ϕ is the angle between the incident photon direction and the direction of the recoil Compton electron.

The corpuscular nature of the photon is assumed and relativistic conservation of total energy and momentum laws are used in the derivation of the well-known Compton wavelength shift relationship

$$\Delta\lambda = \lambda' - \lambda = \lambda_c(1 - \cos\theta)\,, \tag{7.16}$$

where

λ is the wavelength of the incident photon: $\lambda = 2\pi\hbar c/(h\nu)$,
λ' is the wavelength of the scattered photon; $\lambda' = 2\pi\hbar c/(h\nu')$,
$\Delta\lambda$ is the difference between the scattered and incident photon wavelength, i.e., $\Delta\lambda = \lambda' - \lambda$,
λ_c is the so-called Compton wavelength of the electron defined as

$$\lambda_c = h/(m_e c) = 2\pi\hbar c/(m_e c^2) = 0.0243 \text{ Å} . \tag{7.17}$$

The following three relativistic relationships can be written for the conservation of total energy and momentum in a Compton interaction:

1. *Conservation of total energy*

$$h\nu + m_e c^2 = h\nu' + m_e c^2 + E_K \tag{7.18}$$

that results in

$$h\nu = h\nu' + E_K . \tag{7.19}$$

2. *Conservation of momentum* in the direction of the incident photon $h\nu$: *x axis*

$$p_\nu = p_{\nu'} \cos\theta + p_e \cos\phi . \tag{7.20}$$

3. *Conservation of momentum* in the direction normal to that of the incident photon $h\nu$: *y axis*

$$0 = -p_{\nu'} \sin\theta + p_e \sin\phi , \tag{7.21}$$

where
E_K is the kinetic energy of the recoil electron,
p_ν is the momentum of the incident photon: $p_\nu = h\nu/c$,
$p_{\nu'}$ is the momentum of the scattered photon: $p_{\nu'} = h\nu'/c$,
p_e is the momentum of the recoil electron: $p_e = m_e v/\sqrt{1-(v/c)^2}$.

Using the relativistic expression for momentum p of (1.30) in conjunction with the three basic conservation relationships above, one can eliminate any two parameters from the three equations to obtain the Compton wavelength shift equation for $\Delta\lambda$ of (7.16) which in turn leads to relationships for the energy of the scattered photon $h\nu'$ and the energy of the recoil electron E_K as a function of the incident photon energy $h\nu$ and scattering angle θ

$$\Delta\lambda = \lambda' - \lambda = \frac{c}{\nu'} - \frac{c}{\nu} = \frac{h}{m_e c}(1 - \cos\theta) \qquad \text{or}$$
$$\frac{1}{h\nu'} - \frac{1}{h\nu} = \frac{1}{m_e c^2}(1 - \cos\theta) . \tag{7.22}$$

From (7.22) we obtain the following expressions for $h\nu'$ and E_K, respectively:

$$h\nu' = h\nu \frac{1}{1 + \varepsilon(1 - \cos\theta)} , \tag{7.23}$$

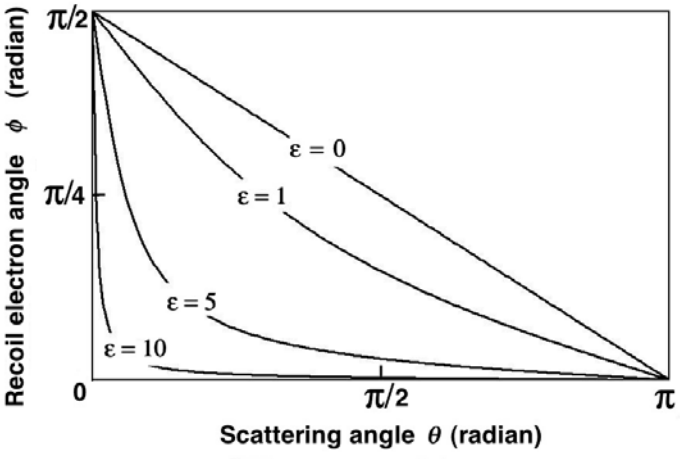

Fig. 7.6. Relationship between the electron recoil angle ϕ and photon scattering angle θ

and

$$E_{\mathrm{K}} = h\nu \frac{\varepsilon(1-\cos\theta)}{1+\varepsilon(1-\cos\theta)} \,, \tag{7.24}$$

where $\varepsilon = h\nu/m_{\mathrm{e}}c^2$ represents the incident photon energy $h\nu$ normalized to the electron rest energy $m_{\mathrm{e}}c^2$.

7.3.1 Relationship Between the Scattering Angle θ and the Recoil Angle ϕ

The scattering angle θ and the recoil electron angle ϕ (see Fig. 7.5) are related as follows:

$$\cot\phi = (1+\varepsilon)\tan(\theta/2) \,. \tag{7.25}$$

The ϕ vs θ relationship is plotted in Fig. 7.6 for various values of $\varepsilon = h\nu/(m_{\mathrm{e}}c^2)$ showing that for a given θ, the higher is the incident photon energy $h\nu$ or the higher is ε, the smaller is the recoil electron angle ϕ.

Equation (7.25) and Fig. 7.6 also show that the range of the scattering angle θ is from 0 to π, while the corresponding range of the recoil electron angle ϕ is limited from $\pi/2$ to 0, respectively.

7.3.2 Scattered Photon Energy $h\nu'$ as a Function of $h\nu$ and θ

The relationship between $h\nu'$ and $h\nu$ of (7.23) is plotted in Fig. 7.7 for various scattering angles θ between 0° (forward scattering) and π (backscattering). The following conclusions can now be made:

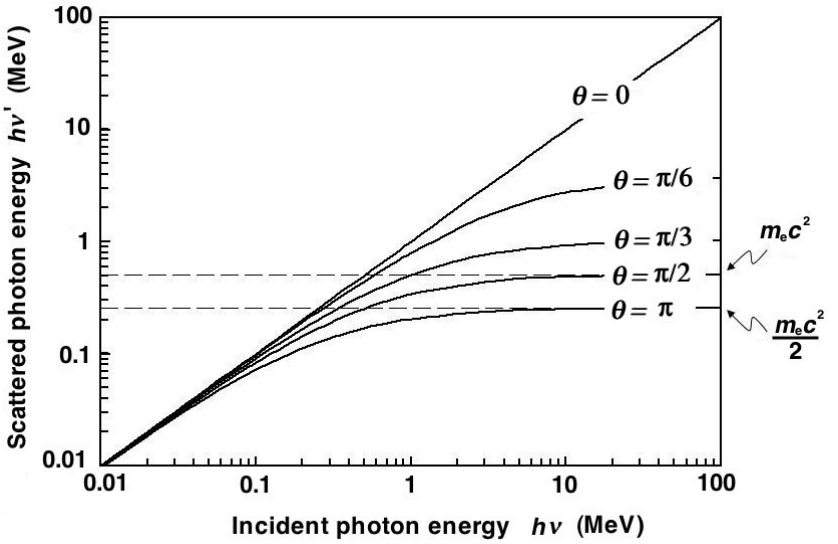

Fig. 7.7. Scattered photon energy $h\nu'$ against the incident photon energy $h\nu$ for various scattering angles θ in the range from 0° to180°

- For $\theta = 0$, the energy of the scattered photon $h\nu'$ equals the energy of the incident photon $h\nu$, irrespective of $h\nu$. Since in this case no energy is transferred to the electron, we are dealing here with classical Thomson scattering.
- For $\theta > 0$ the energy of the scattered photon saturates at high values of $h\nu$; the larger is the scattering angle θ, the lower is the saturation value of $h\nu'$ for $h\nu \to \infty$.
- For example, the saturation values of $h\nu'$ at $\theta = \frac{\pi}{2}$ and $\theta = \pi$ for $h\nu \to \infty$ are

$$h\nu'_{\mathrm{sat}}(\theta = \frac{\pi}{2}) = \lim_{h\nu\to\infty} \frac{h\nu}{1+\varepsilon}$$
$$= \lim_{h\nu\to\infty} \frac{h\nu}{1+\frac{h\nu}{m_e c^2}} = m_e c^2 = 0.511 \text{ MeV} \qquad (7.26)$$

and

$$h\nu'_{\mathrm{sat}}(\theta = \pi) = \lim_{h\nu\to\infty} \frac{h\nu}{1+2\varepsilon}$$
$$= \lim_{h\nu\to\infty} \frac{h\nu}{1+\frac{2h\nu}{m_e c^2}} = \frac{m_e c^2}{2} = 0.255 \text{ MeV}\,, \qquad (7.27)$$

respectively, as shown in Fig. 7.7. These results show that photons scattered with angles θ larger than $\pi/2$ cannot exceed 511 keV no matter how

high is the incident photon energy $h\nu$. This finding is of great practical importance in design of shielding barriers for linear accelerator installations.

- For a given $h\nu$ the scattered photon energy $h\nu'$ will be in the range between $h\nu/(1+2\varepsilon)$ for $\theta = \pi$ and $h\nu$ for $\theta = 0$, i.e.,

$$\left.\frac{h\nu}{1+2\varepsilon}\right|_{\theta=\pi} \leq h\nu' \leq h\nu|_{\theta=0} \ . \tag{7.28}$$

- As shown in (7.22), the Compton shift in wavelength $\Delta\lambda$ is independent of the energy of the incident photon $h\nu$.
- The Compton shift in energy, on the other hand, depends strongly on the incident photon energy $h\nu$. Low-energy photons are scattered with minimal change in energy, while high-energy photons suffer a very large change in energy. The shift in photon energy $h\nu - h\nu'$ is equal to the kinetic energy E_{K} transferred to the Compton recoil electron.

7.3.3 Energy Transfer to the Compton Recoil Electron

The Compton (recoil) electron gains its kinetic energy E_{K} from the incident photon of energy $h\nu$, as given in (7.24)

$$E_{\mathrm{K}} = h\nu - h\nu' = h\nu\frac{\varepsilon(1-\cos\theta)}{1+\varepsilon(1-\cos\theta)} \ . \tag{7.29}$$

The maximum kinetic energy transfer $(E_{\mathrm{K}})_{\max}$ to recoil electron for a given $h\nu$ occurs at $\theta = \pi$ (photon backscattering) which corresponds to electron recoil angle $\phi = 0$, as shown in Fig. 7.8 with a plot of $(E_{\mathrm{K}})_{\max}/(h\nu)$ against $h\nu$. The maximum fraction of the incident photon energy $h\nu$ given to the recoil electron, $(E_{\mathrm{K}})_{\max}/(h\nu)$, is also given in Table 7.1 for photon energies in the range from 0.01 MeV to 100 MeV. In general $(E_{\mathrm{K}})_{\max}/(h\nu)$ is given as follows:

$$\frac{(E_{\mathrm{K}})_{\max}}{h\nu} = \frac{E_{\mathrm{K}}(\theta=\pi)}{h\nu} = \frac{2\varepsilon}{1+2\varepsilon}. \tag{7.30}$$

The expression of (7.29) can be solved for $h\nu$ after inserting $\varepsilon = h\nu/(m_{\mathrm{e}}c^2)$ to obtain a quadratic equation for $h\nu$ with the following solution:

$$h\nu = \frac{1}{2}(E_{\mathrm{K}})_{\max}\left\{1+\sqrt{1+\frac{2m_{\mathrm{e}}c^2}{(E_{\mathrm{K}})_{\max}}}\right\} \ . \tag{7.31}$$

For a given incident photon energy $h\nu$ the kinetic energy E_{K} of the recoil electron is in the range from 0 at $\theta = 0^\circ$ to $2h\nu\varepsilon/(1+2\varepsilon)$ at $\theta = \pi$, i.e.,

$$0 \leq E_{\mathrm{K}} \leq 2h\nu\varepsilon/(1+2\varepsilon) = (E_{\mathrm{K}})_{\max} \ . \tag{7.32}$$

From the dosimetric point of view, the most important curve given in Fig. 7.8 is the one showing $\overline{E}^{\sigma}_{\mathrm{K}}/(h\nu)$, the mean fraction of the incident photon energy $h\nu$ transferred to recoil electrons. Data for $\overline{E}^{\sigma}_{\mathrm{K}}/(h\nu)$ are also given in

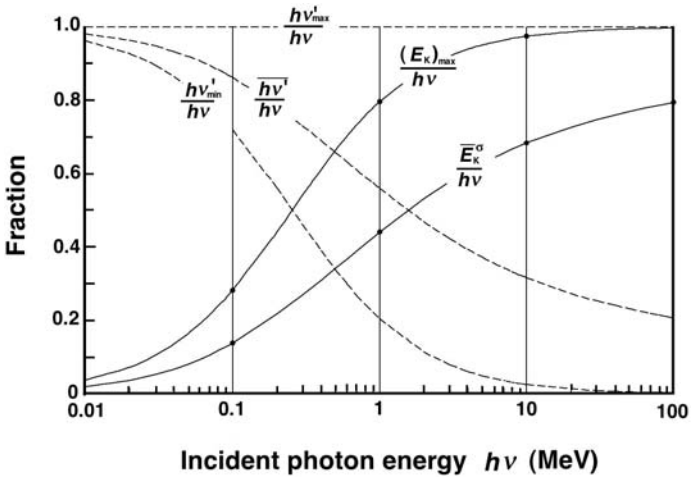

Fig. 7.8. Fraction of incident photon energy $h\nu$ transferred in Compton effect to:
- Maximum energy of recoil electron: $(E_\mathrm{K})_\mathrm{max}/(h\nu)$; $\theta = \pi$ [see (7.30)]
- Mean energy of recoil electron: $\overline{E}^{\sigma}_\mathrm{K}/(h\nu)$ [see (7.54 below)]
- Maximum energy of scattered photon: $h\nu'_\mathrm{max}/(h\nu)$; $\theta = 0^\circ$ [see (7.33)]
- Mean energy of the scattered photon: $\overline{h\nu'}/(h\nu)$ [see (7.34)]
- Minimum energy of the scattered photon: $h\nu'_\mathrm{min}/(h\nu)$; $\theta = \pi$ [see (7.35)]

Table 7.1, showing that the fractional energy transfer to recoil electrons is quite low at low photon energies (0.02 at $h\nu = 0.01$ MeV) and then slowly rises to become 0.44 at $h\nu = 1$ MeV and 0.796 at $h\nu = 100$ MeV. The mean fraction $\overline{E}^{\sigma}_\mathrm{K}/(h\nu)$ is discussed further in (7.53) and (7.54) below.

Figure 7.8 and Table 7.1 also show the *maximum*, *mean* and *minimum fractions* ($h\nu'_\mathrm{max}/h\nu$, $\overline{h\nu'}/h\nu$, $h\nu'_\mathrm{min}/h\nu$, respectively) of the incident photon energy $h\nu$ given to the scattered photon. The fractions are calculated as follows:

$$\frac{h\nu'_\mathrm{max}}{h\nu} = \frac{h\nu'|_{\theta=0}}{h\nu} = 1\,, \tag{7.33}$$

$$\frac{\overline{h\nu'}}{h\nu} = 1 - \frac{\bar{E}_\mathrm{K}}{h\nu}\,, \tag{7.34}$$

$$\frac{h\nu'_\mathrm{min}}{h\nu} = \frac{h\nu'|_{\theta=\pi}}{h\nu} = \frac{1}{1+2\varepsilon} = 1 - \frac{(E_\mathrm{K})_\mathrm{max}}{h\nu}\,, \tag{7.35}$$

where $\varepsilon = h\nu/(m_\mathrm{e}c^2)$.

7.3.4 Differential Cross Section for Compton Scattering $d_\mathrm{e}\sigma^{\mathrm{KN}}_\mathrm{c}/d\Omega$

The probability or cross section for a Compton interaction between a photon and a "free electron" is given by an expression derived by *Oskar Klein* and

Table 7.1. Fractions of the incident phoyton energy transferred through Compton effect to the maximum electron kinetic energy $(E_K)_{max}/(h\nu)$; mean electron kinetic energy $\overline{E}^{\sigma}_K/(h\nu)$; maximum scatterd photon energy $h\nu'_{max}/(h\nu)$; mean scattered photon energy $\overline{h\nu'}/(h\nu)$; and minimum scattered photon energy $h\nu'_{min}/(h\nu)$

$h\nu$ (MeV)	0.01	0.1	1.0	10.0	100.0
$(E^{\sigma}_K)_{max}/(h\nu)$	0.04	0.29	0.80	0.95	0.995
$\overline{E}^{\sigma}_K/(h\nu)$	0.02	0.14	0.44	0.68	0.796
$h\nu'_{max}/(h\nu)$	1.0	1.0	1.0	1.0	1.0
$\overline{h\nu'}/(h\nu)$	0.98	0.86	0.56	0.32	0.21
$h\nu'_{min}/(h\nu)$	0.96	0.71	0.20	0.05	0.005

Yoshio Nishina in 1929. The differential electronic cross section for Compton effect is given as follows:

$$\frac{d_e\sigma_c^{KN}}{d\Omega} = \frac{r_e^2}{2}\left(\frac{\nu'}{\nu}\right)^2\left\{\frac{\nu'}{\nu}+\frac{\nu}{\nu'}-\sin^2\theta\right\}$$
$$= \frac{r_e^2}{2}(1+\cos^2\theta)\,F_{KN} = \frac{d_e\sigma_{Th}}{d\Omega}F_{KN}\,, \tag{7.36}$$

where

$d_e\sigma_c^{KN}/d\Omega$ is the differential Klein-Nishina electronic cross section for the Compton effect,
ν is the frequency of the incident photon,
ν' is the frequency of the scattered photon,
θ is the scattering angle,
r_e is the classical radius of the electron (2.82 fm),
F_{KN} is the Klein-Nishina form factor,
$d_e\sigma_{Th}/d\Omega$ is the differential cross section for Thomson scattering.

The Klein-Nishina form factor F_{KN} for a free electron is given as follows:

$$F_{KN} = \frac{1}{[1+\varepsilon(1-\cos\theta)]^2}\left\{1+\frac{\varepsilon^2(1-\cos\theta)^2}{[1+\varepsilon(1-\cos\theta)](1+\cos^2\theta)}\right\}, \tag{7.37}$$

where again $\varepsilon = h\nu/(m_e c^2)$.

The Klein-Nishina form factor F_{KN} is plotted in Fig. 7.9 against the scattering angle θ for various values of the energy parameter ε. For $\varepsilon = 0$ the form factor is 1 irrespective of the scattering angle θ.

As shown in (7.37) and in Fig. 7.9, the form factor F_{KN} is a complicated function of the scattering angle θ and parameter ε. However, it is easy to show that:

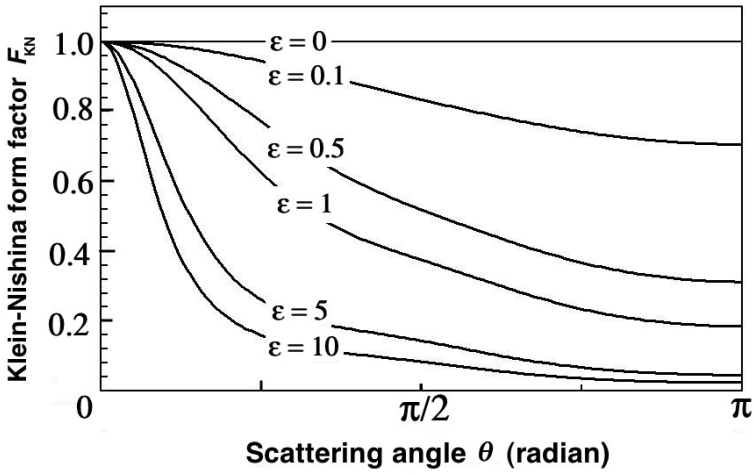

Fig. 7.9. Atomic form factor for Compton effect F_{KN} against scattering angle θ

- $F_{\mathrm{KN}} \leq 1$ for all θ and ε. (7.38)
- $F_{\mathrm{KN}} = 1$ for $\theta = 0$ at any ε. (7.39)
- $F_{\mathrm{KN}} = 1$ for $\varepsilon = 0$ at any θ (Thomson scattering). (7.40)

The differential electronic cross section for the Compton effect $d_{\mathrm{e}}\sigma_{\mathrm{c}}^{\mathrm{KN}}/d\Omega$ when $F_{\mathrm{KN}} = 1$ is equal to the Thomson electronic differential cross section $d_{\mathrm{e}}\sigma_{\mathrm{Th}}/d\Omega$ given in (7.12)

$$\frac{d_{\mathrm{e}}\sigma_{\mathrm{c}}^{\mathrm{KN}}}{d\Omega}\,|_{F_{\mathrm{KN}}=1} = \frac{d_{\mathrm{e}}\sigma_{\mathrm{Th}}}{d\Omega} = \frac{r_{\mathrm{e}}^2}{2}(1+\cos^2\theta)\,. \tag{7.41}$$

The differential Compton electronic cross section $d_{\mathrm{e}}\sigma_{\mathrm{c}}^{\mathrm{KN}}/d\Omega$ is given in Fig. 7.10 against the scattering angle θ for various values of ε ranging from $\varepsilon \approx 0$ which results in $F_{\mathrm{KN}} = 1$ for all θ, (i.e., Thomson scattering) to $\varepsilon = 10$ for which the F_{KN} causes a significant deviation from the Thomson electronic cross section for all angles θ except for $\theta = 0$.

The data of Fig. 7.10 are replotted in Fig. 7.11 in a polar coordinate system that gives a better illustration of the Compton scattering phenomenon.

- At low ε the probabilities for forward scattering and back scattering are equal and amount to 79.4 mb (Thomson scattering).
- As the energy $h\nu$ increases the probability for back scattering decreases and the probability for forward scattering remains constant at 79.4 mb.
- The polar diagram of Fig. 7.11 is sometimes colloquially referred to as the "peanut diagram" to help students remember its shape.

At low incident photon energies (Thomson limit) the probabilities for forward scattering and back scattering are equal and twice as large as the probability

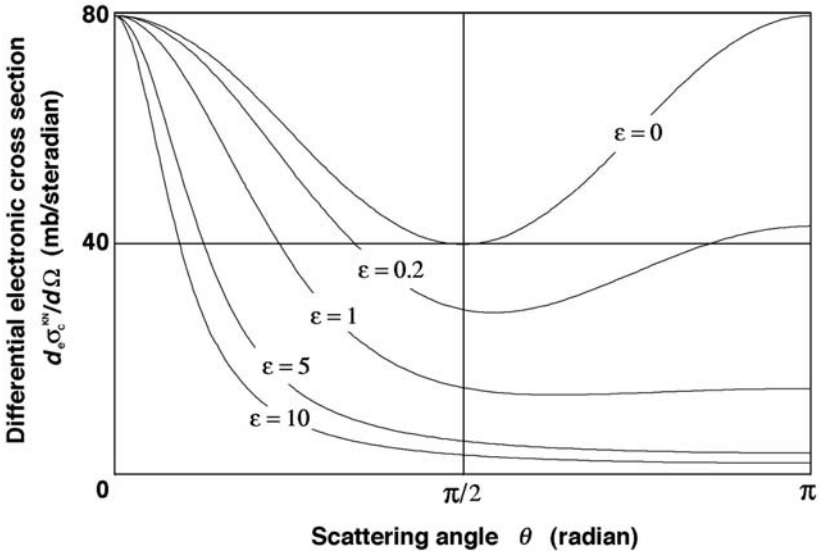

Fig. 7.10. Differential electronic cross section for Compton effect $d_e\sigma_c^{KN}/d\Omega$ against scattering angle θ for various values of $\varepsilon = h\nu/(m_e c^2)$, as given by (7.36). The differential electronic cross section for Compton effect $d_e\sigma_c^{KN}/d\Omega$ for $\varepsilon = 0$ is equal to the differential electronic cross section for Thomson scattering $d_e\sigma_{Th}/d\Omega$ (see Fig. 7.2)

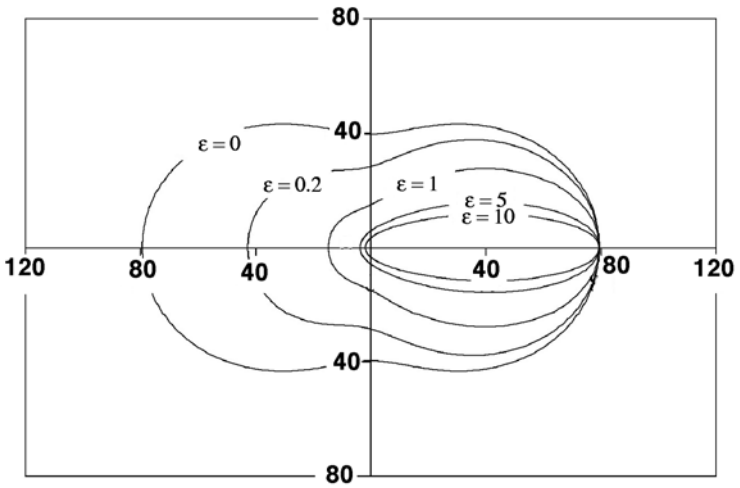

Fig. 7.11. Polar representation of the angular dependence of the differential electronic cross section $d_e\sigma_c^{KN}/d\Omega$ for Compton scattering, as given by (7.36) and plotted for various values of $\varepsilon = h\nu/(m_e c^2)$. The differential electronic cross section for Compton effect $d_e\sigma_c^{KN}/d\Omega$ for $\varepsilon = 0$ is equal to the differential electronic cross section for Thomson scattering $d_e\sigma_{Th}/d\Omega$ (see Fig. 7.3)

for side scattering. As the incident photon energy, i.e., ε, increases, the scattering becomes increasingly more forward peaked and backscattering rapidly diminishes.

7.3.5 Differential Energy Transfer Cross Section $(d_e\sigma_c^{KN})_{tr}/d\Omega$

The differential energy transfer coefficient $(d_e\sigma_c^{KN})_{tr}/d\Omega$ for the Compton effect is determined from the differential electronic cross section $d_e\sigma_c/d\Omega$ given in (7.36) as follows:

$$\begin{aligned}\frac{(d_e\sigma_c^{KN})_{tr}}{d\Omega} &= \frac{d_e\sigma_c^{KN}}{d\Omega}\frac{\overline{E}_K}{h\nu} = \frac{r_e^2}{2}\left(\frac{\nu'}{\nu}\right)^2\left\{\frac{\nu'}{\nu}+\frac{\nu}{\nu'}-\sin^2\theta\right\}\left(\frac{\nu-\nu'}{\nu}\right)\\ &= \frac{d_e\sigma_{Th}}{d\Omega}F_{KN}\frac{\overline{E}_K^{\sigma}}{h\nu} = \frac{r_e^2}{2}(1+\cos^2\theta)\frac{\varepsilon(1-\cos\theta)}{[1+\varepsilon(1-\cos\theta)]^3}\\ &\quad\left\{1+\frac{\varepsilon^2(1-\cos\theta)^2}{[1+\varepsilon(1-\cos\theta)](1+\cos^2\theta)}\right\}\frac{\overline{E}_K^{\sigma}}{h\nu}\,, \qquad (7.42)\end{aligned}$$

where $\overline{E}_K^{\sigma}/(h\nu)$ is given in Fig. 7.8 and in Table 7.1 for incident photon energies in the range 0.01 MeV $\leq h\nu \leq$ 100 MeV.

7.3.6 Energy Distribution of Recoil Electrons $d_e\sigma_c^{KN}/dE_K$

The differential electronic Klein-Nishina cross section $d_e\sigma_c^{KN}/dE_K$ expressing the initial energy spectrum of Compton recoil electrons averaged over all scattering angles θ is calculated from the general Klein-Nishina relationship for $d_e\sigma_c^{KN}/d\Omega$ as follows:

$$\begin{aligned}\frac{d_e\sigma_c^{KN}(E_K)}{dE_K} &= \frac{d_e\sigma_c^{KN}}{d\Omega}\frac{d\Omega}{d\theta}\frac{d\theta}{dE_K} =\\ &= \frac{\pi r_e^2}{\varepsilon h\nu}\left\{2-\frac{2E_K}{\varepsilon(h\nu-E_K)}+\frac{E_K^2}{\varepsilon^2(h\nu-E_K)^2}+\frac{E_K^2}{h\nu(h\nu-E_K)}\right\}\,,\end{aligned} \qquad (7.43)$$

where

$d_e\sigma_c^{KN}/d\Omega$ is given in (7.36),
$d\Omega/d\theta$ is $2\pi\sin\theta$,
$d\theta/dE_K$ is $(dE_K/d\theta)^{-1}$ with $E_K(\theta)$ given in (7.29).

The differential electronic cross section $d_e\sigma_c^{KN}/dE_K$ is plotted in Fig. 7.12 against the kinetic energy E_K of the recoil electron for various values of the incident photon energy $h\nu$. The following features can now be recognized:

- The distribution of kinetic energies given to the Compton recoil electrons is essentially flat from zero almost up to the maximum electron kinetic energy $(E_K)_{max}$ where a higher concentration occurs.

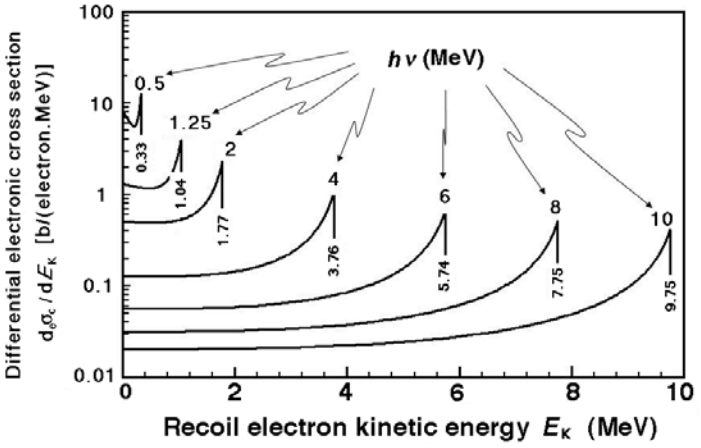

Fig. 7.12. Differential electronic Klein-Nishina cross section per unit kinetic energy $d_e\sigma_c^{KN}/dE_K$ calculated from (7.43) and plotted against the kinetic energy of the Compton recoil electron E_K for various incident photon energies $h\nu$. For a given photon energy the maximum kinetic energy of the recoil electron, calculated from (7.44), is indicated on the graph

- $(E_K)_{max}$ is calculated from

$$(E_K)_{max} = 2h\nu\varepsilon/(1+2\varepsilon) = h\nu - h\nu'_{min} \,, \tag{7.44}$$

as given by (7.30). Since, as shown in (7.27), $h\nu'_{min}$ approaches $m_e c^2/2$ for high $h\nu$, we note that $(E_K)_{max}$ approaches $h\nu - (m_e c^2/2)$.

7.3.7 Total Electronic Klein-Nishina Cross Section for Compton Scattering $_e\sigma_c^{KN}$

The total cross section for the Compton scattering on a free electron $_e\sigma_c^{KN}$ is calculated by integrating the differential cross section $d_e\sigma_c^{KN}/d\Omega$ of (7.36) over the whole solid angle

$$\begin{aligned} {}_e\sigma_c^{KN} &= \int \frac{d_e\sigma_c^{KN}}{d\Omega} d\Omega \\ &= 2\pi r_e^2 \left\{ \frac{1+\varepsilon}{\varepsilon^2} \left[\frac{2(1+\varepsilon)}{1+2\varepsilon} - \frac{\ln(1+2\varepsilon)}{\varepsilon} \right] + \frac{\ln(1+2\varepsilon)}{2\varepsilon} - \frac{1+3\varepsilon}{(1+2\varepsilon)^2} \right\} . \end{aligned} \tag{7.45}$$

The numerical value of $_e\sigma_c^{KN}$ can also be obtained through a determination of the area under the $d_e\sigma_c^{KN}/d\theta$ curve for a given ε. For $\varepsilon = 0$ the area is equal to the Thomson result of 0.665 b [see (7.14)].

Two extreme cases are of special interest, since they simplify the expression for $_e\sigma_c^{KN}$:

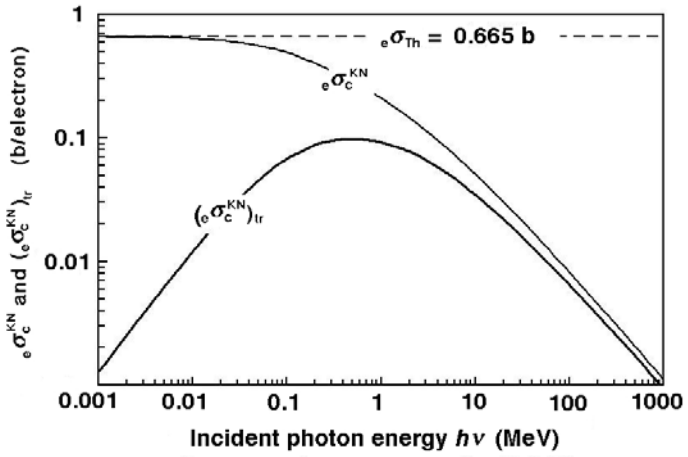

Fig. 7.13. Compton electronic cross section ${}_e\sigma_c^{KN}$ and electronic energy transfer cross section $({}_e\sigma_c^{KN})_{tr}$ for a free electron against incident photon energy $h\nu$ in the energy range from 0.001 MeV to 1000 MeV, determined from Klein-Nishina Eqs. (7.45) and (7.51), respectively. For very low photon energies ${}_e\sigma_c^{KN} = {}_e\sigma_{Th} = 0.665$ b

- For small incident photon energies $h\nu$ we get the following relationship:

$$ {}_e\sigma_c^{KN} = \frac{8\pi}{3} r_e^2 (1 - 2\varepsilon + \frac{26}{5}\varepsilon^2 - \frac{133}{10}\varepsilon^3 + \frac{1144}{35}\varepsilon^4 - \ldots) , \qquad (7.46) $$

  which for $\varepsilon \to 0$ approaches the classical Thomson result of (7.14), i.e.,

$$ {}_e\sigma_c^{KN}\big|_{\varepsilon \to 0} \approx {}_e\sigma_{Th} = \frac{8\pi}{3} r_e^2 = 0.665 \text{ b} . \qquad (7.47) $$

- For very large incident photon energies $h\nu$, i.e., $\varepsilon \gg 1$, we get

$$ {}_e\sigma_c^{KN} \approx \pi r_e^2 \frac{1 + 2\ln\varepsilon}{2\varepsilon} . \qquad (7.48) $$

Figure 7.13 shows the Compton electronic cross section ${}_e\sigma_c^{KN}$ as determined by the Klein-Nishina relationship of (7.45) against the incident photon energy $h\nu$ in the energy range from 0.001 MeV to 1000 MeV. The following features can be identified:

- At low photon energies ${}_e\sigma_c^{KN}$ is approximately equal to the classical Thomson cross section ${}_e\sigma_{Th}$ which, with its value of 0.665 b, is independent of photon energy.
- For intermediate photon energies ${}_e\sigma_c^{KN}$ decreases gradually with photon energy to read 0.46 b at $h\nu = 0.1$ MeV, 0.21 b at $h\nu = 1$ MeV, 0.05 b at $h\nu = 10$ MeV, and 0.08 b at $h\nu = 100$ MeV.
- At very high photon energies $h\nu$, the Compton electronic cross section ${}_e\sigma_c^{KN}$ attains $1/(h\nu)$ dependence, as shown in (7.48).

- The Compton electronic cross section ${}_{\mathrm{e}}\sigma_{\mathrm{c}}^{\mathrm{KN}}$ is independent of atomic number Z of the absorber, since in the Compton theory the electron is assumed free and stationary, i.e., the electron's binding energy to the atom is assumed to be negligible.

The Compton atomic cross section ${}_{\mathrm{a}}\sigma_{\mathrm{c}}^{\mathrm{KN}}$ is determined from the electronic cross section of (7.45) using the standard relationship

$$ {}_{\mathrm{a}}\sigma_{\mathrm{c}}^{\mathrm{KN}} = Z\, {}_{\mathrm{e}}\sigma_{\mathrm{c}}^{\mathrm{KN}} \,, \tag{7.49} $$

where Z is the atomic number of the absorber.

The Compton mass attenuation coefficient $\sigma_{\mathrm{c}}^{\mathrm{KN}}/\rho$ is given as follows:

$$ \frac{\sigma_{\mathrm{c}}^{\mathrm{KN}}}{\rho} = \frac{N_{\mathrm{A}}}{A}\, {}_{\mathrm{a}}\sigma_{\mathrm{c}}^{\mathrm{KN}} = \frac{ZN_{\mathrm{A}}}{A}\, {}_{\mathrm{e}}\sigma_{\mathrm{c}}^{\mathrm{KN}} \approx \frac{1}{2} N_{\mathrm{A}}\, {}_{\mathrm{e}}\sigma_{\mathrm{c}}^{\mathrm{KN}} \,. \tag{7.50} $$

The atomic Compton cross section (attenuation coefficient) ${}_{\mathrm{a}}\sigma_{\mathrm{c}}^{\mathrm{KN}}$ is linearly proportional to Z, while the Compton mass attenuation coefficient $\sigma_{\mathrm{c}}^{\mathrm{KN}}/\rho$ is essentially independent of Z insofar as Z/A is independent of Z. In reality Z/A ranges from 1 for hydrogen, to 0.5 for low atomic number elements down to 0.4 for high Z, allowing us to make the approximation $Z/A \approx 0.5$.

7.3.8 Energy Transfer Cross Section for Compton Effect $({}_{\mathrm{e}}\boldsymbol{\sigma}_{\mathbf{c}}^{\mathbf{KN}})_{\mathbf{tr}}$

The electronic energy transfer cross section $({}_{\mathrm{e}}\sigma_{\mathrm{c}}^{\mathrm{KN}})_{\mathrm{tr}}$ is obtained by integrating the differential energy cross section $d({}_{\mathrm{e}}\sigma_{\mathrm{c}}^{\mathrm{KN}})_{\mathrm{tr}}/d\Omega$ of (7.42) over all photon scattering angles θ from 0° to 180° to get

$$ ({}_{\mathrm{e}}\sigma_{\mathrm{c}}^{\mathrm{KN}})_{\mathrm{tr}} = $$

$$ 2\pi r_{\mathrm{e}}^2 \left\{ \begin{array}{l} \dfrac{2(1+\varepsilon)^2}{\varepsilon^2(1+2\varepsilon)} - \dfrac{1+3\varepsilon}{(1+2\varepsilon)^2} - \\ \\ -\dfrac{(1+\varepsilon)(2\varepsilon^2-2\varepsilon-1)}{\varepsilon^2(1+2\varepsilon)^2} - \dfrac{4\varepsilon^2}{3(1+2\varepsilon)^3} - \left[\dfrac{1+\varepsilon}{\varepsilon^3} - \dfrac{1}{2\varepsilon} + \dfrac{1}{2\varepsilon^3}\right] \ln(1+2\varepsilon) \end{array} \right\} . \tag{7.51} $$

In addition to the Compton electronic cross section ${}_{\mathrm{e}}\sigma_{\mathrm{c}}^{\mathrm{KN}}$, Fig. 7.13 also shows the energy transfer cross section for the Compton effect $({}_{\mathrm{e}}\sigma_{\mathrm{c}}^{\mathrm{KN}})_{\mathrm{tr}}$ calculated with (7.51) and plotted against the incident photon energy $h\nu$ in the energy range from 0.001 MeV to 1000 MeV.

Since $({}_{\mathrm{e}}\sigma_{\mathrm{c}}^{\mathrm{KN}})_{\mathrm{tr}}$ and ${}_{\mathrm{e}}\sigma_{\mathrm{c}}^{\mathrm{KN}}$ are related through the following relationship:

$$ ({}_{\mathrm{e}}\sigma_{\mathrm{c}}^{\mathrm{KN}})_{\mathrm{tr}} = {}_{\mathrm{e}}\sigma_{\mathrm{c}}^{\mathrm{KN}} \overline{E}_{\mathrm{tr}}^{\sigma}/(h\nu) \,, \tag{7.52} $$

where $\overline{E}_{\mathrm{tr}}^{\sigma}/h\nu$ is the mean fraction of the incident photon energy transferred to the kinetic energy of the Compton recoil electron, we can calculate

$\overline{E}^{\sigma}_{\mathrm{K}}/h\nu$ as

$$\frac{\overline{E}^{\sigma}_{\mathrm{K}}}{h\nu} = \frac{({}_{\mathrm{e}}\sigma_{\mathrm{c}}^{\mathrm{KN}})_{\mathrm{tr}}}{{}_{\mathrm{e}}\sigma_{\mathrm{c}}^{\mathrm{KN}}} \,, \tag{7.53}$$

with $({}_{\mathrm{e}}\sigma_{\mathrm{c}}^{\mathrm{KN}})_{\mathrm{tr}}$ and ${}_{\mathrm{e}}\sigma_{\mathrm{c}}^{\mathrm{KN}}$ given in (7.51) and (7.45), respectively.

Inserting (7.45) and (7.51) into (7.53) gives the following result for the mean fraction of the incident photon energy transferred to the kinetic energy of the recoil electron in Compton effect $\overline{E}^{\sigma}_{\mathrm{K}}/h\nu$:

$$\frac{\overline{E}^{\sigma}_{\mathrm{K}}}{h\nu} = \frac{\left\{\frac{2(1+\varepsilon)^2}{\varepsilon^2(1+2\varepsilon)} - \frac{1+3\varepsilon}{(1+2\varepsilon)^2} - \frac{(1+\varepsilon)(2\varepsilon^2-2\varepsilon-1)}{\varepsilon^2(1+2\varepsilon)^2} - \frac{4\varepsilon^2}{3(1+2\varepsilon)^3} - \left[\frac{1+\varepsilon}{\varepsilon^3} - \frac{1}{2\varepsilon} + \frac{1}{2\varepsilon^3}\right]\ln(1+2\varepsilon)\right\}}{\left\{\frac{1+\varepsilon}{\varepsilon^2}\left[\frac{2(1+\varepsilon)}{1+2\varepsilon} - \frac{\ln(1+2\varepsilon)}{\varepsilon}\right] + \frac{\ln(1+2\varepsilon)}{2\varepsilon} - \frac{1+3\varepsilon}{(1+2\varepsilon)^2}\right\}} \,. \tag{7.54}$$

At first glance (7.54) looks very cumbersome; however, it is simple to use once the appropriate value for ε at a given photon energy $h\nu$ has been established. For example, an incident photon of energy $h\nu = 1.02$ MeV results in $\varepsilon = 2$ that, when inserted into (7.54), gives $\overline{E}^{\sigma}_{\mathrm{K}}/(h\nu) = 0.440$ or $\overline{E}^{\sigma}_{\mathrm{K}} = 0.440$ MeV. The energy of the corresponding scattered photon is $h\nu' = h\nu - \overline{E}^{\sigma}_{\mathrm{K}} = 0.660$ MeV.

$\overline{E}^{\sigma}_{\mathrm{K}}/(h\nu)$ is plotted in Fig. 7.8 (the "Compton Graph") in the incident photon energy $h\nu$ range between 0.01 MeV and 100 MeV. Table 7.1 gives several values of $\overline{E}^{\sigma}_{\mathrm{K}}/(h\nu)$ in the same energy range.

The plot of $\overline{E}^{\sigma}_{\mathrm{K}}/(h\nu)$ against incident photon energy $h\nu$ of Fig. 7.8 shows that when low energy photons interact in a Compton process, very little energy is transferred to recoil electrons and most energy goes to the scattered photon. On the other hand, when high energy photons ($h\nu > 10$ MeV) interact in a Compton process, most of the incident photon energy is given to the recoil electron and very little is given to the scattered photon.

7.3.9 Binding Energy Effects and Corrections

The Compton electronic cross section ${}_{\mathrm{e}}\sigma_{\mathrm{c}}^{\mathrm{KN}}$ and energy transfer coefficient $({}_{\mathrm{e}}\sigma_{\mathrm{c}}^{\mathrm{KN}})_{\mathrm{tr}}$ were calculated with Klein-Nishina relationships for free electrons and are plotted in Fig. 7.13 with solid curves. At very low incident photon energies the assumption of free electrons breaks down and the electronic binding energy E_{B} affects the Compton atomic cross sections; the closer is the photon energy $h\nu$ to E_{B}, the larger is the deviation of the atomic cross section ${}_{\mathrm{a}}\sigma_{\mathrm{c}}$ from the calculated free-electron Klein-Nishina cross sections ${}_{\mathrm{e}}\sigma_{\mathrm{c}}^{\mathrm{KN}}$.

This discrepancy is evident from Fig. 7.14 that displays, for various absorbers ranging from hydrogen to lead, the atomic cross sections ${}_{\mathrm{a}}\sigma_{\mathrm{c}}$ (solid curves) and the calculated Klein-Nishina atomic cross sections ${}_{\mathrm{a}}\sigma_{\mathrm{c}}^{\mathrm{KN}}$. Note that ${}_{\mathrm{a}}\sigma_{\mathrm{c}}^{\mathrm{KN}} = Z\,{}_{\mathrm{e}}\sigma_{\mathrm{c}}^{\mathrm{KN}}$, where ${}_{\mathrm{e}}\sigma_{\mathrm{c}}^{\mathrm{KN}}$ is calculated with (7.45). It is also shown

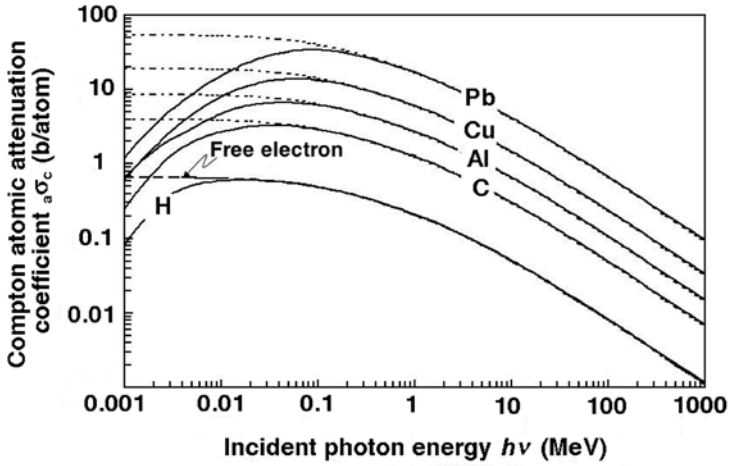

Fig. 7.14. Compton atomic cross sections $_a\sigma_c$ plotted against incident photon energy $h\nu$ for various absorbers, ranging from hydrogen to lead. The *dotted curves* represent $_a\sigma_c^{KN}$ data calculated with Klein-Nishina free-electron relationships; the *solid curves* represent the $_a\sigma_c$ data that incorporate the binding effects of the orbital electrons. The *dashed curve* represents the Klein-Nishina free electron coefficients $_e\sigma_c^{KN}$ for the Compton effect

in Fig. 7.14 that at low incident photon energies $h\nu$, the larger is the atomic number Z of the absorber, the more pronounced is the discrepancy and the higher is the energy at which $_a\sigma_c$ and $_a\sigma_c^{KN}$ begin to coincide.

Various theories have been developed to account for electronic binding energy effects on Compton atomic cross sections. Most notable is the method developed by *John Hubbell* from the National Institute for Science and Technology (NIST) in Washington, USA, who treated the binding energy corrections to the Klein-Nishina relationships in the impulse approximation taking into account all orbital electrons of the absorber atom. This involves applying a multiplicative correction function $S(x, Z)$, referred to as the *incoherent scattering function*, to the Klein-Nishina atomic cross sections as follows:

$$\frac{d_a\sigma_c}{d\Omega} = \frac{d_a\sigma_c^{KN}}{d\Omega} S(x, Z) \,, \tag{7.55}$$

where x, the *momentum transfer variable*, stands for $\sin(\theta/2)/\lambda$.

The total Compton atomic cross section $_a\sigma_c$ is obtained from the following integral:

$$_a\sigma_c = \int_{\theta=0}^{\theta=\pi} S(x, Z)\, d_e\sigma_c^{KN}(\theta) \,, \tag{7.56}$$

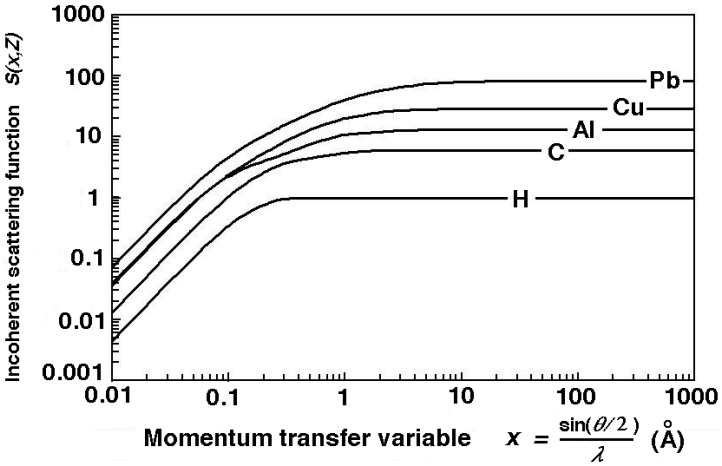

Fig. 7.15. Incoherent scattering function $S(x, Z)$ plotted against the momentum transfer variable x for various absorbers in the range from hydrogen to lead

where the incoherent scattering function $S(x, Z)$ relates to the properties of the absorber atom and is important for collisions in which the electron momentum p_e is small enough so that the electron has a finite probability for not escaping from the atom.

From Fig. 7.5, in conjunction with the application of the law of cosines on the triangle $(\vec{p}_\nu, \vec{p}_{\nu'}, \vec{p}_e)$, we obtain the following relationship for p_e^2:

$$p_e^2 = p_\nu^2 + p_{\nu'}^2 - 2p_\nu p_{\nu'} \cos\theta \tag{7.57}$$

or

$$p_e = \sqrt{\left(\frac{h\nu}{c}\right)^2 + \left(\frac{h\nu'}{c}\right)^2 - 2\frac{h\nu}{c}\frac{h\nu'}{c}\cos\theta}\,. \tag{7.58}$$

For small $h\nu$ we know that $h\nu' \approx h\nu$ (see Fig. 7.7) and p_e of (7.58) is approximated as follows:

$$p_e \approx \frac{h\nu}{c}\sqrt{2(1-\cos\theta)} = \frac{h\nu}{c}\sqrt{4\sin^2\frac{\theta}{2}} = 2h\frac{\sin\frac{\theta}{2}}{\lambda} = 2hx\,, \tag{7.59}$$

where $x = (\sin\theta/2)/\lambda$ is defined as the *momentum transfer variable* with λ the wavelength of the incident photon.

Hubbell also compiled extensive tables of the incoherent scattering function $S(x, Z)$. Figure 7.15 presents Hubbell's data for $S(x, Z)$ plotted against $x = \sin(\theta/2)/\lambda$ for several absorbers in the range from hydrogen to lead. The figure shows that $S(x, Z)$ saturates at Z for relatively large values of x; the higher is Z, the larger is x at which the saturation sets in. With decreasing

x, the function $S(x, Z)$ decreases and attains at $x = 0.01$ a value that is less than 1% of its saturation Z value. The following features can be recognized:

- The electron binding correction is effective only when $S(x, Z) < Z$.
- For $S(x, Z) = Z$ there is no correction and the Klein-Nishina coefficients ${}_{\mathrm{e}}\sigma_{\mathrm{c}}^{\mathrm{KN}}$ provide correct values for the atomic cross sections ${}_{\mathrm{a}}\sigma_{\mathrm{c}}$ through the simple relationship ${}_{\mathrm{a}}\sigma_{\mathrm{c}} = Z({}_{\mathrm{e}}\sigma_{\mathrm{c}}^{\mathrm{KN}})$.
- The binding energy correction is only important at photon energies of the order of E_{B}, and this occurs in the photon energy region where photoeffect and Rayleigh scattering are much more probable than the Compton effect. Thus, ignoring the binding correction on Compton cross sections will not adversely affect the determination of the total cross section for photon interactions at relatively low photon energies, since, at these low energies, effects other than the Compton effect make a much larger contribution to the total attenuation coefficient than does the Compton effect.

The effects of binding energy corrections on Klein-Nishina differential atomic cross sections per unit angle $d_{\mathrm{a}}\sigma_{\mathrm{c}}^{\mathrm{KN}}/d\theta$ are shown in Fig. 7.16 for various incident photon energies in the range from 1 keV to 10 MeV, for hydrogen in part (a), carbon in part (b), and lead in part (c). The data points are for Klein-Nishina expressions $d_{\mathrm{a}}\sigma_{\mathrm{c}}^{\mathrm{KN}}/d\theta = Z\, d_{\mathrm{e}}\sigma_{\mathrm{c}}^{\mathrm{KN}}/d\theta$, the solid curves represent the Klein-Nishina results corrected with the incoherent scattering function $S(x, Z)$, i.e., $d_{\mathrm{a}}\sigma_{\mathrm{c}}/d\theta = S(x, Z)\, d_{\mathrm{e}}\sigma_{\mathrm{c}}^{\mathrm{KN}}/d\theta$.

The following conclusions may be made from Fig. 7.16:

- For a given absorber Z, the binding energy correction is more significant at lower photon energies. For example, in lead the uncorrected and corrected 1 keV curves differ considerably, the 10 keV curves differ less, the 0.1 MeV curves even less, while the 1 MeV and 10 MeV curves are identical.
- For a given photon energy $h\nu$, the binding energy correction is more significant at higher atomic numbers Z. For example, the uncorrected and corrected 0.1 MeV curves in hydrogen are identical, for carbon they are almost identical, and for lead they are significantly different.

7.3.10 Mass Attenuation Coefficient for Compton Effect

The Compton mass attenuation coefficient σ_{c}/ρ is calculated from the Compton atomic cross section ${}_{\mathrm{a}}\sigma_{\mathrm{c}}$ with the standard relationship as follows:

$$\frac{\sigma_{\mathrm{c}}}{\rho} = \frac{N_{\mathrm{A}}}{A}{}_{\mathrm{a}}\sigma_{\mathrm{c}} \,. \tag{7.60}$$

In the energy region not affected by electron binding effects the following relationships hold:

$${}_{\mathrm{a}}\sigma_{\mathrm{c}} = Z({}_{\mathrm{e}}\sigma_{\mathrm{c}}^{\mathrm{KN}}) \tag{7.61}$$

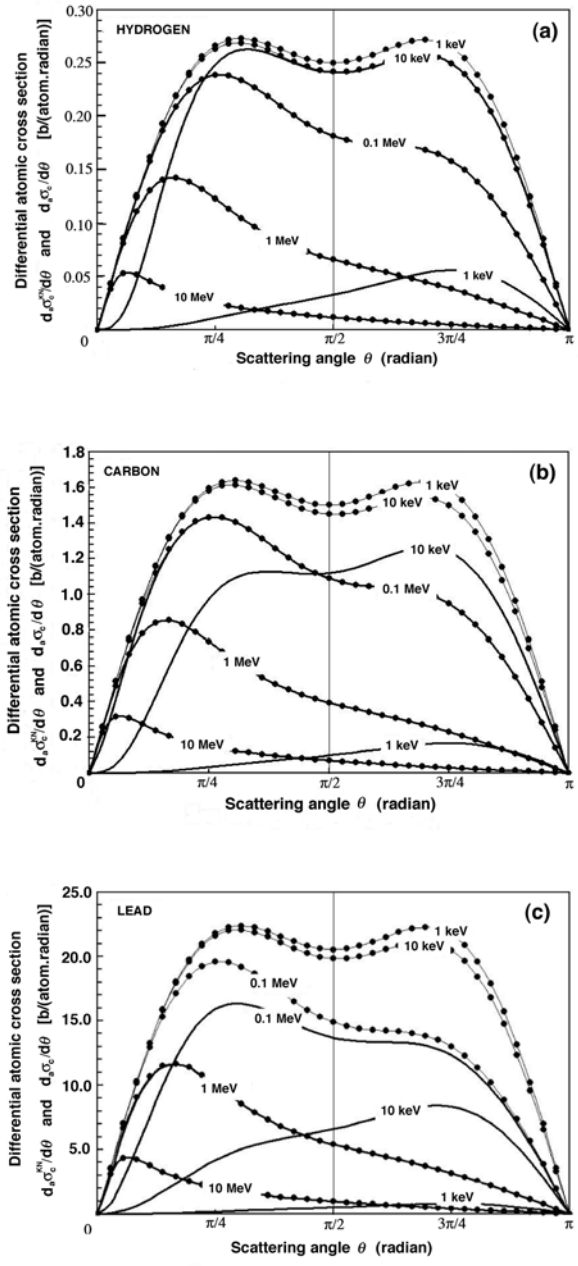

Fig. 7.16. Differential atomic cross-section per unit angle for Compton effect, $d_a\sigma_c/d\theta$, against scattering angle θ for hydrogen in part **a**, carbon in part **b**, and lead in part **c**. The *dotted curves (data points)* are for Klein-Nishina data, the *solid lines* represent the Klein-Nishina data corrected with the incoherent scattering function $S(x, Z)$

and

$$\frac{\sigma_c}{\rho} = \frac{ZN_A}{A} {}_e\sigma_c^{KN} \approx \frac{N_A}{2} {}_e\sigma_c^{KN} , \tag{7.62}$$

where Z and A are the atomic number and atomic mass, respectively, of the absorber and their ratio Z/A is of the order of 0.5.

The following conclusions may now be drawn from (7.62):

1. Since ${}_e\sigma_c^{KN}$ is given for free electrons, it is independent of Z. This makes ${}_a\sigma_c$ linearly dependent on Z.
2. Since $Z/A \approx 0.5$ for all elements with the exception of hydrogen for which $Z/A = 1$, σ_c/ρ is essentially independent of Z. In reality, as often stated before, $Z/A = 0.5$ for low atomic number absorbers but with increasing Z the ratio Z/A gradually falls to $Z/A = 0.4$ for high atomic number absorbers.

Since the Compton atomic coefficient ${}_a\sigma_c$ is linearly proportional to the atomic number Z of the absorber, as shown in (7.61), the mass attenuation coefficient σ_c/ρ is essentially independent of Z, as shown in (7.62), insofar as Z/A is considered independent of Z.

Tables 7.2 and 7.3 list the Compton atomic cross section ${}_a\sigma_c$ and mass attenuation coefficient σ_c/ρ, respectively, for 10 keV and 1 MeV photons interacting with various absorbers in the range from hydrogen to lead. Columns (5) display the atomic cross sections ${}_a\sigma_c$ incorporating binding energy corrections, while columns (6) display the Klein-Nishina atomic cross sections ${}_a\sigma_c^{KN} = Z({}_e\sigma_c^{KN})$. The two coefficients (${}_a\sigma_c$ and ${}_a\sigma_c^{KN}$) agree well for the photon energy of 1 MeV; however, the discrepancy between the two is significant for the photon energy of 10 keV, as also shown in Fig. 7.14.

We also note that at $h\nu = 1$ MeV, the σ_c/ρ values follow straight from the Klein-Nishina electronic cross sections and are affected only by the specific value for Z/A. This is not the case for σ_c/ρ at 10 keV that are affected not only by Z/A but also by the electronic binding effects that are significant in this energy range for all Z; the larger is Z, the larger is the binding effect, as shown in columns (5) and (6) of Table 7.2.

7.3.11 Compton Mass Energy Transfer Coefficient

The Compton mass energy transfer coefficient $(\sigma_c/\rho)_{tr}$ is calculated from the mass attenuation coefficient σ_c/ρ using the standard relationship

$$\left(\frac{\sigma_c}{\rho}\right)_{tr} = \frac{\sigma_c}{\rho} \frac{\overline{E}_K^{\sigma}}{h\nu}, \tag{7.63}$$

where $\overline{E}_K^{\sigma}$ is the average energy transferred to the kinetic energy of recoil electrons in the Compton effect. $\overline{E}_K^{\sigma}$ is given by (7.54) and in Table 7.1. It is plotted as "*The Compton Graph*" in Fig. 7.8. $\overline{E}_K^{\sigma}/(h\nu)$ is the average fraction of the incident photon energy that is transferred to the recoil (Compton)

Table 7.2. Compton atomic cross sections ${}_{\mathrm{a}}\sigma_{\mathrm{c}}$ and mass attenuation coefficients σ_{c}/ρ at photon energy of 10 keV for various absorbers

(1) Element	(2) Symbol	(3) Atomic number Z	(4) Atomic mass A	(5) (*a*) ${}_{\mathrm{a}}\sigma_{\mathrm{c}}$ (b/atom)	(6) (*b*) $Z\,{}_{\mathrm{e}}\sigma_{\mathrm{c}}^{\mathrm{KN}}$ (b/atom)	(7) (*c*) σ_{c}/ρ (cm^2/g)
Hydrogen	H	1	1.008	0.60	0.64	0.0358
Carbon	C	6	12.01	2.70	3.84	0.0135
Aluminum	Aℓ	13	26.98	4.74	8.33	0.0106
Copper	Cu	29	63.54	8.15	18.57	0.0176
Tin	Sn	50	118.69	12.00	32.03	0.0607
Lead	Pb	82	207.2	15.60	52.52	0.0153

(a) Data are from the NIST

(b) ${}_{\mathrm{e}}\sigma_{\mathrm{c}}^{\mathrm{KN}}(h\nu = 10\ \mathrm{keV}) = 0.6405 \times 10^{-24}\ \mathrm{cm}^2/\mathrm{electron} = 0.6405\ \mathrm{b/electron}$

(c) $$\frac{\sigma_{\mathrm{c}}}{\rho} = \frac{N_{\mathrm{A}}}{A}{}_{\mathrm{a}}\sigma_{\mathrm{c}} = \frac{ZN_{\mathrm{A}}}{A}{}_{\mathrm{e}}\sigma_{\mathrm{c}}^{\mathrm{KN}} \approx \frac{N_{\mathrm{A}}}{2}{}_{\mathrm{e}}\sigma_{\mathrm{c}}^{\mathrm{KN}} = 0.193\ \mathrm{cm}^2/\mathrm{g} \tag{7.64}$$

Table 7.3. Compton atomic cross sections ${}_{\mathrm{a}}\sigma_{\mathrm{c}}$ and mass attenuation coefficients σ_{c}/ρ at photon energy of 1 MeV for various absorbers

(1) Element	(2) Symbol	(3) Atomic number Z	(4) Atomic mass A	(5) (*a*) ${}_{\mathrm{a}}\sigma_{\mathrm{c}}$ (b/atom)	(6) (*b*) $Z\,{}_{\mathrm{e}}\sigma_{\mathrm{c}}^{\mathrm{KN}}$ (b/atom)	(7) (*c*) σ_{c}/ρ (cm^2/g)
Hydrogen	H	1	1.008	0.211	0.211	0.1261
Carbon	C	6	12.01	1.27	1.27	0.0636
Aluminum	Aℓ	13	26.98	2.75	2.75	0.0613
Copper	Cu	29	63.54	6.12	6.12	0.0580
Tin	Sn	50	118.69	10.5	10.56	0.0534
Lead	Pb	82	207.2	17.19	17.32	0.0500

(a) Data are from the NIST

(b) ${}_{\mathrm{e}}\sigma_{\mathrm{c}}^{\mathrm{KN}}(h\nu = 1\ \mathrm{MeV}) = 0.2112 \times 10^{-24}\ \mathrm{cm}^2/\mathrm{electron} = 0.2112\ \mathrm{b/electron}$

(c) $$\frac{\sigma_{\mathrm{c}}}{\rho} = \frac{N_{\mathrm{A}}}{A}{}_{\mathrm{a}}\sigma_{\mathrm{c}} = \frac{ZN_{\mathrm{A}}}{A}{}_{\mathrm{e}}\sigma_{\mathrm{c}}^{\mathrm{KN}} \approx \frac{N_{\mathrm{A}}}{2}{}_{\mathrm{e}}\sigma_{\mathrm{c}}^{\mathrm{KN}} = 0.0636\ \mathrm{cm}^2/\mathrm{g} \tag{7.65}$$

electron. As shown in Fig. 7.8, this average fraction increases with increasing energy from a low value of 0.01 at 10 keV, through 0.44 at 1 MeV, to reach a value of 0.8 at 100 MeV.

- For low incident photon energies $(\sigma_{\mathrm{c}}/\rho)_{\mathrm{tr}} \ll \sigma/\rho$.
- For high incident photon energies $(\sigma_{\mathrm{c}}/\rho)_{\mathrm{tr}} \approx \sigma/\rho$.

Figure 7.17 shows the ${}_{\mathrm{a}}\sigma_{\mathrm{c}}$ and ${}_{\mathrm{a}}\sigma_{\mathrm{c}}^{\mathrm{KN}}$ data for lead from Fig. 7.14 and in addition, it also shows the binding energy effect on the Compton atomic energy transfer coefficients of lead by displaying $({}_{\mathrm{a}}\sigma_{\mathrm{c}})_{\mathrm{tr}}$ and $({}_{\mathrm{a}}\sigma_{\mathrm{c}}^{\mathrm{KN}})_{\mathrm{tr}}$ both obtained by multiplying the ${}_{\mathrm{a}}\sigma_{\mathrm{c}}$ and ${}_{\mathrm{a}}\sigma_{\mathrm{c}}^{\mathrm{KN}}$ data, respectively, with the appropriate

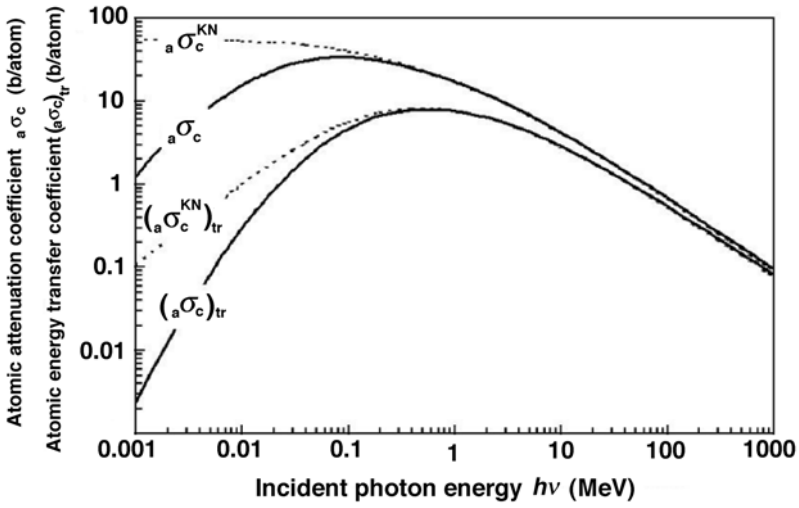

Fig. 7.17. The Compton atomic cross section for lead of Fig. 7.14 and the Compton atomic energy transfer coefficients for lead; *dashed curves* are Klein-Nishina data for free unbound electrons; *solid curves* are data incorporating electronic binding effects. Data are from the NIST

average kinetic energy transferred to the recoil electron given by (7.54) and plotted in Fig. 7.8.

7.4 Rayleigh Scattering

Rayleigh scattering is a photon interaction process in which photons are scattered by bound atomic electrons. The atom is neither excited nor ionized and after the interaction the bound electrons revert to their original state. The atom as a whole absorbs the transferred momentum but its recoil energy is very small and the incident photon scattered with scattering angle θ has essentially the same energy as the original photon. The scattering angles are relatively small because the recoil imparted to the atom must not produce atomic excitation or ionization.

The Rayleigh scattering is named after the physicist *John W. Rayleigh* who in 1900 developed a classical theory for scattering of electromagnetic radiation by atoms. The effect occurs mostly at low photon energies $h\nu$ and for high atomic number Z of the absorber, in the energy region where electron binding effects severely diminish the Compton Klein-Nishina cross sections. As a result of a coherent contribution of all atomic electrons to the Rayleigh (i.e., coherent) atomic cross section, the Rayleigh cross section exceeds the Compton cross section in this energy region.

7.4.1 Differential Atomic Cross Sections for Rayleigh Scattering

The differential Rayleigh atomic cross section $d_a\sigma_R/d\Omega$ per *unit solid angle* is given as follows:

$$\frac{d_a\sigma_R}{d\Omega} = \frac{d_e\sigma_{Th}}{d\Omega}\{F(x,Z)\}^2 = \frac{r_e^2}{2}(1+\cos^2\theta)\{F(x,Z)\}^2 \ , \qquad (7.66)$$

where

$d_e\sigma_{Th}/d\Omega$	is the differential Thomson electronic cross section,
$F(x,Z)$	is the so-called *atomic form factor* with the momentum transfer variable $x = \sin(\theta/2)/\lambda$, as given in (7.59),
λ	is the wavelength of the incident photon,
Z	is the atomic number of the absorber.

The differential Rayleigh atomic cross section $d_a\sigma_R/d\theta$ per *unit scattering angle* θ is

$$\frac{d_a\sigma_R}{d\theta} = \frac{d_a\sigma_R}{d\Omega}\frac{d\Omega}{d\theta} = \frac{r_e^2}{2}(1+\cos^2\theta)\{F(x,Z)\}^2 2\pi\sin\theta =$$
$$= \pi r_e^2 \sin\theta(1+\cos^2\theta)\{F(x,Z)\}^2 \ . \qquad (7.67)$$

7.4.2 Form Factor $F(x,Z)$ for Rayleigh Scattering

Calculations of the atomic form factor $F(x,Z)$ are difficult and, since they are based on atomic wavefunctions, they can be carried out analytically only for the hydrogen atom. For all other atoms the calculations rely on various approximations and atomic models, such as the Thomas-Fermi, Hartree, or Hartree-Fock.

The atomic form factor $F(x,Z)$ is equal to Z for small scattering angles θ and approaches zero for large scattering angles θ. Its values are plotted in Fig. 7.18 against the momentum transfer variable $x = \sin(\theta/2)/\lambda$ for various absorbers ranging in atomic number Z from 1 to 82.

Figure 7.19 is a plot of the differential Rayleigh atomic cross section $d_a\sigma_R/d\theta$ against the scattering angle θ for hydrogen and carbon, respectively, consisting of a product of the differential Thomson electronic cross section $d_e\sigma_{Th}/d\theta$ given in (7.13) and the square of the atomic form factor $F(x,Z)$, as given in (7.67). For comparison the differential Thomson atomic cross section $d_a\sigma_{Th}/d\theta$ is also shown in Fig. 7.19. For hydrogen $d_a\sigma_{Th}/d\theta = d_e\sigma_{Th}/d\theta$, while for carbon $d_a\sigma_{Th}/d\theta = 6\,d_e\sigma_{Th}/d\theta$, with both curves symmetrical about $\theta = \pi/2$.

The $d_a\sigma_R/d\theta$ curves for various energies shown in Fig. 7.19 are not symmetrical about $\theta = \pi/2$ because of the peculiar shape of the atomic form factor $F(x,Z)$ that causes a predominance in forward Rayleigh scattering; the larger the photon energy, the more asymmetrical is the $d_a\sigma_R/d\theta$ curve and the more forward peaked is the Rayleigh scattering. The area under each $d_a\sigma_R/d\theta$ curve gives the total Rayleigh atomic cross-section ${}_a\sigma_R$ for a given photon energy.

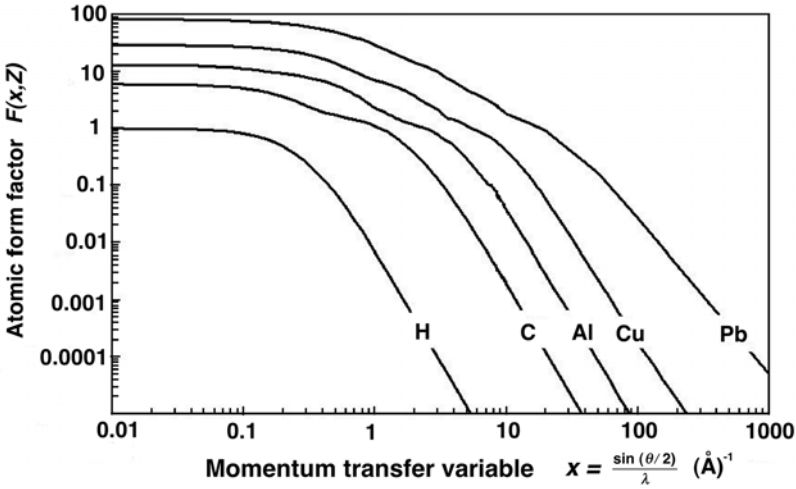

Fig. 7.18. Atomic form factor $F(x, Z)$ plotted against the momentum transfer variable $x = \sin(\theta/2)/\lambda$

7.4.3 Scattering Angles in Rayleigh Scattering

The angular spread of Rayleigh scattering depends on the photon energy $h\nu$ and the atomic number Z of the absorber. It can be estimated from the following relationship:

$$\theta_{\mathrm{R}} \approx 2 \arcsin\left(\frac{0.026 Z^{1/3}}{\varepsilon}\right) , \tag{7.68}$$

where

θ_{R} is the characteristic angle for Rayleigh scattering, representing the opening half angle of a cone that contains 75% of the Rayleigh-scattered photons,
Z is the atomic number of the absorber,
ε is the reduced photon energy, *i.e.*, $\varepsilon = h\nu/(m_{\mathrm{e}}c^2)$.

As suggested by (7.68), the angle θ_{R} increases with increasing Z of the absorber for the same $h\nu$ and decreases with increasing photon energy $h\nu$ for the same Z. Table 7.4 lists the characteristic angle θ_{R} for Rayleigh scattering for photon energies in the range from 100 keV to 10 MeV and various absorbers (carbon, copper and lead), calculated from (7.68).

- At high photon energies ($h\nu > 1$ MeV) Rayleigh scattering is confined to small angles for all absorbers.
- At low energies, particularly for high Z absorbers, the angular distribution of Rayleigh-scattered photons is much broader. In this energy range the Rayleigh atomic cross section ${}_{\mathrm{a}}\sigma_{\mathrm{R}}$ exceeds the Compton atomic cross

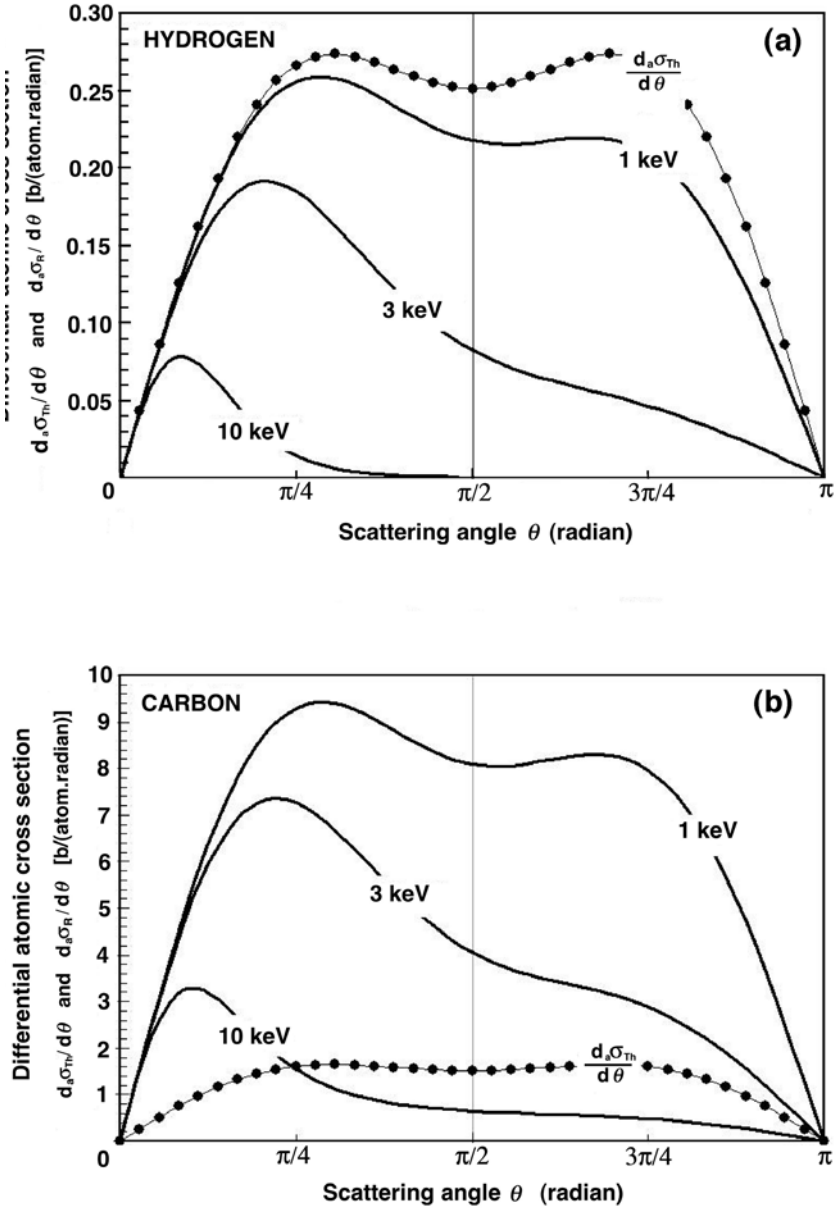

Fig. 7.19. Differential atomic cross section per unit angle for Rayleigh scattering $d_{\mathrm{a}}\sigma_{\mathrm{R}}/d\theta$, given by (7.67), for incident photon energies of 1, 3, and 10 keV for hydrogen in part **a** and carbon in part **b**. The differential Thomson cross-section $d_{\mathrm{a}}\sigma_{\mathrm{Th}}/d\theta$ for the two absorbing materials is shown by the *dotted curves* (data points) for comparison

Table 7.4. The characteristic angle θ_R for Rayleigh scattering for various absorber materials and photon energies in the range from 100 keV to 10 MeV

Absorber	*Symbol*	Z	*Photon energy* (MeV)				
			0.1	0.5	1	5	10
Carbon	C	6	28°	6°	3°	0.6°	0.3°
Copper	Cu	29	48°	9°	5°	0.9°	0.5°
Lead	Pb	82	70°	13°	7°	1.3°	0.7°

section ${}_a\sigma_c$ but is nonetheless very small in comparison with the photoelectric atomic cross section ${}_a\tau$. The atomic Rayleigh cross section ${}_a\sigma_R$ is therefore often ignored in gamma ray transport as well as in shielding barrier calculations.

- Rayleigh scattering plays no role in radiation dosimetry, since no energy is transferred to charged particles through Rayleigh scattering.

7.4.4 Atomic Cross Sections for Rayleigh Scattering ${}_a\sigma_R$

The Rayleigh atomic cross section ${}_a\sigma_R$ can be obtained by determining the area under the appropriate $d_a\sigma_R/d\theta$ curve plotted against θ, as shown in Fig. 7.19, or it can be calculated by integrating the differential cross section $d_a\sigma_R/d\theta$ of (7.67) over all possible scattering angles θ from 0 to π, i.e.,

$$ {}_a\sigma_R = \pi r_e^2 \int_0^\pi \sin\theta(1+\cos^2\theta)\,[F(x,Z)]^2\,d\theta \; . \tag{7.69} $$

Rayleigh atomic cross section ${}_a\sigma_R$ is shown with solid curves against incident photon energy $h\nu$ in the range from 1 keV to 1000 MeV in Fig. 7.20. For comparison, the figure also shows the Compton atomic cross-section ${}_a\sigma_c$ of Fig. 7.14 in the same energy range. The following conclusions may be reached from Fig. 7.20:

- At low photon energies ${}_a\sigma_R$ exceeds ${}_a\sigma_c$; the higher is the atomic number of the absorber, the larger is the difference. However, at low photon energies both ${}_a\sigma_R$ and ${}_a\sigma_c$ are negligible in comparison with the atomic cross section for the photoelectric effect ${}_a\tau$, so both are usually ignored in calculations of the total atomic cross section ${}_a\mu$ for a given absorber at very low photon energies.
- The photon energy $h\nu_{eq}$ at which the atomic cross sections for Rayleigh and Compton scattering are equal, i.e., ${}_a\sigma_R = {}_a\sigma_c$, is proportional to the atomic number Z of the absorber. From Fig. 7.20 we also note that for photon energies exceeding $h\nu_{eq}$ the Rayleigh atomic cross section ${}_a\sigma_R$ is inversely proportional to $(h\nu)^2$; i.e.,

$$ {}_a\sigma_R \propto (1/h\nu)^2 \; . \tag{7.70} $$

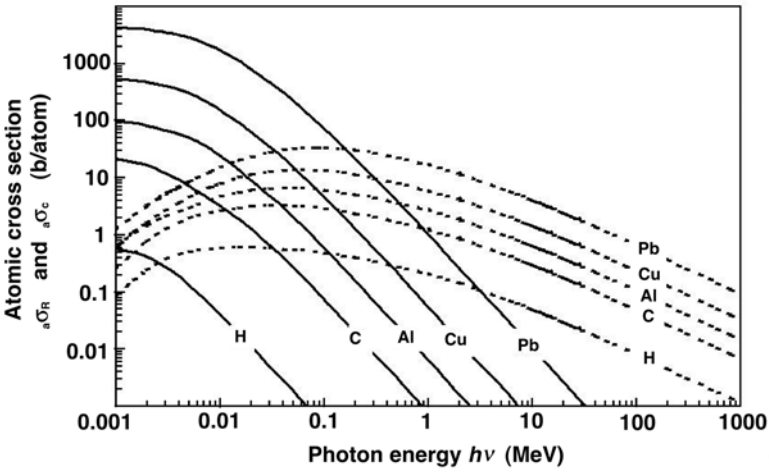

Fig. 7.20. Atomic cross sections for Rayleigh scattering $_a\sigma_R$ and Compton scattering $_a\sigma_c$ against incident photon energy $h\nu$ in the range from 1 keV to 1000 MeV for various absorbers ranging from hydrogen to lead. $_a\sigma_R$ is shown by *solid curves;* $_a\sigma_c$ is shown by *dashed curves* for comparison. For very low photon energies the $_a\sigma_R$ *curves* exhibit a plateau with a value of $_e\sigma_{Th}\, Z^2$ where $_e\sigma_{Th}$ is the energy independent Thomson cross-section and Z is the atomic number of the absorber (note that $F(x, Z) \to Z$ for low $h\nu$, i.e., large λ). Data are from the NIST

- In general, as evident from Fig. 7.20, we may also state that $_a\sigma_R$ is proportional to Z^2, where Z is the atomic number of the absorber.

7.4.5 Mass Attenuation Coefficient for Rayleigh Scattering

The Rayleigh mass attenuation coefficient σ_R/ρ is determined through the standard relationship

$$\frac{\sigma_R}{\rho} = \frac{N_A}{A} {}_a\sigma_R \, . \tag{7.71}$$

- Since $_a\sigma_R \propto Z^2/(h\nu)^2$ and $A \approx 2Z$, we conclude that $\sigma_R/\rho \propto Z/(h\nu)^2$, where Z and A are the atomic number and atomic mass, respectively, of the absorber.
- Since no energy is transferred to charged particles in Rayleigh scattering, the energy transfer coefficient for Rayleigh scattering is zero.

7.5 Photoelectric Effect

An interaction between a photon and a tightly bound orbital electron of an absorber atom is called *photoelectric effect* (photoeffect). In the interaction

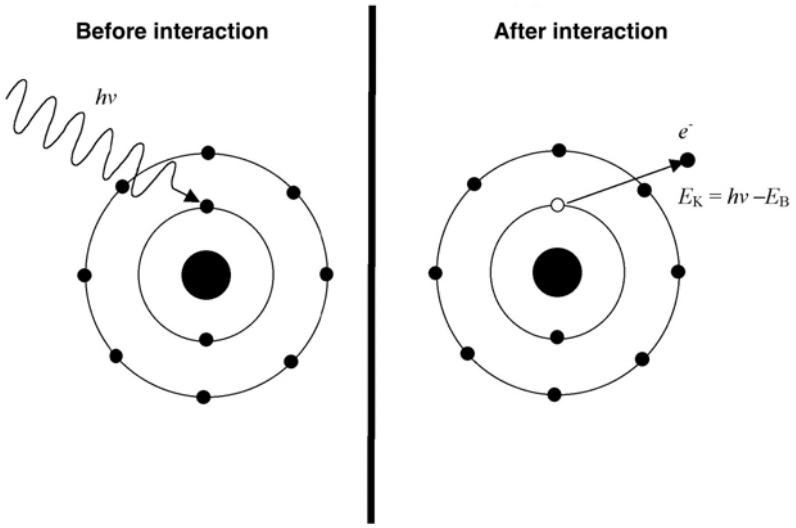

Fig. 7.21. Schematic diagram of the photoelectric effect. A photon with energy $h\nu$ interacts with a K-shell electron. The photon is absorbed completely and the K-shell electron is ejected as photoelectron from the atom with a kinetic energy $E_K = h\nu - E_B(K)$, where $E_B(K)$ is the binding energy of the K-shell electron. The vacancy in the K shell will subsequently be filled with a higher orbit electron and the energy of the electronic transition will be emitted either in the form of a characteristic (fluorescent) photon or in the form of an Auger electron

the photon is absorbed completely and the orbital electron is ejected with kinetic energy E_K. The ejected orbital electron is referred to as a *photoelectron*. The photoelectric interaction between a photon of energy $h\nu$ and a K-shell atomic electron is shown schematically in Fig. 7.21.

Conservation of energy and momentum considerations show that the photoelectric effect can only occur on a tightly bound electron rather than on a "free electron", so that the atom as a whole picks up the difference between the momentum of the photon ($p_\nu = h\nu/c$) and that of the photoelectron ($p_e = \sqrt{E^2 - E_o^2}/c$), where E and E_o are the total energy and rest energy, respectively, of the photoelectron.

Figure 7.22 shows that energy and momentum cannot be conserved simultaneously in a photon-free electron interaction. In part (a) the total energy is conserved but, as a result of total energy conservation, the total momentum is not conserved. In part (b) the total momentum is conserved but, as a result of total momentum conservation, the total energy is not conserved. Thus, an extra interaction partner must absorb the extra momentum and this is achieved when the electron is tightly bound to the nucleus, so that the whole atom picks up the extra momentum

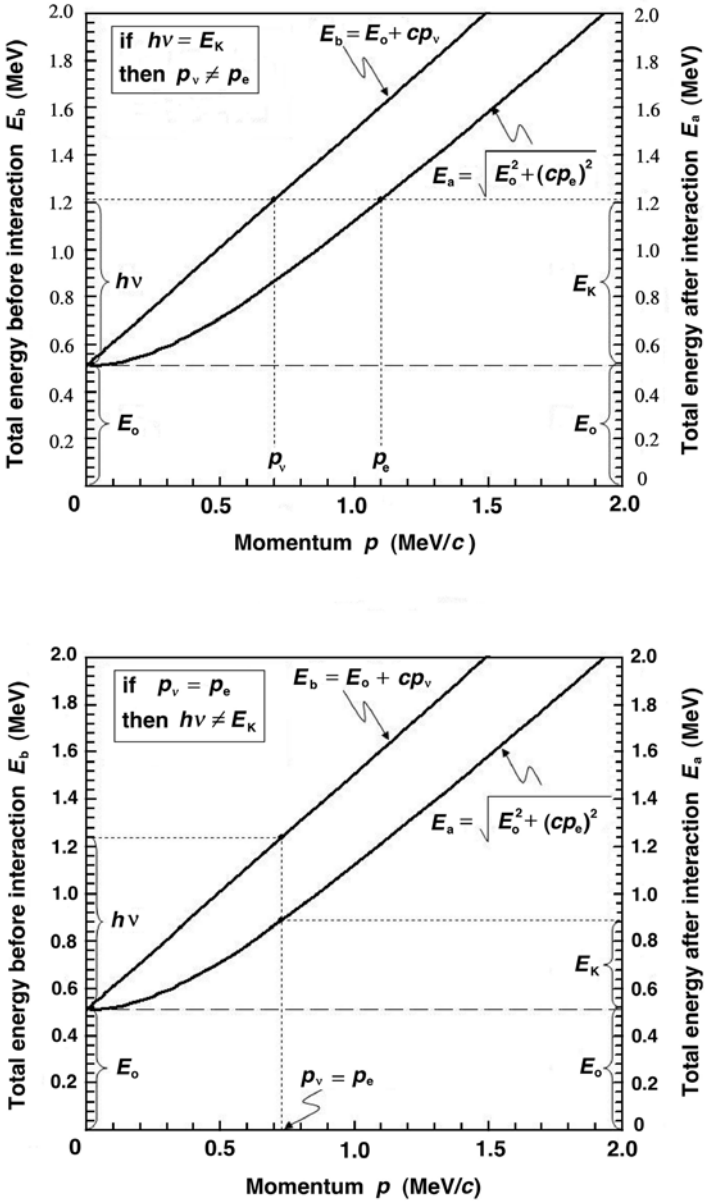

Fig. 7.22. Energy and momentum conservation considerations in photoelectric effect occurring on a free electron. In part **a** the total energy is conserved ($E_\mathrm{b} = E_\mathrm{a}$) but not the momentum; in part **b** the total momentum is conserved ($p_\nu = p_\mathrm{e}$) but not the total energy

- Because of the relatively large nuclear mass, the atomic recoil energy is exceedingly small and may be neglected. The kinetic energy E_{K} of the ejected photoelectron then equals the incident photon energy $h\nu$ less the binding energy E_{B} of the orbital electron, i.e.,

$$E_{\mathrm{K}} = h\nu - E_{\mathrm{B}} \ . \tag{7.72}$$

- When the photon energy $h\nu$ exceeds the K-shell binding energy $E_{\mathrm{B}}(\mathrm{K})$ of the absorber, i.e., $h\nu > E_{\mathrm{B}}(\mathrm{K})$, about 80% of all photoelectric absorptions occur with the K-shell electrons of the absorber.
- The energy uptake by the photoelectron may be insufficient to bring about its ejection from the atom (ionization), but may be sufficient to raise it to a higher orbit (excitation).
- The vacancy that results from the emission of the photoelectron will be filled by a higher shell electron and the transition energy will be emitted either as a characteristic (fluorescent) photon or as an Auger electron, the probability for each governed by the fluorescent yield (see Sect. 3.1).

7.5.1 Atomic Cross Section for Photoelectric Effect

The atomic cross section for the photoelectric effect ${}_{\mathrm{a}}\tau$ as a function of the incident photon energy $h\nu$ exhibits a characteristic sawtooth structure in which the sharp discontinuities (absorption edges) arise whenever the photon energy coincides with the binding energy of a particular electron shell. Since all shells except for the K shell exhibit a fine structure, the ${}_{\mathrm{a}}\tau$ curve plotted against the incident photon energy $h\nu$ also exhibits a fine structure in the L, M, ... etc. absorption edges.

Three distinct energy regions characterize the atomic cross section ${}_{\mathrm{a}}\tau$: (1) *Region in the immediate vicinity of absorption edges*; (2) *Region at some distance from the absorption edge*; and (3) *Region in the relativistic region far from the K absorption edge.*

1. Theoretical predictions for ${}_{\mathrm{a}}\tau$ in region (1) are difficult and uncertain.
2. For region (2) the atomic attenuation coefficient (cross section) for K-shell electrons ${}_{\mathrm{a}}\tau_{\mathrm{K}}$ is given as follows:

$${}_{\mathrm{a}}\tau_{\mathrm{K}} = \alpha^4 {}_{\mathrm{e}}\sigma_{\mathrm{Th}} Z^n \sqrt{\frac{32}{\varepsilon^7}} \ , \tag{7.73}$$

where

ε	is the usual normalized photon energy, *i.e.*, $\varepsilon = h\nu/(m_{\mathrm{e}}c^2)$,
α	is the fine structure constant (1/137),
Z	is the atomic number of the absorber,
${}_{\mathrm{e}}\sigma_{\mathrm{Th}}$	is the total Thomson electronic cross section given in (7.14),
n	is the power for the Z dependence of ${}_{\mathrm{a}}\tau_{\mathrm{K}}$ ranging from $n = 4$ at relatively low photon energies to $n = 4.6$ at high photon energies,

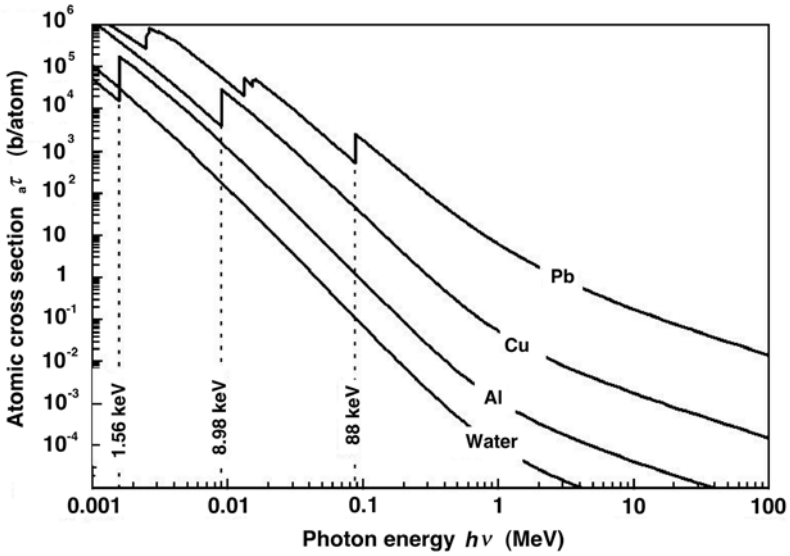

Fig. 7.23. Photoelectric atomic cross section ${}_a\tau$ against photon energy $h\nu$ for various absorbers. Energies of K-absorption edges are also indicated. Data are from the NIST

3. In the relativistic region ($\varepsilon \gg 1$), ${}_a\tau_K$ is given as follows:

$$ {}_a\tau_K = \frac{1.5}{\varepsilon}\alpha^4 Z^5 {}_e\sigma_{Th} \, . \tag{7.74}$$

The following conclusions may be reached with regard to energy and atomic number dependence of ${}_a\tau_K$:

- The energy dependence of ${}_a\tau_K$ is assumed to go as $(1/h\nu)^3$ at low photon energies $h\nu$ gradually transforming into $1/h\nu$ at high $h\nu$.
- The energy dependences for regions (2) and (3) can be identified from Fig. 7.23 that displays the atomic cross section for the photoeffect against incident photon energy for various absorbers ranging from water to lead. Absorption edges are clearly shown in Fig. 7.23, the K absorption edges are identified for aluminum (1.56 eV), copper (8.98 eV) and lead (88 keV). The fine structures of the L and M absorption edges are also shown.
- The atomic number Z dependence (${}_a\tau \propto Z^n$) of ${}_a\tau$, where n ranges from 4 to 5, is also evident from Fig. 7.23.

7.5.2 Angular Distribution of Photoelectrons

The angular distribution of photoelectrons depends on the incident photon energy $h\nu$. At low $h\nu$ photoelectrons tend to be emitted at 90° to the incident photon direction. As $h\nu$ increases, however, the photoelectron emis-

sion peak moves progressively to more forward photoelectron emission angles, somewhat akin to the emission of bremsstrahlung photons in electron bremsstrahlung interaction.

7.5.3 Energy Transfer to Photoelectrons in Photoelectric Effect

The photoelectron attains a kinetic energy of $E_K = h\nu - E_B$ as it leaves the atom but also leaves behind a vacancy in a shell that is most often a K-shell for $h\nu > E_B(K)$, where $E_B(K)$ is the binding energy of the K-shell electron. The vacancy is filled with an upper shell electron and the transition energy is emitted either in the form of a characteristic (fluorescent) photon or in the form of an Auger electron depending on the fluorescent yield ω for the particular interaction.

Because of the presence of Auger electrons, the mean energy transfer to electrons in a photoelectric effect $\overline{E}^{\tau}_{tr}$ for $h\nu > E_B(K)$ is in general between $h\nu - E_B(K)$ and $h\nu$.

- $\overline{E}^{\tau}_{tr} = h\nu - E_B(K)$ when $\omega_K \approx 1$, i.e., no Auger electrons are produced as a result of the photoelectric effect and the emission of a photoelectron.
- $\overline{E}^{\tau}_{tr} = h\nu$ when $\omega_K = 0$, i.e., no characteristic photons are produced as a result of the photoelectric effect and emission of a photoelectron.
- $h\nu - E_B(K) < \overline{E}^{\tau}_{tr} < h\nu$ is the general case in which a combination of characteristic photons and Auger electrons is released.

The general relationship for $\overline{E}^{\tau}_{tr}$ is given as follows:

$$\overline{E}^{\tau}_{tr} = h\nu - P_K\,\omega_K\,\overline{h\nu}_K\ , \tag{7.75}$$

where

P_K is the fraction of all photoelectric interactions that occur in the K-shell for photons $h\nu > E_B(K)$. Typical values of P_K are of the order of 0.8 or larger, as shown in Fig. 3.3;

ω_K is the fluorescent yield for the K-shell, as discussed in Sect. 3.1.2 and displayed in Fig. 3.3;

$\overline{h\nu}_K$ is a K-shell weighted mean value of all possible fluorescent transition energies, ranging from the L $\rightarrow$ K transition through the M $\rightarrow$ K transition, etc. to a limit $E_B(K)$. Since the K_α transitions are the most probable fluorescent transitions for the K shell, the value of $\overline{h\nu}_K$ is weighted toward the energy of the K_α transition and typically amounts to about 86% of the $E_B(K)$ value for a given Z of the absorber.

Figure 7.24 provides a plot of the K-shell binding energy $E_B(K)$, the K-shell weighted mean fluorescence energy $\overline{h\nu}_K \approx 0.86 E_B(K)$, and the average energy emitted in the form of K fluorescent photons $P_K\omega_K\overline{h\nu}_K$ against the atomic number Z of the absorber. The range of the K-shell binding energies in nature is from 13.6 eV for hydrogen to about 150 keV for the highest atomic number elements. $E_B(K)$ can be estimated from the Hartree relationship given in (2.83).

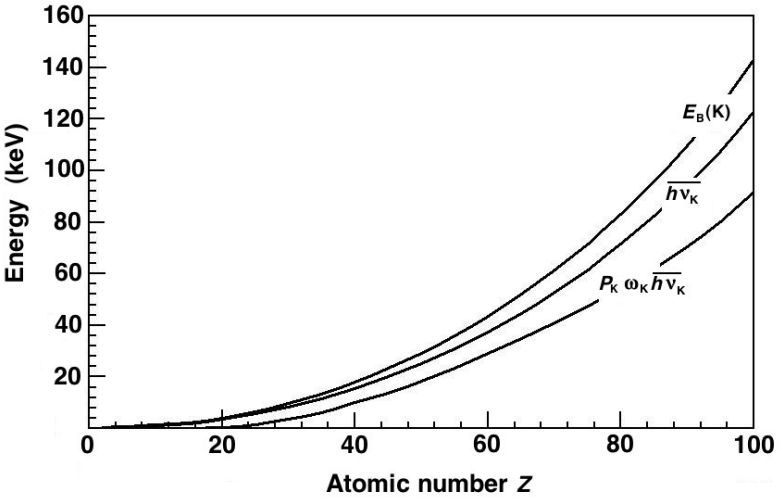

Fig. 7.24. The electron binding energy in the K shell, $E_{\mathrm{B}}(K)$; the weighted mean characteristic x-ray energy for the K shell, $\overline{h\nu}_{\mathrm{K}}$; and the mean energy emitted in the form of K-shell characteristic photons, $P_{\mathrm{K}}\omega_{\mathrm{K}}\overline{h\nu}_{\mathrm{K}}$ against the atomic number Z of the absorber

7.5.4 Mass Attenuation Coefficient for the Photoelectric Effect

The mass attenuation coefficient for the photoelectric effect τ/ρ is calculated from the atomic cross section ${}_{\mathrm{a}}\tau$ with the standard relationship

$$\frac{\tau}{\rho} = \frac{N_{\mathrm{A}}}{A}{}_{\mathrm{a}}\tau \,, \tag{7.76}$$

where A and ρ are the atomic mass and density, respectively, of the absorber.

7.5.5 Mass Energy Transfer Coefficient for the Photoelectric Effect

The mass energy transfer coefficient for the photoelectric effect $(\tau_{\mathrm{K}}/\rho)_{\mathrm{tr}}$ for incident photon energy $h\nu$ that exceeds the K-shell binding energy $E_{\mathrm{B}}(\mathrm{K})$, i.e., $h\nu \geq E_{\mathrm{B}}(\mathrm{K})$ is calculated from the relationship

$$\begin{aligned}\left(\frac{\tau_{\mathrm{K}}}{\rho}\right)_{\mathrm{tr}} &= \frac{\tau_{\mathrm{K}}}{\rho}\frac{\overline{E}^{\tau}_{\mathrm{tr}}}{h\nu} = \frac{\tau_{\mathrm{K}}}{\rho}\frac{h\nu - P_{\mathrm{K}}\,\omega_{\mathrm{K}}\,\overline{h\nu}_{\mathrm{K}}}{h\nu} \\ &= \frac{\tau_{\mathrm{K}}}{\rho}\left(1 - \frac{P_{\mathrm{K}}\,\omega_{\mathrm{K}}\,\overline{h\nu}_{\mathrm{K}}}{h\nu}\right) = \frac{\tau_{\mathrm{K}}}{\rho}\bar{f}^{\tau} \,,\end{aligned} \tag{7.77}$$

where $\bar{f}^{\tau} = 1 - P_{\mathrm{K}}\,\omega_{\mathrm{K}}\,\overline{h\nu}_{\mathrm{K}}/(h\nu)$ is the mean fraction of energy $h\nu$ transferred to electrons.

Table 7.5. Parameters for photoelectric effect in various absorbers for photon energies $h\nu$ exceeding the K-shell binding energy $E_B(K)$

Element	Z	ω_K	P_K	$E_B(K)$ (keV)	$\overline{h\nu}_K$ (keV)	$P_K\omega_K\overline{h\nu}_K$ (keV)	$\bar{f}^\tau(E_B(K))$
C	6	0	0.95	0.28	0.24	0	1.0
Cu	29	0.50	0.87	9.0	7.7	3.35	0.62
Sn	50	0.85	0.85	29.2	25.0	18.1	0.38
Pb	82	0.97	0.78	88.0	75.7	64.6	0.27

Table 7.5 gives the fluorescent yield ω_K, the fraction P_K, the K-shell binding energy $E_B(K)$, the mean K-shell characteristic radiation energy $\overline{h\nu}_K$, the product $P_K\,\omega_K\,\overline{h\nu}_K$; and $\bar{f}^\tau(E_B(K))$, the mean fraction of the photon energy transferred to electrons in photoelectric effect for photons of energy $h\nu = E_B(K)$.

The fraction $\bar{f}^\tau$, plotted against photon energy $h\nu$ for various elements in Fig. 7.25, starts at its lowest value at $h\nu = E_B(K)$ and then gradually approaches 1 with increasing photon energy. For $f^\tau = 1$, the incident photon energy $h\nu$ is transferred to electrons in full: the photoelectron receives a kinetic energy $h\nu - E_B(K)$ and the available energy $E_B(K)$ either goes to Auger electrons for low Z absorbers or is essentially negligible in comparison to $h\nu$ for all absorbers at very high photon energies $h\nu$.

The formalism that was used above for K-shell electrons when $h\nu > E_B(K)$ will apply for L-shell electrons when $E_B(L) < h\nu < E_B(K)$, etc. The tightest bound electron available for a photoelectric interaction is by far

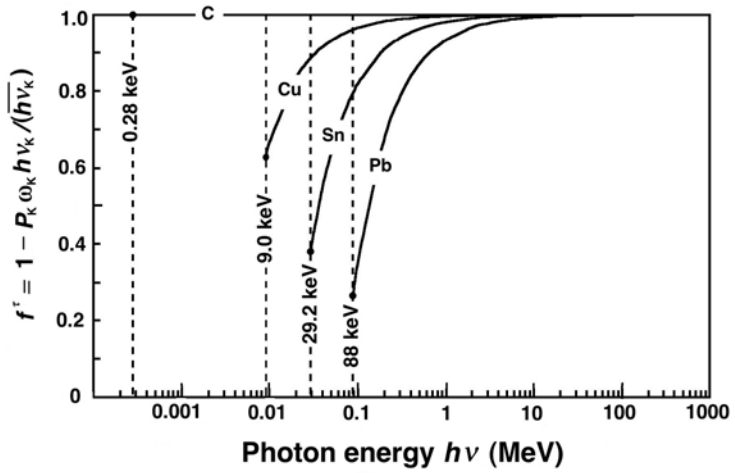

Fig. 7.25. The photoelectric fraction $\bar{f}_K^\tau$, the mean fraction of photon energy $h\nu$ transferred to electrons in a K-shell photoelectric effect interaction in carbon, copper, tin, and lead, against photon energy $h\nu$

the most likely to have a photoelectric interaction with the photon; thus only electrons most likely to have an interaction are considered in calculation of the photoelectric coefficients.

7.6 Pair Production

When the photon energy $h\nu$ exceeds $2m_e c^2 = 1.02$ MeV, the production of an electron-positron pair in conjunction with a complete absorption of the photon becomes energetically possible. For the effect to occur, three quantities must be conserved: *energy*, *charge* and *momentum*.

For $h\nu > 2m_e c^2$, energy and charge can be conserved even if pair production occurs in free space. However, to conserve the linear momentum the effect cannot occur in free space; it can only occur in the Coulomb field of a collision partner (either atomic nucleus or orbital electron) that can take up a suitable fraction of the momentum carried by the photon.

The pair production and triplet production interactions are shown schematically in Fig. 7.26.

7.6.1 Conservation of Energy, Momentum and Charge for Pair Production in Free Space

Before the pair production interaction there is photon energy $E_\nu = h\nu > 2m_e c^2$ and photon momentum $p_\nu = h\nu/c$. In the interaction an electron-positron pair is produced with a total energy $E_{\text{pair}} = 2\gamma m_e c^2$ and total momentum $p_{\text{pair}} = 2\gamma m_e \upsilon$.

- *Conservation of Energy:*
  $E_\nu = h\nu \equiv E_{\text{pair}} = 2\gamma m_e c^2$
- *Conservation of Momentum:*
  $$p_\nu = \frac{h\nu}{c} \equiv p_{\text{pair}} = 2\gamma m_e \upsilon \rightarrow 2\gamma m_e c^2 \frac{\upsilon}{c^2} = E_\nu \frac{\upsilon}{c^2} = p_\nu \frac{\upsilon}{c}$$
  Since the particle velocity υ is always smaller than c, it follows that p_ν, the momentum before the pair production interaction, is always larger than p_{pair}, the total momentum after the pair production interaction. Thus, the photon possesses momentum excess that is not absorbed by the electron-positron pair. This momentum excess must be absorbed by a collision partner, be it the atomic nucleus or an orbital electron of an absorber. Therefore, pair production interaction cannot occur in free space (vacuum) where no collision partner is available.
- When the extra momentum is absorbed by the atomic nucleus of the absorber, the recoil energy, as a result of the relatively large nuclear mass, is exceedingly small and the effect is described as the standard pair production (usually referred to as *pair production*). Two particles (electron and positron) leave the interaction site.

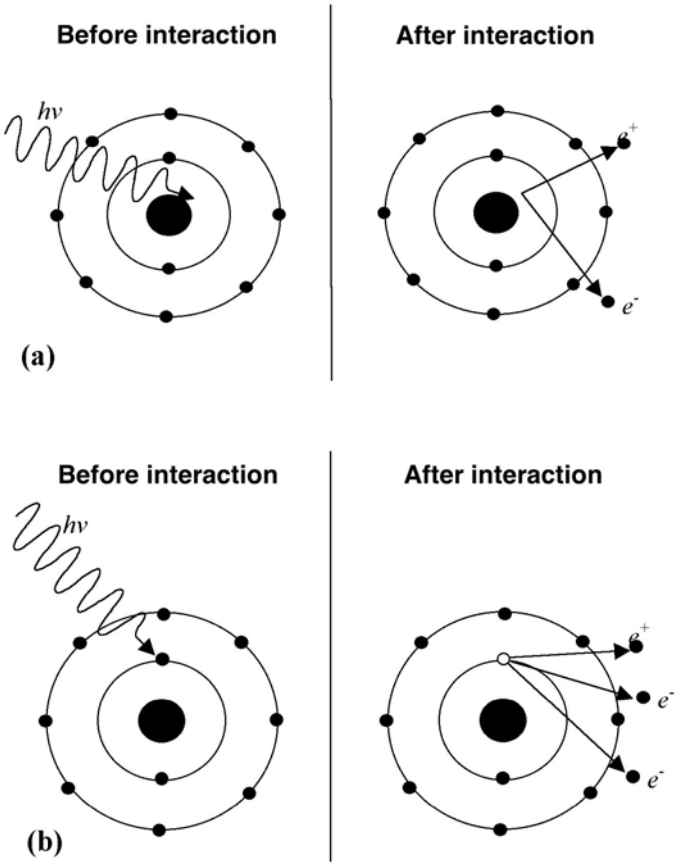

Fig. 7.26. Schematic representation of pair production (**a**) in the Coulomb field of a nucleus and (**b**) triplet production (in the Coulomb field of an orbital electron)

- When an orbital electron of the absorber picks up the extra momentum, the recoil energy of the orbital electron may be significant and the effect is described as the pair production in the Coulomb field of electron, i.e., *triplet production*. Three particles (two electrons and a positron) leave the interaction site.
- *Conservation of Charge:*
  The total charge before the interaction is zero and the total charge after the interaction is also zero.

7.6.2 Threshold Energy for Pair Production and Triplet Production

In contrast to other common photon interactions, such as photoelectric effect, Rayleigh scattering and Compton scattering, pair production exhibits a

threshold energy below which the effect cannot happen. The threshold energy is derived following the procedure described in detail in Section 4.2.3 that is based on the invariant: $E^2 - p^2c^2 = inv$ where E and p are the total energy and total momentum, respectively, before and after the interaction.

For *pair production* in the field of the nucleus the conditions for before the interaction (in the laboratory system) and for after the interaction (in the center-of-mass system) are written as follows:

- *Total energy before:* $(h\nu)^{\rm pp}_{\rm thr} + m_{\rm A}c^2$, where $m_{\rm A}c^2$ is the rest mass of the nucleus, the interaction partner.
- *Total momentum before:* $(h\nu)^{\rm pp}_{\rm thr}/c$.
- *Total energy after:* $(m_{\rm A}c^2 + 2m_{\rm e}c^2)$.
- *Total momentum after:* 0

The invariant for before and after the pair production event is

$$\left\{(h\nu)^{\rm pp}_{\rm thr} + m_{\rm A}c^2\right\}^2 - \left(\frac{(h\nu)^{\rm pp}_{\rm thr}}{\rm c}\right)^2 c^2 = (m_{\rm A}c^2 + 2m_{\rm e}c^2)^2 - 0\ , \tag{7.78}$$

resulting in the following expression for pair production threshold $E^{\rm pp}_{\rm thr} = (h\nu)^{\rm pp}_{\rm thr}$

$$\begin{aligned} E^{\rm pp}_{\gamma{\rm thr}} &= (h\nu)^{\rm pp}_{\rm thr} = 2m_{\rm e}c^2\left(1 + \frac{m_{\rm e}c^2}{m_{\rm A}c^2}\right) \\ &= (1.022\ {\rm MeV}) \times \left(1 + \frac{m_{\rm e}c^2}{m_{\rm A}c^2}\right)\ . \end{aligned} \tag{7.79}$$

In the first approximation we can use $(h\nu)^{\rm pp}_{\rm thr} \approx 2m_{\rm e}c^2$, since the ratio $m_{\rm e}c^2/m_{\rm A}c^2$ is very small, indicating that the recoil energy of the nucleus is exceedingly small.

For *triplet production* the conditions for before the interaction (in the laboratory system) and for after the interaction (in the center-of-mass system) are written as follows:

- *Total energy before:* $(h\nu)^{\rm tp}_{\rm thr} + m_{\rm e}c^2$, where $m_{\rm e}c^2$ is the rest mass of the orbital electron, the interaction partner.
- *Total momentum before:* $(h\nu)^{\rm tp}_{\rm thr}/c$.
- *Total energy after:* $3m_{\rm e}c^2$, accounting for rest energies of the orbital electron as well as for the electron-positron pair.
- *Total momentum after:* 0.

The invariant for before and after the triplet production event is

$$\left\{(h\nu)^{\rm tp}_{\rm thr} + m_{\rm e}c^2\right\}^2 - [(h\nu)^{\rm tp}_{\rm thr}]^2 = (3m_{\rm e}c^2)^2 - 0\ , \tag{7.80}$$

resulting in the following expression for the triplet production threshold:

$$E^{\rm tp}_{\gamma_{\rm thr}} = (h\nu)^{\rm tp}_{\rm thr} = 4m_{\rm e}c^2 = 2.044\ {\rm MeV}\ . \tag{7.81}$$

7.6.3 Energy Transfer to Charged Particles in Pair Production

The total kinetic energy transferred to charged particles (electron and positron) in pair production is

$$(E_{\mathrm{K}}^{\kappa})_{\mathrm{tr}} = h\nu - 2m_{\mathrm{e}}c^2 \,, \tag{7.82}$$

ignoring the minute recoil energy of the nucleus.

Generally, the electron and the positron do not receive equal kinetic energies but their average is given as

$$\overline{E}_{\mathrm{K}}^{\mathrm{pp}} = \frac{h\nu - 2m_{\mathrm{e}}c^2}{2} \,. \tag{7.83}$$

The exact energy distribution of electrons and positrons in pair production is a complex function of photon energy $h\nu$ and atomic number Z of the absorber. In the first approximation we assume that all distributions of the available energy $(h\nu - 2m_{\mathrm{e}}c^2)$ are equally probable, except for the extreme case where one particle obtains all the available energy and the other particle obtains none.

7.6.4 Angular Distribution of Charged Particles

The angular distribution of the electrons and positrons produced in pair production is peaked increasingly in the forward direction with increasing incident photon energy $h\nu$. For very high energies ($\varepsilon = h\nu/(m_{\mathrm{e}}c^2) \gg 1$) the mean angle $\bar{\theta}$ of positron and electron emission is of the order of $\theta \approx 1/\varepsilon$.

7.6.5 Nuclear Screening

For very high photon energies ($h\nu > 20$ MeV) significant contribution to the pair production cross section may come from interaction points that lie outside the orbit of K shell electrons. The Coulomb field in which the pair production occurs is thus reduced because of the screening of the nucleus by the two K-shell electrons, thereby requiring a screening correction in theoretical calculations.

7.6.6 Atomic Cross Sections for Pair Production

The theoretical derivations of atomic cross sections for pair production ${}_{\mathrm{a}}\kappa$ are very complicated, some based on Born approximation, others not, some accounting for nuclear screening and others not.

In general the atomic cross sections for pair production in the field of a nucleus or orbital electron appear as follows:

$${}_{\mathrm{a}}\kappa = \alpha r_{\mathrm{e}}^2 Z^2 P(\varepsilon, Z) \,, \tag{7.84}$$

Table 7.6. Characteristics of atomic cross section for pair production in the field of the nucleus or in the field of an orbital electron

Field	*Energy range*	$P(\varepsilon, Z)$	*Comment*	
nucleus	$1 \ll \varepsilon \ll 1/(\alpha Z^{1/3})$	$\frac{28}{9}\ln 2\varepsilon - \frac{218}{27}$	*no screening*	(7.85)
nucleus	$\varepsilon \gg 1/(\alpha Z^{1/3})$	$\frac{28}{9}\ln\frac{183}{Z^{1/3}} - \frac{2}{27}$	*complete screening*	(7.86)
nucleus	outside the limits above but $\varepsilon > 4$	$\frac{28}{9}\ln 2\varepsilon - \frac{218}{27} - 1.027$	*no screening*	(7.87)
electron	$\varepsilon > 4$	$\frac{1}{Z}\left(\frac{28}{9}\ln 2\varepsilon - 11.3\right)$	*no screening*	(7.88)

where

α	is the fine structure constant ($\alpha = 1/137$),
r_e	is the classical electron radius [$r_\mathrm{e} = e^2/(4\pi\varepsilon_\mathrm{o} m_\mathrm{e} c^2) = 2.818$ fm],
Z	is the atomic number of the absorber,
$P(\varepsilon, Z)$	is a complicated function of the photon energy $h\nu$ and atomic number Z of the absorber, as given in Table 7.6.

It is evident from (7.83) through (7.88) and from Table 7.6, that the atomic cross section for pair production ${}_\mathrm{a}\kappa_\mathrm{pp}$ is proportional to Z^2, while the atomic cross section for triplet production ${}_\mathrm{a}\kappa_\mathrm{tp}$ is linearly proportional to Z. In general, the relationship between ${}_\mathrm{a}\kappa_\mathrm{pp}$ and ${}_\mathrm{a}\kappa_\mathrm{tp}$ is given as follows:

$$ {}_\mathrm{a}\kappa_\mathrm{pp}/{}_\mathrm{a}\kappa_\mathrm{tp} = \eta Z \ , \tag{7.89} $$

where η is a parameter, depending only on $h\nu$, and, according to *Robley Evans*, equal to 2.6 at $h\nu = 6.5$ MeV, 1.2 at $h\nu = 100$ MeV, and approaching unity as $h\nu \to \infty$. This indicates that the atomic cross section for triplet production ${}_\mathrm{a}\kappa_\mathrm{tp}$ is at best about 30% of the pair production cross section ${}_\mathrm{a}\kappa_\mathrm{pp}$ for $Z = 1$ and less than 1% for high Z absorbers.

Since the atomic cross section for pair production in the field of the atomic nucleus exceeds significantly the atomic cross section for triplet production, as shown in Fig. 7.27 for two absorbing materials: carbon with $Z = 6$ and lead with $Z = 82$, both the pair production and the triplet production contributions are usually given under the header of general pair production as follows:

$$ {}_\mathrm{a}\kappa = {}_\mathrm{a}\kappa_\mathrm{pp} + {}_\mathrm{a}\kappa_\mathrm{tp} = {}_\mathrm{a}\kappa_\mathrm{pp}\left\{1 + 1/(\eta Z)\right\} \ , \tag{7.90} $$

where the electronic effects (triplet production) are accounted for with the correction term $1/(\eta Z)$. This term is equal to zero for $h\nu < 4m_\mathrm{e}c^2$, where $4m_\mathrm{e}c^2$ is the threshold energy for triplet production.

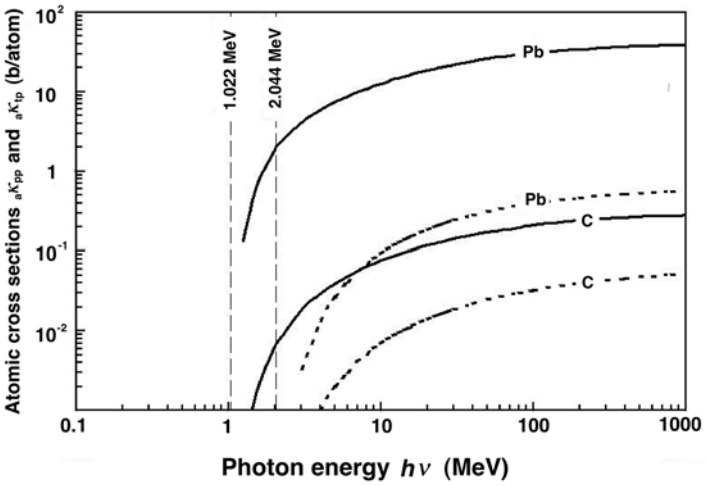

Fig. 7.27. Atomic cross sections for pair production ${}_a\kappa_{pp}$ (*solid curves*) and for triplet production ${}_a\kappa_{tp}$ (*dotted curves*) against incident photon energy $h\nu$ for carbon and lead. Data are from the NIST

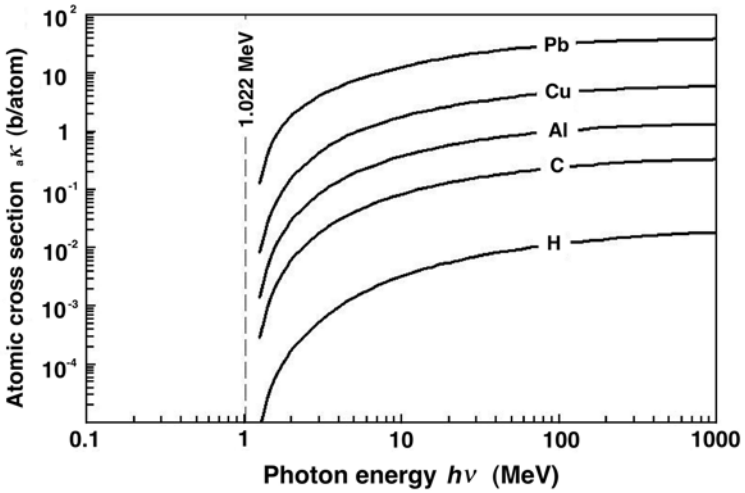

Fig. 7.28. Atomic cross section for pair production (including triplet production) ${}_a\kappa$ against incident photon energy $h\nu$ for various absorbers in the range from hydrogen to lead. Data are from the NIST

The atomic cross sections for general pair production ${}_a\kappa$ are plotted in Fig. 7.28 for various absorbers ranging from hydrogen to lead. The increase of ${}_a\kappa$ with incident photon energy $h\nu$ and with atomic number Z of the absorber is evident.

7.6.7 Mass Attenuation Coefficient for Pair Production

The mass attenuation coefficient for pair production κ/ρ is calculated from the atomic cross section ${}_{\mathrm{a}}\kappa$ with the standard relationship

$$\frac{\kappa}{\rho} = \frac{N_{\mathrm{A}}}{A}\,{}_{\mathrm{a}}\kappa\,, \tag{7.91}$$

where A and ρ are the atomic mass and density, respectively, of the absorber.

7.6.8 Mass Energy Transfer Coefficient for Pair Production

The mass energy transfer coefficient for pair production $(\kappa/\rho)_{\mathrm{tr}}$ for incident photon energy $h\nu$ that exceeds the threshold energy of 1.02 MeV for pair production is calculated from the relationship

$$\left(\frac{\kappa}{\rho}\right)_{\mathrm{tr}} = \frac{\kappa}{\rho}\frac{h\nu - 2m_{\mathrm{e}}c^2}{h\nu} = \frac{\kappa}{\rho}\left(1 - \frac{2m_{\mathrm{e}}c^2}{h\nu}\right) = \bar{f}^{\kappa}\frac{\kappa}{\rho}\,, \tag{7.92}$$

where $\bar{f}^{\kappa}$ is the average fraction of the incident photon energy $h\nu$ that is transferred to charged particles (electron and positron) in pair production.

The pair production fraction $\bar{f}^{\kappa}$ is plotted against photon energy $h\nu$ in Fig. 7.29. The fraction $\bar{f}^{\kappa}$ is 0 for $h\nu \le 2m_{\mathrm{e}}c^2$, rises gradually with increasing energy above $2m_{\mathrm{e}}c^2$, and approaches $\bar{f}^{\kappa} = 1$ asymptotically, showing that at large $h\nu$ the following relationship holds $(\kappa/\rho)_{\mathrm{tr}} \approx (\kappa/\rho)$. Figure 7.30 shows a comparison between the mass attenuation coefficient κ/ρ and mass energy transfer coefficient $(\kappa/\rho)_{\mathrm{tr}}$ against photon energy for carbon and lead. Both coefficients are related through $\bar{f}^{\kappa}$, as given by (7.92).

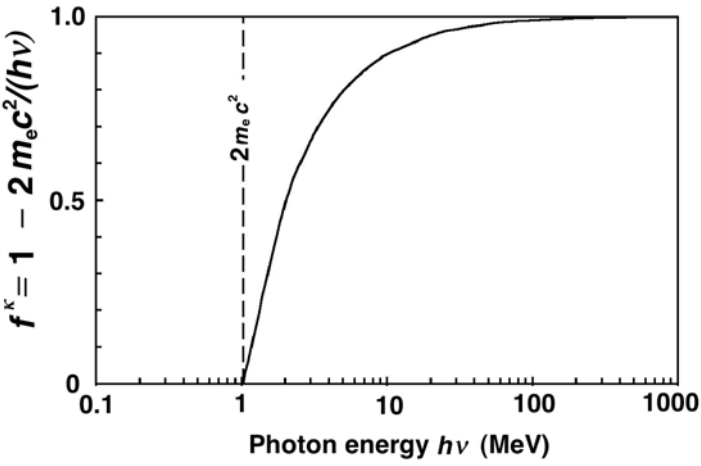

Fig. 7.29. The average pair production fraction $\bar{f}^{\kappa}$ against photon energy $h\nu$

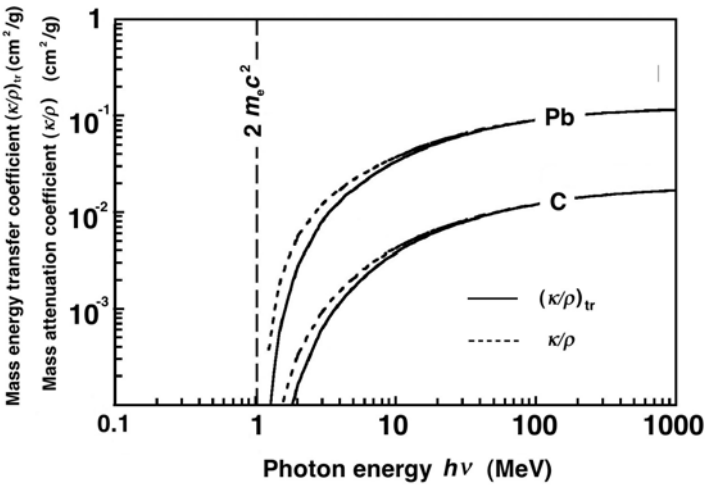

Fig. 7.30. Mass energy transfer coefficient $(\kappa/\rho)_{\rm tr}$ (*solid curves*) and mass attenuation coefficient κ/ρ (*dashed curves*) for pair production against photon energy $h\nu$ for carbon and lead. Data are from the NIST

7.6.9 Positron Annihilation

The positron is an antiparticle to an electron. The two have identical rest masses: $m_{\rm e}c^2 = 0.511$ MeV and opposite signs: electrons are negative, positrons positive. The positron was discovered in 1932 by *Carl Anderson* during his study of cosmic ray tracks in a Wilson cloud chamber.

Of interest in medical physics are positrons produced by:

1. Energetic photons undergoing pair production or triplet production (important in radiation dosimetry and health physics)
2. β^+decay used in positron emission tomography (PET) imaging.

Energetic positrons move through an absorbing medium and experience collisional and radiative losses of their kinetic energy through Coulomb interactions with orbital electrons and nuclei, respectively, of the absorber.

Eventually, positron collides with an electron and the two annihilate directly or they annihilate through an intermediate step forming a metastable hydrogen-like structure (see Sect. 2.3.7) called positronium (Ps). The positron and electron of the positronium revolve about their common center-of-mass in discrete orbits that are subjected to Bohr quantization rules with the reduced mass equal to one half of the electron rest mass and the lowest state with a binding energy of $(1/2)E_{\rm R} = 6.8$ eV.

The process of positron-electron annihilation is an inverse to pair production with the total mass before annihilation transformed into one, two, or three photons.

- The most common electron-positron annihilation occurs when the positron loses all of its kinetic energy and then undergoes annihilation with a "stationary and free" electron. The annihilation results in two photons (annihilation quanta) of energy $m_e c^2 = 0.511$ MeV each and moving in opposite directions (at nearly 180° to one another) ensuring conservation of total charge (zero), total energy ($2m_e c^2 = 1.02$ MeV) and total momentum (zero).
- A less common event (of the order of 2% of all annihilation interactions) is the annihilation-in-flight between a positron with non-zero kinetic energy E_K and either a tightly bound electron or a "free" electron.
  - When the electron is tightly bound to the nucleus, the nucleus can pick up the recoil momentum, and annihilation-in-flight produces only one photon with essentially the total positron energy (sum of rest energy and kinetic energy).
  - When the electron is essentially free, the annihilation-in-flight results in two photons, one of energy $h\nu_1$ and the other of energy $h\nu_2$. It can be shown that, for energetic positrons where $E_K \gg m_e c^2$, the following relationships hold: $h\nu_1 = E_K + (3/2)m_e c^2$ and $h\nu_2 = (1/2)m_e c^2$.

7.7 Photonuclear Reactions (Photodisintegration)

Photonuclear reaction is a direct interaction between an energetic photon and an absorber nucleus. Two other names are often used for the effect: *photodisintegration* and "*nuclear photoeffect*". Neutrons produced in photonuclear reactions are referred to as *photoneutrons*.

In photonuclear reactions the nucleus absorbs a photon and the most likely result of such an interaction is the emission of a single neutron through a (γ, n) reaction, even though emissions of charged particles, gamma rays, more than one neutron, or fission fragments (photofission) are also possible but much less likely to occur.

The most notable feature of the cross section for nuclear absorption of energetic photons is the so-called "giant resonance" exhibiting a broad peak in the cross section centered at about 24 MeV for low atomic number Z absorbers and at about 12 MeV for high Z absorbers. The only exceptions to the high photon energy rule are the two reactions $^2\mathrm{H}(\gamma, \mathrm{n})^1\mathrm{H}$ and $^9\mathrm{Be}(\gamma, \mathrm{n})2\alpha$ that have giant resonance peaks at much lower photon energies.

The full-width-at-half-maximum (FWHM) in the giant resonance cross sections typically ranges from about 3 MeV to 9 MeV. The FWHM depends on the detailed properties of absorber nuclei.

Table 7.7 provides various parameters for the "giant (γ, n) resonance" cross section for selected absorbers.

- The threshold energy represents the separation energy of a neutron from the nucleus that is of the order of 8 MeV or more, except for the deuteron

Table 7.7. Photonuclear (γ, n) giant resonance cross section parameters for selected absorbers

Absorber	Threshold energy (MeV)	Resonance peak energy $h\nu_{\max}$(MeV)	Resonance FWHM (MeV)	% of total electronic cross section at $h\nu_{\max}$
^{12}C	18.7	23.0	3.6	5.9
^{27}Aℓ	13.1	21.5	9.0	3.9
^{63}Cu	10.8	17.0	8.0	2.0
^{208}Pb	7.4	13.6	3.8	2.7

(^{2}H) and berillium-9 (^{9}Be) where it is at 2.22 MeV and 1.67 MeV, respectively.

- The resonance peak energy steadily decreases from 23 MeV for carbon-12 (^{12}C) with increasing Z.
- The magnitude of the atomic cross section for photodisintegration ${}_{\mathrm{a}}\sigma_{\mathrm{PN}}$, even at the resonance peak energy $h\nu_{\max}$, is relatively small in comparison with the sum of competing "electronic" cross sections and amounts to only a few percent of the total "electronic" cross section. As a result, ${}_{\mathrm{a}}\sigma_{\mathrm{PN}}$ is usually neglected in photon attenuation studies in medical physics.

While the photonuclear reactions do not play a role in general photon attenuation studies, they are of considerable importance in shielding calculations whenever photon energies exceed the photonuclear reaction threshold. Neutrons produced through the (γ, n) photonuclear reactions are usually far more penetrating than the photons that produced them. In addition, the daughter nuclei resulting from the (γ, n) reaction may be radioactive and the neutrons, through subsequent neutron capture, may produce radioactivity in the irradiation facility, adding to radiation hazard in the facility. This raises concern over the induced radioactivity in clinical high-energy linear accelerator installations (above 10 MV) and results in choice of appropriate machine components to decrease the magnitude and half-life of the radioactivation as well as adequate treatment room ventilation to expel the nitrogen-13 and oxygen-15 produced in the room (typical air exchanges in treatment rooms are of the order of six to eight per hour).

7.8 General Aspects of Photon Interaction with Absorbers

The most important parameter used for characterization of x-ray or gamma ray penetration into absorbing media is the linear attenuation coefficient μ. This coefficient depends on energy $h\nu$ of the photon and atomic number Z of the absorber, and may be described as the probability per unit path length that a photon will have an interaction with the absorber.

7.8.1 Narrow Beam Geometry

The attenuation coefficient μ is determined experimentally using the so-called *narrow beam geometry* technique that implies a narrowly collimated source of monoenergtic photons and a narrowly collimated detector. As shown in Fig. 7.31a, a slab of absorber material of thickness x is placed between the source and detector. The absorber decreases the detector signal (intensity) from $I(0)$ that is measured without the absorber in place to $I(x)$ that is measured with absorber thickness x in the beam.

A layer of thickness dx' within the absorber reduces the beam intensity by dI and the fractional reduction in intensity, $-dI/I$, is proportional to

- attenuation coefficient μ
- layer thickness dx'

The relationship for $-dI/I$ can thus be written as follows:

$$-dI/I = \mu dx' \tag{7.93}$$

or, after integration from 0 to x, as

$$\int_{I(0)}^{I(x)} \frac{dI}{I} = -\int_0^x \mu dx', \qquad \text{or} \qquad I(x) = I(0)e^{-\int_0^x \mu dx'} . \tag{7.94}$$

For a homogeneous medium $\mu = \text{const}$ and (7.94) reduces to the standard exponential relationship valid for monoenergetic photon beams

$$I(x) = I(0)e^{-\mu x} . \tag{7.95}$$

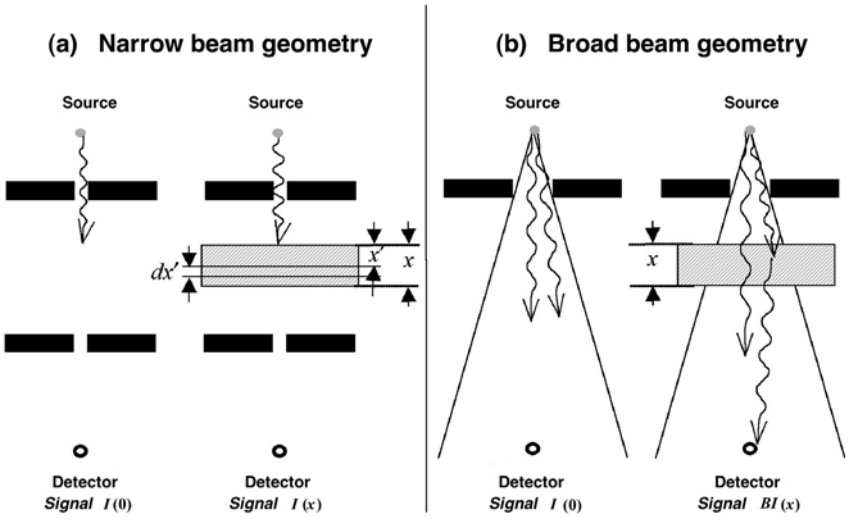

Fig. 7.31. Measurement of photon attenuation in absorbing material. Part **a** is for narrow beam geometry; part **b** is for broad beam geometry

7.8.2 Characteristic Absorber Thicknesses

Several thicknesses of special interest are defined as parameters for monoenergetic photon beam characterization in narrow beam geometry:

1. *First Half-Value Layer* (HVL_1 or $x_{1/2}$) is the thickness of a homogeneous absorber that attenuates the narrow beam intensity $I(0)$ to one half (50%) of the original intensity, i.e., $I(x_{1/2}) = 0.5I(0)$. Half-value layers are often used for characterization of superficial and orthovoltage x-ray beams. The absorbing materials used for this purpose are usually aluminum (for the superficial energy range) and copper (for the orthovoltage energy range).
2. *Mean Free Path* (MFP or $\bar{x}$) is the thickness of a homogeneous absorber that attenuates the beam intensity $I(0)$ to $1/e = 0.368$ (36.8%) of its original intensity, i.e., $I(\bar{x}) = 0.368I(0)$. The photon mean free path is the average distance a photon of energy $h\nu$ travels through a given absorber before undergoing an interaction.
3. *Tenth-Value Layer* (TVL or $x_{1/10}$) is the thickness of a homogeneous absorber that attenuates the beam intensity $I(0)$ to one tenth (10%) of its original intensity, i.e., $I(x_{1/10}) = 0.1I(0)$. Tenth-value layers are often used in radiation protection in treatment room shielding calculations.
4. *Second Half-Value Layer* (HVL_2), measured with the same homogeneous absorber material as the first half value layer (HVL_1), is defined as the thickness of the absorber that attenuates the narrow beam intensity from $0.5I(0)$ to $0.25I(0)$. The ratio between HVL_1 and HVL_2 is called the homogeneity factor χ of the photon beam.
   - When $\chi = 1$, the photon beam is monoenergetic such as a cobalt-60 beam with energy of 1.25 MeV or cesium-137 beam with energy of 0.662 MeV.
   - When $\chi \neq 1$, the photon beam possesses a spectral distribution.
   - For $\chi < 1$ the absorber is hardening the photon beam, i.e., preferentially removing low-energy photons from the spectrum (photoelectric effect region).
   - For $\chi > 1$ the absorber is softening the photon beam, i.e., preferentially removing high-energy photons from the spectrum (pair production region).

In terms of $x_{1/2}$, $\bar{x}$, and $x_{1/10}$ the linear attenuation coefficient μ may be expressed as

$$\mu = \frac{\ln 2}{x_{1/2}} = \frac{1}{\bar{x}} = \frac{\ln 10}{x_{1/10}} \,, \tag{7.96}$$

resulting in the following relationships among the characteristic thicknesses:

$$x_{1/2} = (\ln 2)\bar{x} = \frac{\ln 2}{\ln 10} x_{1/10} \equiv 0.301 x_{1/10} \,. \tag{7.97}$$

The various characteristic thicknesses and their effects on photon beam intensity are summarized in Table 7.8.

Table 7.8. Characteristic absorber thicknesses and their effects upon beam intensity attenuation

Absorber thickness	$\frac{I(x)}{I(0)}$	$100\frac{I(x)}{I(0)}$	*Name*	*Symbol*
$(\ln 2)/\mu$	0.500	50.0%	*Half-Value Layer*	$HVL = x_{1/2}$
$1/\mu$	0.368	36.8%	*Mean Free Path*	$MFP = \bar{x}$
$(\ln 10)/\mu$	0.100	10.0%	*Tenth-Value Layer*	$TVL = x_{1/10}$
$3/\mu$	0.050	5.0%	—	—
$5/\mu$	0.0067	$\sim 0.7\%$	—	—
$7/\mu$	0.0009	$\sim 0.1\%$	—	—
$9/\mu$	0.00012	$\sim 0.012\%$	—	—

7.8.3 Other Attenuation Coefficients and Cross Sections

In addition to the *linear attenuation coefficient* μ, other related coefficients and cross sections are in use for describing photon beam attenuation characteristics, such as

- *mass attenuation coefficient* μ_{m}
- *atomic cross section* ${}_{\mathrm{a}}\mu$
- *electronic cross section* ${}_{\mathrm{e}}\mu$
- *energy transfer coefficient* μ_{tr}
- *energy absorption coefficient* μ_{ab}

The relationship among the various attenuation coefficients and cross sections is given as follows:

$$\mu = \rho\mu_{\mathrm{m}} = n^{\square}\,{}_{\mathrm{a}}\mu = Z\,n^{\square}\,({}_{\mathrm{e}}\mu)\ , \tag{7.98}$$

where

ρ is the density of the absorber:
$n^{\square}$ is the number of atoms N_{a} per volume V of the absorber, i.e., $n^{\square} = N_{\mathrm{a}}/V$, and $N_{\mathrm{a}}/V = \rho N_{\mathrm{a}}/m = \rho N_{\mathrm{A}}/A$ with N_{A} the Avogadro's number of atoms per gram-atom and A the atomic mass of the absorber in g/gram-atom;
Z is the atomic number of the absorber.

Two other coefficients are in use to account for

1. the energy transferred from photons to charged particles (electrons and positrons) in a photon-atom interaction (*energy transfer coefficient* μ_{tr});
2. the energy actually absorbed by the medium (*energy absorption coefficient* μ_{ab}, often labeled as μ_{en} in the literature).

The *energy transfer coefficient* μ_{tr} is defined as follows:

$$\mu_{\mathrm{tr}} = \mu\overline{E}_{\mathrm{tr}}/(h\nu)\ , \tag{7.99}$$

where $\overline{E}_{\rm tr}$ is the average energy transferred from the primary photon with energy $h\nu$ to kinetic energy of charged particles (electrons and positrons).

The *energy absorption coefficient* $\mu_{\rm ab}$ is similarly defined as

$$\mu_{\rm ab} = \mu \overline{E}_{\rm ab}/(h\nu) \ , \tag{7.100}$$

where $\overline{E}_{\rm ab}$ is the average energy absorbed in the volume-of-interest in the medium.

The average energy absorbed in the volume-of-interest in the medium is equal to

$$\bar{E}_{\rm ab} = \bar{E}_{\rm tr} - \bar{E}_{\rm rad} \ , \tag{7.101}$$

where $\bar{E}_{\rm rad}$ is the average energy component of $\bar{E}_{\rm tr}$ that the charged particles lose in the form of radiative collisions and is thus not absorbed in the volume-of-interest.

- The energy absorption coefficient $\mu_{\rm ab}$ can now be written in terms of the energy transfer coefficient $\mu_{\rm tr}$ as follows:

$$\mu_{\rm ab} = \mu \frac{\bar{E}_{\rm ab}}{h\nu} = \mu \frac{\bar{E}_{\rm tr} - \bar{E}_{\rm rad}}{h\nu} = \mu_{\rm tr} - \mu_{\rm tr} \frac{\bar{E}_{\rm rad}}{\bar{E}_{\rm tr}} = \mu_{\rm tr}(1-\bar{g}) \ , \tag{7.102}$$

  where $\bar{g}$ represents the so-called *radiative fraction*, i.e., the average fraction of the energy lost in radiative interactions by the secondary charged particles as they travel through the absorbing medium. These radiative interactions are the bremsstrahlung production (for electrons and positrons) and in-flight annihilation (for positrons).
- The in-flight annihilation is usually ignored and the radiative fraction is often referred to as the bremsstrahlung fraction. As discussed in Sect. 5.7, the radiative fraction $\bar{g}$ is the average value of the radiation yields $B(E_{\rm Ko})$ for the spectrum of all electrons and positrons of various starting energies $E_{\rm Ko}$ produced or released in the medium by primary photons.

Table 7.9 lists the various attenuation coefficients and cross-sections, their relationship to the linear attenuation coefficient and their units.

7.8.4 Broad Beam Geometry

In contrast to the narrow beam geometry that is used in determination of the various attenuation coefficients and cross sections for photon beam attenuation, one can also deal with broad beam geometry in which the detector reading is not only decreased through attenuation of the primary photon beam in the absorber, it is also increased by the radiation scattered from the absorber into the detector. The geometry for a broad beam experiment on photon attenuation in an absorber is shown in Fig. 7.31b.

Table 7.9. Attenuation coefficients and cross sections used in photon attenuation studies

	Symbol	*Relationship to* μ	*Units*
Linear attenuation coefficient	μ	μ	cm^{-1}
Mass attenuation coefficient	μ_{m}	μ/ρ [(a)]	cm^2/g
Atomic cross-section	${}_{\mathrm{a}}\mu$	$\mu/n^{\square}$ [(b)]	$\mathrm{cm}^2/\mathrm{atom}$
Electronic cross-section	${}_{\mathrm{e}}\mu$	$\mu/(Zn^{\square})$ [(c)]	$\mathrm{cm}^2/\mathrm{electron}$

[(a)] ρ is the density of the absorber,
[(b)] $n^{\square}$ is the number of atoms per unit volume of the absorber, i.e., $n^{\square} = \rho N_{\mathrm{A}}/A$,
[(c)] $Zn^{\square}$ is the number of electrons per unit volume of absorber, i.e., $Zn^{\square} = \rho Z N_{\mathrm{A}}/A$.

The signal measured by the detector for an absorber thickness x is then equal to $BI(x)$ where:

$I(x)$ is the narrow beam geometry signal for absorber thickness x,
B is the so-called *build-up factor* that accounts for the secondary photons that are scattered from the absorber into the detector.

Broad beam geometry is used in radiation protection for design of treatment room shielding and in beam transport studies.

7.8.5 Classification of Photon Interactions

As discussed in previous sections and summarized in Table 7.10, there are numerous options available to photons for interacting with matter. The photon interactions may be classified according to the *type of target* and *type of event*.

- As shown in Table 7.11, according to the *type of target* there are two possibilities for photon interaction with an atom:
  - photon/orbital electron interaction,

Table 7.10. Most important photon interactions with atoms of the absorber

Interaction	Symbol for *electronic cross section*	Symbol for *atomic cross section*	Symbol for *linear attenuation coefficient*
Thomson scattering	${}_{\mathrm{e}}\sigma_{\mathrm{Th}}$	${}_{\mathrm{a}}\sigma_{\mathrm{Th}}$	σ_{Th}
Rayleigh scattering	-	${}_{\mathrm{a}}\sigma_{\mathrm{R}}$	σ_{R}
Compton scattering	${}_{\mathrm{e}}\sigma_{\mathrm{c}}$	${}_{\mathrm{a}}\sigma_{\mathrm{c}}$	σ_{C}
Photoelectric effect	-	${}_{\mathrm{a}}\tau$	τ
Pair production	-	${}_{\mathrm{a}}\kappa_{\mathrm{pp}}$	κ_{p}
Triplet production	${}_{\mathrm{e}}\kappa_{\mathrm{tp}}$	${}_{\mathrm{a}}\kappa_{\mathrm{tp}}$	κ_{t}
Photodisintegration	-	${}_{\mathrm{a}}\sigma_{\mathrm{pn}}$	σ_{pn}

Table 7.11. Types of targets in photon interactions with atoms

Photon-orbital electron interactions	*Photon-nucleus interactions*
— with bound electrons *Photoelectric effect* *Rayleigh scattering*	— with nucleus directly *Photodisintegration*
— with "free" electrons *Thomson scattering* *Compton scattering*	— with Coulomb field of nucleus *Pair production*
— with Coulomb field of electron *Triplet production*	

Table 7.12. Types of photon-atom interactions

Complete absorption of photon	*Photon scattering*
Photoelectric effect	Thomson scattering
Pair production	Rayleigh scattering
Triplet production	Compton scattering
Photodisintegration	

  - photon/nucleus interaction.

- As shown in Table 7.12, according to the *type of event* there are two possibilities for photon interaction with an atom:
  - complete absorption of the photon,
  - scattering of the photon.

As far as medical physics is concerned, photon interactions are classified into four categories:

1. *Interactions of major importance:*
   - Photoelectric effect
   - Compton scattering by free electron
   - Pair production (including triplet production)
2. *Interactions of moderate importance:*
   - Rayleigh scattering
   - Thomson scattering by free electron
3. *Interactions of minor importance:*
   - Photonuclear reactions
4. *Negligible interactions:*
   - Thomson scattering by the nucleus
   - Compton scattering by the nucleus

- Meson production
- Delbrück scattering

7.8.6 Mass Attenuation Coefficient of Compounds and Mixtures

The mass attenuation coefficient μ/ρ for a compound or mixture is approximated by a summation of a weighted average of its constituents, i.e.,

$$\frac{\mu}{\rho} = \sum_{\mathrm{i}} w_{\mathrm{i}} \frac{\mu_{\mathrm{i}}}{\rho} \,, \tag{7.103}$$

where

w_{i} is the proportion by weight of the i-th constituent,
μ_{i}/ρ is the mass attenuation coefficient of the i-th constituent.

7.8.7 Tabulation of Attenuation Coefficients

The attenuation coefficients and cross sections listed in Table 7.10 have specific values for a given photon energy $h\nu$ and absorber atomic number Z, and these values represent a sum of values for all individual interactions that a photon may have with an atom (photonuclear reactions are usually neglected).

Thus, for an absorber with density ρ, atomic number Z, and atomic mass A, we write the following relationships for the linear attenuation coefficient μ, mass attenuation coefficient μ_{m}, atomic cross section ${}_{\mathrm{a}}\mu$, and electronic cross-section ${}_{\mathrm{e}}\mu$:

$$\mu = \tau + \sigma_{\mathrm{R}} + \sigma_{\mathrm{c}} + \kappa \,, \tag{7.104}$$

$$\mu_{\mathrm{m}} = \mu/\rho = (\tau + \sigma_{\mathrm{R}} + \sigma_{\mathrm{c}} + \kappa)/\rho \,, \tag{7.105}$$

$$\begin{aligned} {}_{\mathrm{a}}\mu &= \frac{\mu}{\rho}\frac{A}{N_{\mathrm{A}}} = \frac{1}{\rho}\frac{A}{N_{\mathrm{A}}}(\tau + \sigma_{\mathrm{R}} + \sigma_{\mathrm{c}} + \kappa) \\ &= {}_{\mathrm{a}}\tau + {}_{\mathrm{a}}\sigma_{\mathrm{R}} + {}_{\mathrm{a}}\sigma_{\mathrm{c}} + {}_{\mathrm{a}}\kappa \,, \end{aligned} \tag{7.106}$$

$${}_{\mathrm{e}}\mu = \frac{\mu}{\rho}\frac{A}{ZN_{\mathrm{A}}} = \frac{1}{\rho}\frac{A}{ZN_{\mathrm{A}}}(\tau + \sigma_{\mathrm{R}} + \sigma_{\mathrm{c}} + \kappa) \,, \tag{7.107}$$

where

τ is the linear attenuation coefficient for photoelectric effect,
σ_{R} is the linear attenuation coefficient for Rayleigh scattering,
σ_{c} is the linear attenuation coefficient for Compton effect,
κ is the linear attenuation coefficient for pair production (including triplet).

In Fig. 7.32 we show the total mass attenuation coefficients μ/ρ for carbon in part a and lead in part b, plotted against the photon energy $h\nu$. In addition to μ/ρ that represents the sum of the individual coefficients for the photoelectric effect, Rayleigh scattering, Compton scattering and pair production, the coefficients for the individual components are also shown. Also shown are the absorption edges for the lead attenuator; the absorption edges for the carbon attenuator are not visible, because they occur off-scale at energies below 1 keV.

Figure 7.33 is a plot on a $(Z, h\nu)$ diagram of the relative predominance of the three major photon interactions with atoms: photoelectric effect, Compton scattering, and pair production for various absorbers with $Z = 1$ to $Z = 100$. The *two curves* on the graph represent the loci of points in the $(Z, h\nu)$ diagram for which either ${}_{\mathrm{a}}\tau = {}_{\mathrm{a}}\sigma_{\mathrm{c}}$ or ${}_{\mathrm{a}}\sigma_{\mathrm{c}} = {}_{\mathrm{a}}\kappa$, i.e., the *left hand curve* represents $(Z, h\nu)$ points for which the photoelectric atomic cross section ${}_{\mathrm{a}}\tau$ equals the Compton atomic cross section ${}_{\mathrm{a}}\sigma_{\mathrm{c}}$ and the *right hand curve* represents $(Z, h\nu)$ points for which the Compton atomic cross section ${}_{\mathrm{a}}\sigma_{\mathrm{c}}$ equals the pair production atomic cross section ${}_{\mathrm{a}}\kappa$.

From Figs. 7.32 and 7.33 the following conclusions may be made:

- At low photon energies ($h\nu < 100$ keV) and high atomic numbers Z the photoeffect mass coefficient τ/ρ predominates and makes the largest contribution to the total mass attenuation coefficient μ/ρ.
- At intermediate photon energies and low atomic numbers Z the Compton effect mass coefficient σ_{c}/ρ predominates and makes the largest contribution to the total mass attenuation coefficient μ/ρ.
- The width of the region of Compton scattering predominance depends on the atomic number Z of the absorber; the lower is Z, the broader is the Compton scattering predominance region. For water and tissue this region ranges from ~20 keV up to ~20 MeV, indicating that for most of radiotherapy the most important interaction of photon beams with tissues is the Compton scattering.
- The pair production dominates at photon energies $h\nu$ above 10 MeV and at high atomic numbers Z of the absorber.
- In all energy regions the Rayleigh scattering mass coefficient σ_{R}/ρ plays only a secondary role in comparison with the other three coefficients.

7.8.8 Energy Transfer Coefficient

The energy transfer coefficient μ_{tr} consist of three components, each of them representing a photon-atom interaction in which all or part of the photon energy $h\nu$ is transferred to charged particles (electrons or positrons). Rayleigh scattering transfers no energy to charged particles in the absorber and the interactions that generally result in energy transfer to charged particles are the photoelectric effect, Compton scattering and pair production. The energy transfer coefficient μ_{tr} is the sum of the energy transfer coefficients for the

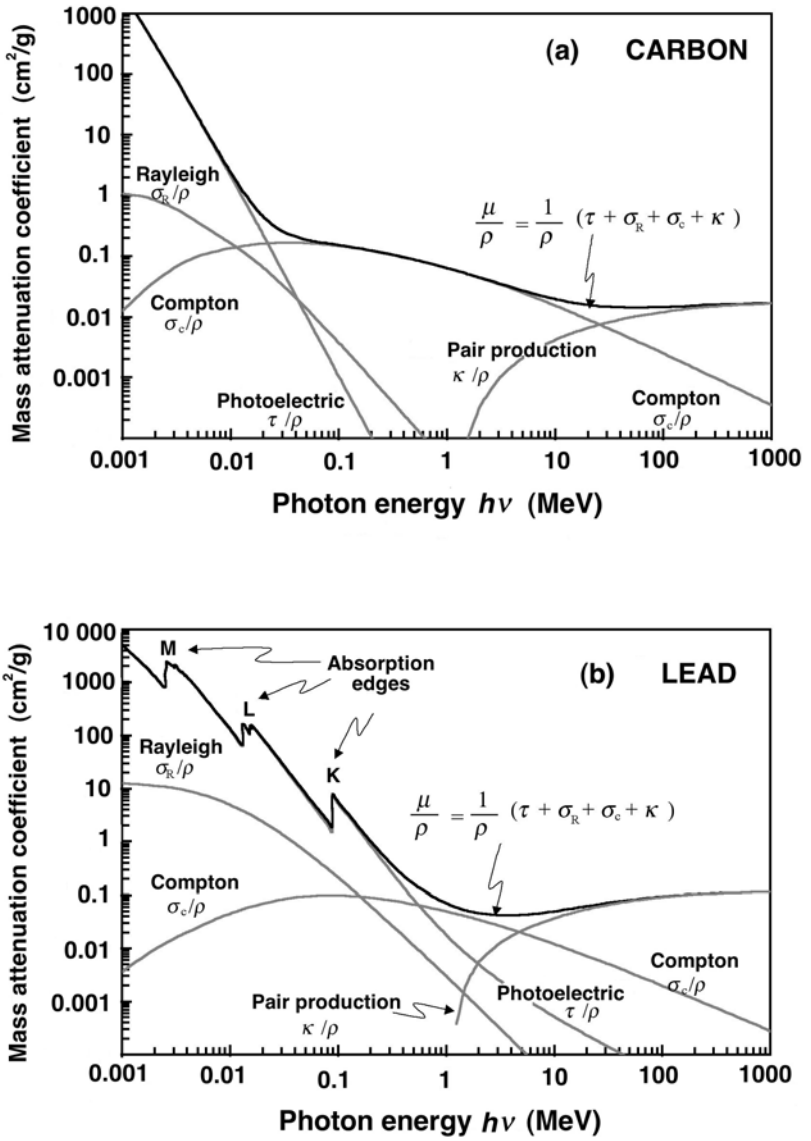

Fig. 7.32. Mass attenuation coefficient μ/ρ against photon energy $h\nu$ in the range from 1 keV to 1000 MeV for carbon in part **a** and lead in part **b**. In addition to the total coefficient μ/ρ, the individual coefficients for photoelectric effect, Rayleigh scattering, Compton scattering, and pair production (including triplet production) are also shown. The mass attenuation coefficient μ/ρ is the sum of the coefficients for individual effects, i.e., $\mu/\rho = (\tau + \sigma_{\mathrm{R}} + \sigma_{\mathrm{c}} + \kappa)/\rho$

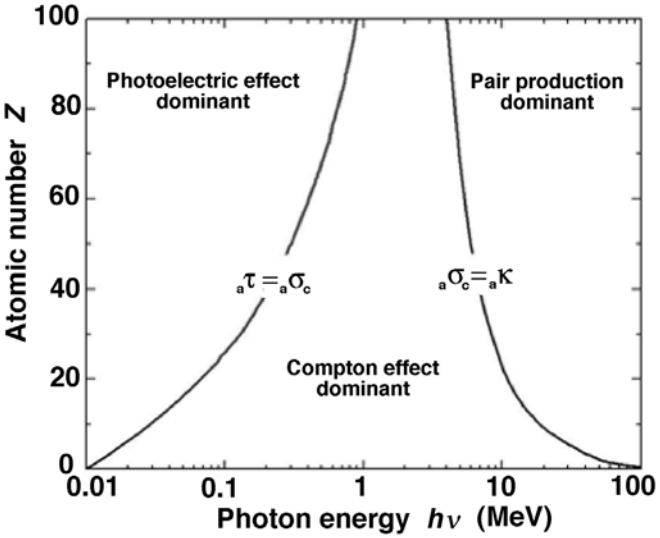

Fig. 7.33. Regions of relative predominance of the three main processes of photon interactions with an absorber: photoelectric effect, Compton scattering, and pair production. The *left curve* represents the loci of points on the (Z,$h\nu$) diagram where the atomic cross section for photoelectric effect equals the atomic cross section for Compton scattering, i.e., ${}_a\tau = {}_a\sigma_c$. The *right curve* represents the loci of points on the (Z,$h\nu$) diagram where the atomic cross section for Compton scattering equals the atomic cross section for pair production, i.e., ${}_a\sigma_c = {}_a\kappa$

three individual effects, i.e.,

$$\begin{aligned}\mu_{tr} &= \mu\frac{\overline{E}_{tr}}{h\nu} = \tau_{tr} + (\sigma_c)_{tr} + \kappa_{tr} = \\ &= \tau\frac{\overline{E}^{\tau}_{tr}}{h\nu} + \sigma_c\frac{\overline{E}^{\sigma}_{tr}}{h\nu} + \kappa\frac{\overline{E}^{\kappa}_{tr}}{h\nu} = f^{\tau}\tau + f^{\sigma}\sigma + f^{\kappa}\kappa = \\ &= \tau\left\{1 - \frac{P_K\omega_K\overline{h\nu}_K}{h\nu}\right\} + \sigma_c\frac{\overline{E}^{\sigma}_{tr}}{h\nu} + \kappa\left\{1 - \frac{2m_ec^2}{h\nu}\right\}, \qquad (7.108)\end{aligned}$$

where

$\overline{E}^{\tau}_{tr}$ is the average energy transferred to electrons (photoelectron and Auger electrons) in a photoelectric effect process,

$\overline{E}^{\sigma}_{tr}$ is the average energy transferred to recoil electron in a Compton effect process,

$\overline{E}^{\kappa}_{tr}$ is the average energy transferred to electron and positron in a pair production process (including triplet production).

$\bar{f}^{\tau} = 1 - P_K\omega_K\overline{h\nu}_K/(h\nu)$ is the average fraction of the photon energy given to the photoelectron and Auger electrons in a pho-

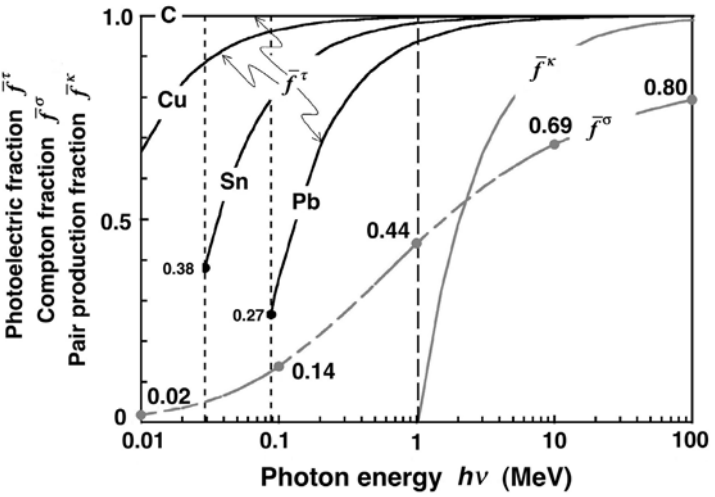

Fig. 7.34. Average energy transfer fractions $\bar{f}^{\tau}$, $\bar{f}^{\sigma}$, and $\bar{f}^{\kappa}$ for photoelectric effect, Compton effect and pair production, respectively, for carbon, copper, tin, and lead. Only the photoeffect fraction $\bar{f}^{\tau}$ depends on the atomic number Z of the absorber; the Compton effect and pair production fractions are independent of Z and depend only on photon energy $h\nu$

toelectric effect interaction (for photons with energy above the K edge of the absorbing medium).

$\bar{f}^{\sigma} = \overline{E}^{\sigma}_{\mathrm{tr}}/(h\nu)$ is the average fraction of the photon energy given to the recoil (Compton) electron in a Compton interaction (see Fig. 7.8).

$\bar{f}^{\kappa} = 1 - 2m_{\mathrm{e}}c^2/(h\nu)$ is the average fraction of the photon energy given to the electron/positron pair in a pair production interaction (including triplet production).

Figure 7.34 summarizes the three energy fractions $\bar{f}^{\tau}$, $\bar{f}^{\sigma}$, and $\bar{f}^{\kappa}$ for energy transfer in an absorber from photon to charged particles in photoelectric effect, Compton scattering, and pair production, respectively.

- All three fractions depend upon photon energy $h\nu$, increase with increasing photon energy $h\nu$, and converge to 1 at large $h\nu$.
- The photoelectric fraction $\bar{f}^{\tau}$ also depends on the atomic number Z of the absorber; the higher is Z, the lower is $\bar{f}^{\tau}$ in the vicinity of the absorption edge and the slower is the convergence to 1. The photoelectric fraction $\bar{f}^{\tau}$ was given in Fig. 7.25.
- The Compton Klein-Nishina fraction $\bar{f}^{\sigma}$ and the pair production fraction $\bar{f}^{\kappa}$ are independent of Z and depend on photon energy $h\nu$ only. The Compton Klein-Nishina fraction $\bar{f}^{\sigma}$ and the pair production fraction $\bar{f}^{\kappa}$ are given in Figs. 7.8 and 7.29, respectively.

From (7.108) we note that $\overline{E}_{\mathrm{tr}}$, the average energy transferred to charged particles, is in general given as

$$\begin{aligned}\overline{E}_{\mathrm{tr}} &= h\nu\frac{\mu_{\mathrm{tr}}}{\mu} = \sum_{\mathrm{i}} w_{\mathrm{i}}\overline{E}^{\mathrm{i}}_{\mathrm{tr}} = \frac{\tau}{\mu}\overline{E}^{\tau}_{\mathrm{tr}} + \frac{\sigma_{\mathrm{c}}}{\mu}\overline{E}^{\sigma}_{\mathrm{tr}} + \frac{\kappa}{\mu}\overline{E}^{\kappa}_{\mathrm{tr}} \\ &= w_\tau\overline{E}^{\tau}_{\mathrm{tr}} + w_\sigma\overline{E}^{\sigma}_{\mathrm{tr}} + w_\kappa\overline{E}^{\kappa}_{\mathrm{tr}} \\ &= \frac{\tau}{\mu}(h\nu - P_{\mathrm{K}}\omega_{\mathrm{K}}\overline{h\nu}_K) + \frac{\sigma_{\mathrm{c}}}{\mu}\overline{E}^{\sigma}_{\mathrm{tr}} + \frac{\kappa}{\mu}(h\nu - 2m_{\mathrm{e}}c^2)\ , \end{aligned} \tag{7.109}$$

where

i refers to a particular interaction of the photon with an atom of the absorber,

w_{i} is the weight of the particular interaction i of photon with absorber atoms.

Figure 7.35 gives a plot of the mass energy transfer coefficient μ_{tr}/ρ for carbon and lead in the photon energy range from 1 keV to 100 MeV. The mass attenuation coefficient μ/ρ is shown with dashed curves for comparison.

- For lead the K, L, and M absorption edges are visible, for carbon they are not because they all occur below the lower 1 keV limit of the graph.
- At photon energies between 1 keV and 10 keV in the photoeffect region $\mu/\rho \approx \mu_{\mathrm{tr}}/\rho \approx \mu_{\mathrm{ab}}/\rho$.
- At intermediate photon energies in the Compton region the Compton fraction $\bar{f}^{\sigma}$ correction to μ/ρ is very effective (see Fig. 7.34) and clearly separates μ/ρ from μ_{tr}/ρ.
- At very high photon energies in the pair production region the pair production fraction is 1 and $\mu/\rho \approx \mu_{\mathrm{tr}}/\rho$ (see Fig. 7.34).

7.8.9 Energy Absorption Coefficient

The energy absorption coefficient μ_{ab} is related to the energy transfer coefficient μ_{tr} by

$$\mu_{\mathrm{ab}} = \mu_{\mathrm{tr}}(1 - \bar{g})\ , \tag{7.110}$$

with $\bar{g}$ representing the so-called *radiative fraction*, i.e., the average fraction of secondary charged particle energy lost in radiative interactions that the secondary charged particles experience in their travel through the absorbing medium. These radiative interactions are the bremsstrahlung production (for electrons and positrons) and in-flight annihilation (for positrons).

- For low absorber atomic number Z and low photon energies $h\nu$ the radiative fraction $\bar{g}$ approaches zero and $\mu_{\mathrm{tr}} \approx \mu_{\mathrm{ab}}$.
- For increasing Z or $h\nu$ the radiative fraction $\bar{g}$ increases gradually, so that, for example, in lead at $h\nu = 10$ MeV, $\bar{g} = 0.26$ and $\mu_{\mathrm{ab}} = 0.74\ \mu_{\mathrm{tr}}$.

Figure 7.35 also shows, in addition to the mass attenuation coefficient μ/ρ and mass energy transfer coefficient μ_{tr}/ρ, the mass energy absorption

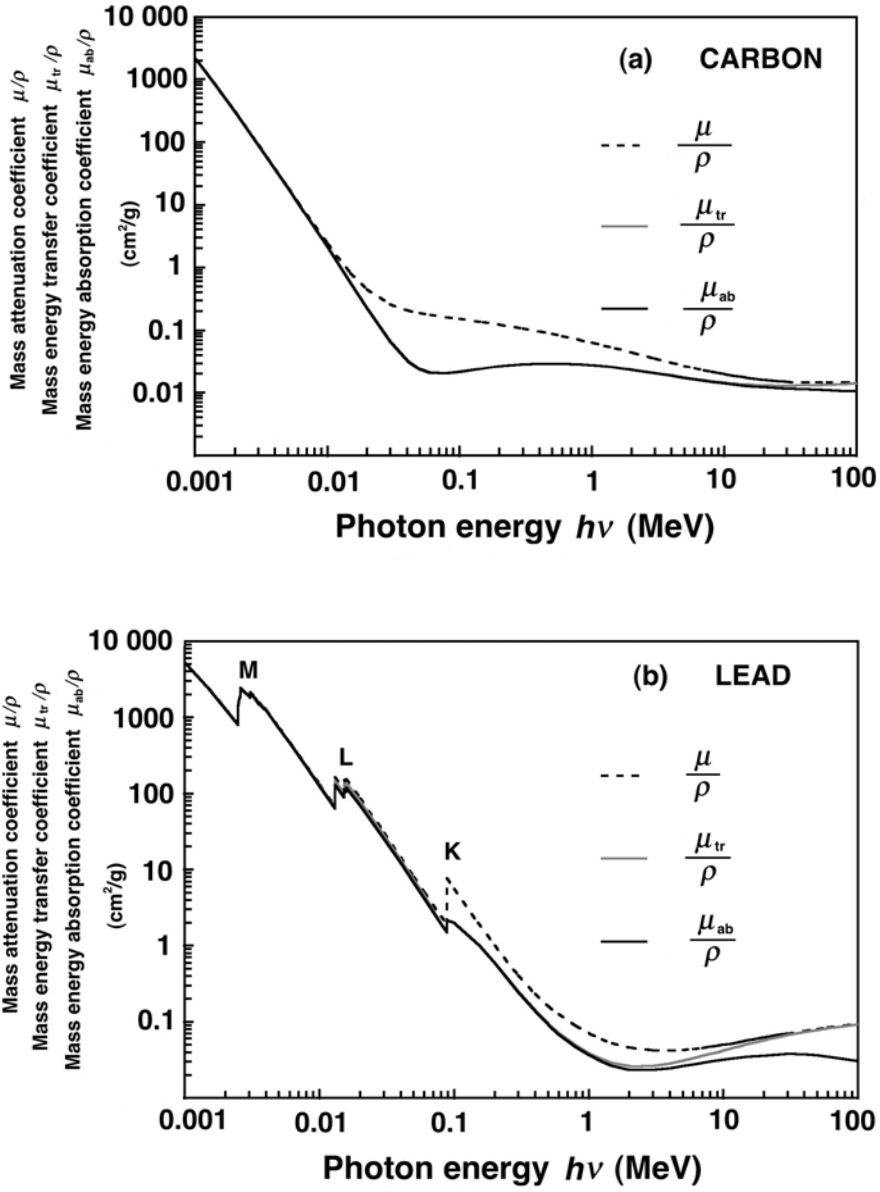

Fig. 7.35. Mass energy transfer coefficient μ_{tr}/ρ (*dark solid curves*), mass attenuation coefficient μ/ρ (*dashed curves*) and mass energy absorption coefficient μ_{ab}/ρ (*light solid curves*) against photon energy $h\nu$ for carbon in part **a** and lead in part **b**

coefficent μ_{ab}/ρ for carbon and lead in the photon energy range from 1 keV to 100 MeV.

The following interesting observations can be made:

- The K, L, and M absorption edges are clearly visible in the plots for lead. The plots for carbon, on the other hand, do not exhibit any absorption edges because the edges occur below 1 keV in the energy range that is not shown.
- Up to a photon energy of a few MeV, $\mu_{tr}/\rho \approx \mu_{ab}/\rho$.
- At photon energies above 10 MeV, μ_{ab}/ρ diverges from μ_{tr}/ρ because of the radiative loss $\bar{g}$ of charged particles released in the medium by the high-energy photons. With an increasing photon energy the radiative fraction $\bar{g}$ increases and so does the difference between μ_{ab}/ρ and μ_{tr}/ρ.
- The radiative fraction $\bar{g}$ also depends on the atomic number Z of the absorber; the higher is Z, the higher is $\bar{g}$ for the same photon energy, as indicated in Fig. 7.35. For example, at a photon energy of 10 MeV, $\bar{g} = 0.035$ for carbon and $\bar{g} = 0.26$ for lead; at 100 MeV, $\bar{g} = 0.25$ for carbon and $\bar{g} = 0.67$ for lead.

7.8.10 Effects Following Photon Interactions

In photoelectric effect, Compton effect, and triplet production vacancies are produced in atomic shells through the ejection of orbital electrons.

- For orthovoltage and megavoltage photons used in diagnosis and treatment of disease with radiation, the shell vacancies occur mainly in inner atomic shells of the absorber.
- Pair production, Rayleigh scattering and photodisintegration do not produce shell vacancies.
- Vacancies in inner atomic shells are not stable; they are followed by emission of characteristic x rays or Auger electrons depending on the fluorescent yield of the absorbing material and cascade to the outer shell of the ion. The ion eventually attracts an electron from its surroundings and becomes a neutral atom.
- Pair production and triplet production are followed by the annihilation of the positron with an orbital electron of the absorber, most commonly producing two annihilation quanta of 0.511 MeV each and moving at approximately 180^{o} to each other. Annihilation of a positron before it expanded all of its kinetic energy is referred to as annihilation-in-flight and may produce photon exceeding 0.511 MeV.

7.9 Summary of Photon Interactions

As is evident from discussions in this chapter, photons have numerous options for interaction with absorbers. The probabilities for interaction in general depend on the incident photon energy $h\nu$ and the atomic number Z of

the absorber. While over a dozen different photon interactions are known in nuclear physics, four of these are of importance to medical physics because they govern: (1) the transfer of energy from photons to light charged particles and the ultimate absorption of energy in irradiated tissues (radiation dosimetry) and (2) the attenuation and scattering of photons by tissues (imaging physics). The four important photon interactions are:

1. Photoelectric effect
2. Rayleigh scattering
3. Compton effect
4. Pair production

Photoelectric Effect

- The photoelectric effect (sometimes also referred to as photoeffect) is an interaction between a photon with energy $h\nu$ and a tightly bound orbital electron of an absorber atom. The interaction is thus between a photon and an absorber atom as a whole. The electron is ejected from the atom and referred to as a photoelectron.
- A tightly bound orbital electron is defined as an orbital electron with binding energy E_B either larger than $h\nu$ or of the order of $h\nu$. For $E_B > h\nu$ the photoeffect cannot occur; for $h\nu > E_B$ the photoelectric effect is possible. The closer is $h\nu$ to E_B, the larger is the probability for photoelectric effect to happen, provided, of course, that $h\nu$ exceeds E_B. At $h\nu = E_B$ the probability abruptly drops and exhibits the so-called absorption edge.
- When the photon energy $h\nu$ exceeds the K-shell binding energy E_B (K) of the absorber atoms, the photoelectric effect is most likely to occur with a K-shell electron in comparison with higher shell electrons. Over 80% of all photoelectric interactions occur with K-shell electrons when $h\nu \geq E_B(K)$.
- With increasing incident photon energy $h\nu$, the atomic, linear, and mass photoelectric attenuation coefficients decrease from their absorption edge value approximately as $1/(h\nu)^3$.
- The atomic photoelectric attenuation coefficient ${}_a\tau$ varies approximately as Z^5 for low Z absorbers and as Z^4 for high Z absorbers.
- The mass photoelectric attenuation coefficient $\tau_m = \tau/\rho$ varies approximately as Z^4 for low Z absorbers and as Z^3 for high Z absorbers.
- In water and tissue $\bar{E}^{\tau}_{tr}$, the average energy transferred to electrons (photoelectrons and Auger electrons) is equal to $\bar{E}^{\tau}_{ab}$, the average energy absorbed in the medium because the radiative fraction $\bar{g}$ is negligible; i.e., $\bar{g} \approx 0$.
- Furthermore, in water and tissue $\bar{E}^{\tau}_{tr}$ is approximately equal to the photon energy $h\nu$ because the fluorescent yield ω_K is approximately equal to zero. Thus in water and tissue the following relationship holds for the photoelectric effect: $\bar{E}^{\tau}_{tr} = \bar{E}^{\tau}_{ab} \approx h\nu$.

Rayleigh Scattering

- Rayleigh scattering is an interaction between a photon with energy $h\nu$ and the whole atom. All orbital electrons contribute to the scattering event and the phenomenon is referred to as coherent scattering because the photon is scattered by the constructive action of the tightly bound electrons of the whole atom.
- The photon leaves the point of interaction with the incident energy $h\nu$ intact but is redirected through a small scattering angle. Since no energy is transferred to charged particles, Rayleigh scattering plays no role in radiation dosimetry; however, it is of some importance in imaging physics because the scattering event has an adverse effect on image quality.
- The atomic Rayleigh attenuation coefficient ${}_{\mathrm{a}}\sigma_{\mathrm{R}}$ decreases approximately as $1/(h\nu)^2$ and is approximately proportional to Z^2 of the absorber.
- Even at very small incident photon energies $h\nu$, the Rayleigh component of the total attenuation coefficient is small and amounts to only a few percent.

Compton Effect

- Compton effect (often referred to as Compton scattering) is an interaction between a photon with energy $h\nu$ and a free orbital electron.
- A free electron is defined as an orbital electron whose binding energy E_{B} is much smaller than the photon energy $h\nu$; i.e., $h\nu \gg E_{\mathrm{B}}$.
- In each Compton interaction a scattered photon and a free electron (referred to as Compton or recoil electron) are produced. The sum of the scattered photon energy $h\nu'$ and the Compton recoil electron kinetic energy E_{K} is equal to the incident photon energy $h\nu$. The relative distribution of the two energies depends on the incident photon energy $h\nu$ and on the angle of emission (scattering angle θ) of the scattered photon.
- The electronic and mass Compton attenuation coefficients ${}_{\mathrm{e}}\sigma_{\mathrm{c}}$ and σ_{c}/ρ, respectively, are essentially independent of the atomic number Z of the absorber.
- The atomic Compton attenuation coefficient ${}_{\mathrm{a}}\sigma_{\mathrm{c}}$ is linearly proportional to the atomic number Z of the absorber.
- The atomic and mass Compton attenuation coefficients ${}_{\mathrm{a}}\sigma_{\mathrm{c}}$ and σ_{c}/ρ, respectively, decrease with increasing incident photon energy $h\nu$.
- The average fraction of the incident photon energy $h\nu$ transferred to recoil electron increases with $h\nu$ (see *The Graph* in Fig. 7.8). At low photon energies the Compton energy transfer coefficient $(\sigma_{\mathrm{c}})_{\mathrm{tr}}$ is much smaller than the Compton attenuation coefficient σ_{c}; i.e., $(\sigma_{\mathrm{c}})_{\mathrm{tr}} \ll \sigma_{\mathrm{c}}$. At high photon energies, on the other hand, $(\sigma_{\mathrm{c}})_{\mathrm{tr}} \approx \sigma_{\mathrm{c}}$.
- In water and tissue the Compton process is the predominant mode of photon interaction in the wide photon energy range from ~100 keV to ~10 MeV (see Fig. 7.33).

Pair Production

- Pair production is an interaction between a photon with energy $h\nu$ exceeding $2m_e c^2 = 1.02$ MeV and the Coulomb field of a nucleus. The photon disappears and an electron-positron pair is produced. The process is an example of mass-energy equivalence and is sometimes referred to as materialization.
- Pair production in the Coulomb field of an orbital electron of the absorber is referred to as triplet production. The process is much less probable than nuclear pair production and has threshold energy of $4m_e c^2 = 2.044$ MeV. The photon disappears and three light charged particles are released: the orbital electron and the electron-positron pair.
- The probability for pair production increases rapidly with the incident photon energy $h\nu$ for photon energies above the threshold energy.
- The atomic pair production attenuation coefficient ${}_a\kappa$ varies approximately as Z^2 of the absorber.
- The mass pair production coefficient $\kappa_m = \kappa/\rho$ varies approximately linearly with the atomic number Z of the absorber.
- The average energy transferred from the incident photon $h\nu$ to charged particles, $\bar{E}_{tr}^{\kappa}$, is $h\nu - 2m_e c^2$.

Table 7.13 provides a summary of the main characteristics for the photoelectric effect, Rayleigh scattering, Compton effect, and pair production.

7.10 Example 1: Interaction of 2 MeV Photons with Lead

For *2 MeV photons in lead* ($Z = 82$; $A = 207.2$ g/g-atom; $\rho = 11.36$ g/cm^3) the photoeffect, coherent scattering, Compton effect, and pair production linear attenuation coefficients are: $\tau = 0.055$ cm^{-1}, $\sigma_R = 0.008$ cm^{-1}, $\sigma_c = 0.395$ cm^{-1}, and $\kappa = 0.056$ cm^{-1}. The average energy transferred to charged particles $\bar{E}_{tr} = 1.13$ MeV and the average energy absorbed in lead is $\bar{E}_{ab} = 1.04$ MeV.

Calculate the linear attenuation coefficient μ; mass attenuation coefficient μ_m; atomic attenuation coefficient ${}_a\mu$; mass energy transfer coefficient μ_{tr}; mass energy absorption coefficient μ_{ab}; and radiative fraction $\bar{g}$.

$$\begin{aligned}\mu &= \tau + \sigma_R + \sigma_c + \kappa = (0.055 + 0.008 + 0.395 + 0.056)\ \text{cm}^{-1} \\ &= 0.514\ \text{cm}^{-1}\end{aligned} \tag{7.111}$$

$$\mu_m = \frac{\mu}{\rho} = \frac{0.514\ \text{cm}^{-1}}{11.36\ \text{g/cm}^3} = 0.0453\ \text{cm}^2/\text{g} \tag{7.112}$$

Table 7.13. Main characteristics of photoelectric effect, Rayleigh scattering, Compton effect, and pair production

	Photoeffect	*Rayleigh scattering*	*Compton effect*	*Pair production*
Photon interaction	With whole atom (bound electron)	With bound electrons	With free electron	With nuclear Coulomb field
Mode of photon interaction	Photon disappears	Photon scattered	Photon scattered	Photon disappears
Energy dependence	$\frac{1}{(h\nu)^3}$	$\frac{1}{(h\nu)^2}$	Decreases with energy	Increases with energy
Threshold	Shell binding energy	No	Shell binding energy	$\sim 2m_e c^2$
Linear attenuation coefficient	τ	σ_R	σ_c	κ
Atomic coefficient dependence on Z	${}_a\tau \propto Z^4$	${}_a\sigma_R \propto Z^2$	${}_a\sigma_c \propto Z$	${}_a\kappa \propto Z^2$
Mass coefficient dependence on Z	$\frac{\tau}{\rho} \propto Z^3$	$\frac{\sigma_R}{\rho} \propto Z$	Independent of Z	$\frac{\kappa}{\rho} \propto Z$
Particles released in absorber	Photoelectron	None	Compton (recoil) electron	Electron-positron pair
Average energy transferred to charged part's	$h\nu - P_K\omega_K\overline{h\nu}_K$	0	$\overline{E}^{\sigma}_{tr}$ (see Fig. 7.8)	$h\nu - 2m_e c^2$
Fraction of energy $h\nu$ transferred	$1 - \frac{P_K\omega_K\overline{h\nu}_K}{h\nu}$	0	$\frac{\overline{E}^{\sigma}_{tr}}{h\nu}$	$1 - \frac{2m_e c^2}{h\nu}$
Subsequent effect	Characteristic x ray, Auger effect	None	Characteristic x ray, Auger effect	Annihilation radiation
Significant energy region for water	<20 keV	<20 keV	20 keV–10 MeV	>10 MeV
Significant energy region for lead	<500 keV	<100 keV	500 keV–3 MeV	>3 MeV

$$
\begin{aligned}
{}_{\mathrm{a}}\mu &= \left\{\frac{\rho N_{\mathrm{A}}}{A}\right\}^{-1}\mu = \frac{207.2\ \text{(g/g-atom)}\ 0.514\ \text{cm}^{-1}}{11.36\ \text{g/cm}^3\ 6.022\times 10^{23}\ \text{(atom/g-atom)}} \\
&= 1.56\times 10^{-23}\ \text{cm}^2/\text{atom} \qquad (7.113)
\end{aligned}
$$

$$
\frac{\mu_{\mathrm{tr}}}{\rho} = \frac{\bar{E}_{\mathrm{tr}}}{h\nu}\frac{\mu}{\rho} = \frac{1.13\ \text{MeV}\ 0.0453\ \text{cm}^2/\text{g}}{2\ \text{MeV}} = 0.0256\ \text{cm}^2/\text{g} \qquad (7.114)
$$

$$
\begin{aligned}
\frac{\mu_{\mathrm{ab}}}{\rho} &= \frac{\mu_{\mathrm{en}}}{\rho} = \frac{\bar{E}_{\mathrm{ab}}}{h\nu}\frac{\mu}{\rho} \\
&= \frac{1.04\ \text{MeV}0.0453\ \text{cm}^2/\text{g}}{2\ \text{MeV}} = 0.0236\ \text{cm}^2/\text{g} \qquad (7.115)
\end{aligned}
$$

$$
\bar{g} = \frac{\bar{E}_{\mathrm{tr}} - \bar{E}_{\mathrm{ab}}}{\bar{E}_{\mathrm{tr}}} = 1 - \frac{\bar{E}_{\mathrm{ab}}}{\bar{E}_{\mathrm{tr}}} = 1 - \frac{1.04\ \text{MeV}}{1.13\ \text{MeV}} = 0.08 \qquad (7.116)
$$

or

$$
\bar{g} = 1 - \frac{\mu_{\mathrm{ab}}/\rho}{\mu_{\mathrm{tr}}/\rho} = 1 - \frac{0.0236\ \text{cm}^2/\text{g}}{0.0256\ \text{cm}^2/\text{g}} = 0.08. \qquad (7.117)
$$

The mass energy transfer coefficient μ_{tr}/ρ can also be determined using (7.108) with the appropriate average energy transfer fractions, given in Fig. 7.34, as follows:

$$
\bar{f}^{\tau} = (h\nu - P_{\mathrm{K}}\omega_{\mathrm{K}}\overline{h\nu}_{\mathrm{K}})/(h\nu) = 0.965\ , \qquad (7.118)
$$

$$
\bar{f}^{\sigma} = \bar{E}^{\sigma}_{\mathrm{tr}}/(h\nu) = 0.53\ , \qquad (7.119)
$$

$$
\bar{f}^{\kappa} = (h\nu - 2\,m_{\mathrm{e}}c^2)/(h\nu) = 0.50\ . \qquad (7.120)
$$

The mass energy transfer coefficient μ_{tr}/ρ is now given as follows:

$$
\begin{aligned}
\frac{\mu_{\mathrm{tr}}}{\rho} &= \frac{1\ \text{cm}^3}{11.36\ \text{g}}\left(0.965\times 0.055 + 0.53\times 0.395 + 0.50\times 0.056\right)\ \text{cm}^{-1} \\
&= 0.0256\,\frac{\text{cm}^2}{\text{g}} \qquad (7.121)
\end{aligned}
$$

in good agreement with the result obtained in (7.114).

Thus, as shown schematically in Fig. 7.36, a *2 MeV photon* in lead will on the average:

- *Transfer 1.13 MeV* to charged particles (electrons and positrons)
- *0.87 MeV will be scattered* through Rayleigh and Compton scattering.

Of the 1.13 MeV of energy transferred,

- *1.04 MeV will be absorbed* in lead and
- *0.09 MeV will be re-emitted* through bremsstrahlung radiative loss.

The radiative fraction $\bar{g}$ for 2 MeV photons in lead is 0.08.

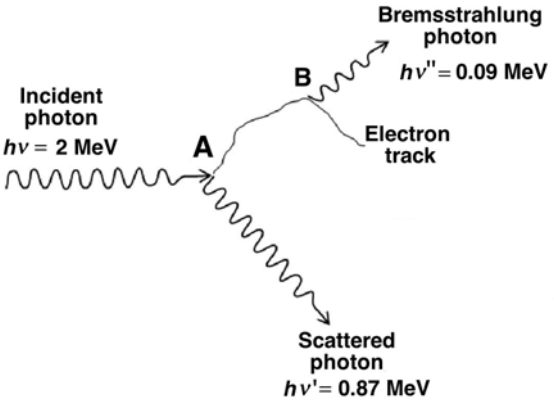

Fig. 7.36. Schematic diagram for general photon interactions with an atom. In this example a 2 MeV photon $h\nu$ interacts with a lead atom. An individual 2 MeV photon, as it encounters a lead atom at point A, may interact with the atom through photoelectric effect, Rayleigh scattering, Compton effect or pair production, or it may not interact at all. However, for a large number of 2 MeV photons striking lead, we may state that on the average:

- 1.13 MeV will be transferred at point A to charged particles (mainly to fast energetic electrons, but possibly also to positrons if the interaction is pair production);
- 0.87 MeV will be scattered through Rayleigh and Compton scattering ($h\nu'$)

Of the 1.13 MeV transferred to charged particles:

- 1.04 MeV will be absorbed in lead over the fast charged particle tracks, and
- 0.09 MeV will be emitted in the form of bremsstrahlung photons ($h\nu''$)

7.11 Example 2: Interaction of 8 MeV Photons with Copper

Monoenergetic photons with energy $h\nu = 8$ MeV ($\varepsilon = 15.66$) interact with a copper absorber ($Z = 29$, $A = 63.54$ g/g-atom; $\rho = 8.96$ g/cm^3). Using only the relationships and graphs given in this chapter, **determine**:

1. atomic cross section ${}_{\mathrm{a}}\mu$
2. mass attenuation coefficient μ_{m}
3. linear attenuation coefficient μ
4. average energy transferred to charged particles $\overline{E}_{\mathrm{tr}}$
5. mass energy transfer coefficient μ_{tr}/ρ
6. average radiative fraction $\bar{g}$
7. average energy absorbed in the copper absorber $\overline{E}_{\mathrm{ab}}$
8. mass energy absorption coefficient μ_{ab}/ρ

1. To determine the total **atomic cross section** ${}_{\mathrm{a}}\boldsymbol{\mu}$ we first calculate the individual atomic cross sections for photoelectric effect ${}_{\mathrm{a}}\tau$, Compton scattering ${}_{\mathrm{a}}\sigma_{\mathrm{c}}$, and pair production ${}_{\mathrm{a}}\kappa$. The total atomic cross section will be the sum of the three individual atomic cross sections. We ignore the atomic cross sections for Rayleigh scattering ${}_{\mathrm{a}}\sigma_{\mathrm{R}}$ and for photonuclear reactions ${}_{\mathrm{a}}\sigma_{\mathrm{PN}}$ because they are very small in comparison with the photoelectric, Compton and pair production cross sections.

Photoelectric Effect

Since $\varepsilon \gg 1$, we use (7.74) to estimate ${}_{\mathrm{a}}\tau$ for K-shell electrons in copper

$$\begin{aligned} {}_{\mathrm{a}}\tau_{\mathrm{K}} &= \frac{1.5}{\varepsilon}\alpha^4 Z^5 {}_{\mathrm{e}}\sigma_{\mathrm{Th}} \\ &= \frac{1.5}{15.66}\frac{29^5}{137^4}0.665\,\frac{\mathrm{b}}{\mathrm{atom}} = 0.004\ \mathrm{b/atom} \end{aligned} \tag{7.122}$$

Compton Effect

We use the Klein-Nishina relationship for the electronic cross section ${}_{\mathrm{e}}\sigma_{\mathrm{c}}^{\mathrm{KN}}$, given in (7.45), and then calculate ${}_{\mathrm{a}}\sigma_{\mathrm{c}}^{\mathrm{KN}}$ from ${}_{\mathrm{a}}\sigma_{\mathrm{c}}^{\mathrm{KN}} = Z\,{}_{\mathrm{e}}\sigma_{\mathrm{c}}^{\mathrm{KN}}$

$$\begin{aligned} &{}_{\mathrm{e}}\sigma_{\mathrm{c}}^{\mathrm{KN}} \\ &= 2\pi r_{\mathrm{e}}^2 \left\{ \frac{1+\varepsilon}{\varepsilon^2}\left[\frac{2(1+\varepsilon)}{1+2\varepsilon} - \frac{\ln(1+2\varepsilon)}{\varepsilon}\right] + \frac{\ln(1+2\varepsilon)}{2\varepsilon} - \frac{1+3\varepsilon}{(1+2\varepsilon)^2}\right\} \\ &= 0.0599\ \mathrm{b/electron} \end{aligned} \tag{7.123}$$

The atomic cross section is calculated from the electronic cross section as follows:

$${}_{\mathrm{a}}\sigma_{\mathrm{c}}^{\mathrm{KN}} = Z\,{}_{\mathrm{e}}\sigma_{\mathrm{c}}^{\mathrm{KN}} = 29 \times 0.0599\ \mathrm{b/atom} = 1.737\ \mathrm{b/atom}. \tag{7.124}$$

Pair Production

Since the photon energy of 8 MeV is significantly above the nuclear pair production threshold of 1.02 MeV and also above the triplet production threshold of 2.04 MeV, both effects (pair production and triplet production) will occur and will contribute to the total atomic cross section ${}_{\mathrm{a}}\mu$. To determine the atomic pair production cross-section we use (7.84)

$${}_{\mathrm{a}}\kappa_{\mathrm{pp}} = \alpha r_{\mathrm{e}}^2 Z^2 P_{\mathrm{pp}}(\varepsilon, Z)\ . \tag{7.125}$$

Since $1 \ll \varepsilon \ll \frac{1}{\alpha Z^{1/3}}$, where for our example $\varepsilon = 15.66$ and $1/(\alpha Z^{1/3}) = 44.6$, we use (7.84) to determine $P_{\mathrm{pp}}(\varepsilon, Z)$ as follows:

$$P_{\mathrm{pp}}(\varepsilon, Z) = \frac{28}{9}\ln(2\varepsilon) - \frac{218}{27} = 10.73 - 8.07 = 2.65\ . \tag{7.126}$$

The atomic cross-section for pair production ${}_{\mathrm{a}}\kappa_{\mathrm{pp}}$ is now calculated as follows:

$$
\begin{aligned}
{}_{\mathrm{a}}\kappa_{\mathrm{pp}} &= \alpha r_{\mathrm{e}}^2 Z^2 P_{\mathrm{pp}}(\varepsilon, Z) = \frac{7.94 \times 10^{-2} \times 29^2 \times 2.65}{137} \frac{\mathrm{b}}{\mathrm{atom}} \\
&= 1.292 \text{ b/atom.}
\end{aligned} \tag{7.127}
$$

To account for the *triplet production* contribution we use (7.90) to get

$$
\begin{aligned}
{}_{\mathrm{a}}\kappa &= {}_{\mathrm{a}}\kappa_{\mathrm{pp}} \left\{ 1 + \frac{1}{\eta Z} \right\} = 1.292 \frac{\mathrm{b}}{\mathrm{atom}} \left\{ 1 + \frac{1}{2.5 \times 29} \right\} \\
&= 1.310 \text{ b/atom.}
\end{aligned} \tag{7.128}
$$

Two observations can now be made:

- For 8 MeV photons interacting with copper, triplet production contributes only of the order of 1.5% to the total atomic pair production cross section.
- The atomic cross-sections ${}_{\mathrm{a}}\sigma_{\mathrm{c}}$ and ${}_{\mathrm{a}}\kappa$ for Compton scattering and pair production, respectively, are almost identical. This can actually be surmised from Fig. 7.33 that shows the loci of points $(Z, h\nu)$ for which ${}_{\mathrm{a}}\tau = {}_{\mathrm{a}}\sigma_{\mathrm{c}}$ and ${}_{\mathrm{a}}\sigma_{\mathrm{c}} = {}_{\mathrm{a}}\kappa$. The point ($Z = 29$, $h\nu = 8$ MeV) is very close to the ${}_{\mathrm{a}}\sigma_{\mathrm{c}} = {}_{\mathrm{a}}\kappa$ curve and thus must possess similar atomic cross-sections ${}_{\mathrm{a}}\sigma_{\mathrm{c}}$ and ${}_{\mathrm{a}}\kappa$.

The total *atomic cross section* ${}_{\mathrm{a}}\mu$ is the sum of the cross sections for individual non-negligible effects, as given in (7.106)

$$
\begin{aligned}
{}_{\mathrm{a}}\mu &= {}_{\mathrm{a}}\tau + {}_{\mathrm{a}}\sigma_{\mathrm{R}} + \sigma_{\mathrm{c}} + {}_{\mathrm{a}}\kappa = (0.004 + 0 + 1.737 + 1.310)\mathrm{b/atom} \\
&= 3.051 \text{ b/atom .}
\end{aligned} \tag{7.129}
$$

2. The **mass attenuation coefficient $\boldsymbol{\mu_{\mathrm{m}}}$** is calculated, as suggested in (7.98), from

$$
\begin{aligned}
\mu_{\mathrm{m}} &= \frac{\mu}{\rho} = {}_{\mathrm{a}}\mu \frac{N_{\mathrm{A}}}{A} = 3.051 \frac{\mathrm{b}}{\mathrm{atom}} \frac{6.022 \times 10^{23} \,\mathrm{atom/g\text{-}atom}}{63.54 \text{ g/g-atom}} \\
&= 0.0289 \frac{\mathrm{cm}^2}{\mathrm{g}} \text{ .}
\end{aligned} \tag{7.130}
$$

3. The **linear attenuation coefficient $\boldsymbol{\mu}$** is determined by multiplying μ_{m} with the absorber density ρ to get

$$
\mu = \rho \mu_{\mathrm{m}} = 8.96 \frac{\mathrm{g}}{\mathrm{cm}^3} \; 0.0289 \; \frac{\mathrm{cm}^2}{\mathrm{g}} = 0.259 \text{ cm}^{-1}. \tag{7.131}
$$

4. The **average energy $\boldsymbol{\overline{E}_{\mathrm{tr}}}$ transferred** from photons to charged particles is determined using (7.109)

$$
\overline{E}_{\mathrm{tr}} = w_\tau \overline{E}_{\mathrm{tr}}^{\tau} + w_\sigma \overline{E}_{\mathrm{tr}}^{\sigma} + w_\kappa \overline{E}_{\mathrm{tr}}^{\kappa}, \tag{7.132}
$$

where

$$w_\tau = \frac{{}_{\mathrm{a}}\tau}{{}_{\mathrm{a}}\mu} = \frac{0.004}{3.051} = 1.3 \times 10^{-3}, \tag{7.133}$$

$$w_\sigma = \frac{{}_{\mathrm{a}}\sigma_{\mathrm{c}}}{{}_{\mathrm{a}}\mu} = \frac{1.737}{3.051} = 0.57, \tag{7.134}$$

$$w_\kappa = \frac{{}_{\mathrm{a}}\kappa}{{}_{\mathrm{a}}\mu} = \frac{1.310}{3.051} = 0.43, \tag{7.135}$$

$$\begin{aligned} \overline{E}^{\tau}_{\mathrm{tr}} &= h\nu - P_{\mathrm{K}}\omega_{\mathrm{K}}\overline{h\nu}_{\mathrm{K}} = 8\ \mathrm{MeV} - 0.5 \times 0.85 \times 7.7 \times 10^{-3}\ \mathrm{MeV} \\ &\approx 8\ \mathrm{MeV}, \end{aligned} \tag{7.136}$$

(see Figs. 7.24 and 7.25 for values of P_{K}, ω_{K}, and $\overline{h\nu}_{\mathrm{K}}$)

$$\overline{E}^{\sigma}_{\mathrm{tr}} = 0.67 \times 8\ \mathrm{MeV} \approx 5.36\ \mathrm{MeV}, \tag{7.137}$$

(see "*The Compton Graph*" in Fig. 7.8)

$$\overline{E}^{\kappa}_{\mathrm{tr}} = h\nu - 2m_{\mathrm{e}}c^2 = 8\ \mathrm{MeV} - 1.02\ \mathrm{MeV} \approx 7\ \mathrm{MeV}. \tag{7.138}$$

Inserting into (7.121) the weights w_{i} and the average energy transfers $\overline{E}^{\mathrm{i}}_{\mathrm{tr}}$ for the individual effects, we now calculate the average energy transferred from 8 MeV photons to charged particles in copper

$$\begin{aligned} \overline{E}_{\mathrm{tr}} &= 1.3 \times 10^{-3} \times 8\ \mathrm{MeV} + 0.57 \times 5.36\ \mathrm{MeV} + 0.43 \times 7\ \mathrm{MeV} \\ &= 6.07\ \mathrm{MeV}\ . \end{aligned} \tag{7.139}$$

5. The **mass energy transfer coefficient $\boldsymbol{\mu_{\mathrm{tr}}/\rho}$** is determined from the following:

$$\frac{\mu_{\mathrm{tr}}}{\rho} = \frac{\mu}{\rho}\frac{\overline{E}_{\mathrm{tr}}}{h\nu} = 0.0289\ \frac{\mathrm{cm}^2}{\mathrm{g}}\ \frac{6.07}{8} = 0.0219\ \mathrm{cm}^2/\mathrm{g}\ . \tag{7.140}$$

6. The **radiative fraction $\bar{g}$** represents an average radiative yield $B(E_{\mathrm{Ko}})$ given in (5.49) for the spectrum of charged particles released by 8 MeV photons in the copper absorber. This charged particle spectrum is composed of recoil Compton electrons (average energy of 5.36 MeV) as well as electrons and positrons from the pair production (average energy of 0.5×7 MeV, i.e., 3.5 MeV).
The $\overline{E}_{\mathrm{tr}}$ exceeds $\overline{E}_{\mathrm{o}}$, the average of the initial energies acquired by charged particles that are set in motion in the absorber, because in pair production two charged particles with a combined energy of 7 MeV are set in motion and the initial average energy for each of the two charged particles is 3.5 MeV.

The *average initial energy* $\overline{E}_{\mathrm{o}}$ of all charged particles released in copper by 8 MeV photons is given as

$$\begin{aligned}\overline{E}_{\mathrm{o}} &= \overline{E}_{\mathrm{tr}} \frac{{}_{\mathrm{a}}\sigma + {}_{\mathrm{a}}\kappa}{{}_{\mathrm{a}}\sigma + 2_{\mathrm{a}}\kappa} = 6.07 \text{ MeV} \frac{1.737 + 1.310}{1.737 + 2 \times 1.310} \\ &= 4.25 \text{ MeV}. \end{aligned} \tag{7.141}$$

The spectrum of charged particles released by 8 MeV photons in the copper absorber can only be determined reliably by Monte Carlo calculations.

In the first approximation, however, we assume that all charged particles are produced with monoenergetic initial energies $\overline{E}_{\mathrm{o}}$. Then the radiative yield $B(E_{\mathrm{Ko}})$, given in Fig. 5.7, can be equated with the radiative fraction $\bar{g}$ to get $\bar{g} \approx 0.1$.

The *average energy* $\overline{E}_{\mathrm{rad}}$ *radiated* by charged particles as bremsstrahlung is given by (5.50) as

$$\overline{E}_{\mathrm{rad}} = B(E_{\mathrm{Ko}})\overline{E}_{\mathrm{tr}} = 0.1 \times 6.07 \text{ MeV} = 0.61 \text{ MeV}. \tag{7.142}$$

7. The **average energy $\overline{E}_{\mathrm{ab}}$ absorbed** in the copper absorber is

$$\begin{aligned}\overline{E}_{\mathrm{ab}} &= \overline{E}_{\mathrm{tr}} - \overline{E}_{\mathrm{rad}} = 6.07 \text{ MeV} - 0.61 \text{ MeV} \\ &= 5.46 \text{ MeV}. \end{aligned} \tag{7.143}$$

8. The **mass energy absorption coefficient μ_{ab}/ρ** is

$$\frac{\mu_{\mathrm{ab}}}{\rho} = \frac{\mu}{\rho}\frac{\overline{E}_{\mathrm{ab}}}{h\nu} = 0.0289 \frac{\mathrm{cm}^2}{\mathrm{g}} \frac{5.46}{8} = 0.0197 \text{ cm}^2/\mathrm{g} \tag{7.144}$$

The *mass energy absorption coefficient* μ_{ab}/ρ may also be calculated from the mass energy transfer coefficient μ_{tr}/ρ and the radiative fraction $\bar{g}$ as follows:

$$\begin{aligned}\frac{\mu_{\mathrm{ab}}}{\rho} &= \frac{\mu_{\mathrm{tr}}}{\rho}(1 - \bar{g}) = 0.0219 \frac{\mathrm{cm}^2}{\mathrm{g}}(1 - 0.1) \\ &= 0.0197 \text{ cm}^2/\mathrm{g}. \end{aligned} \tag{7.145}$$

In summary, as shown schematicall in Fig. 7.37, we determined for 8 MeV photons interacting with a copper absorber that on the average:

(a) **6.07** MeV will be transferred to charged particles; **1.93** MeV will be scattered.
(b) **5.46** MeV will be absorbed in copper; **0.61** MeV will be radiated in the form of bremmstrahlung.
(c) The atomic cross-section ${}_{\mathrm{a}}\mu$, the mass attenuation coefficient μ_{m}, and the linear attenuation coefficient μ for 8 MeV photons in copper are: 3.051 b/atom; 0.0289 cm^2/g; and 0.259 cm^{-1}, respectively.

(d) The mass energy transfer coefficient μ_{tr}/ρ and mass energy absorption coefficient μ_{ab}/ρ are: 0.0219 cm^2/g and 0.0197 cm^2/g, respectively.
(e) The radiative fraction $\bar{g}$ for 8 MeV photons in copper is $\sim$0.1.

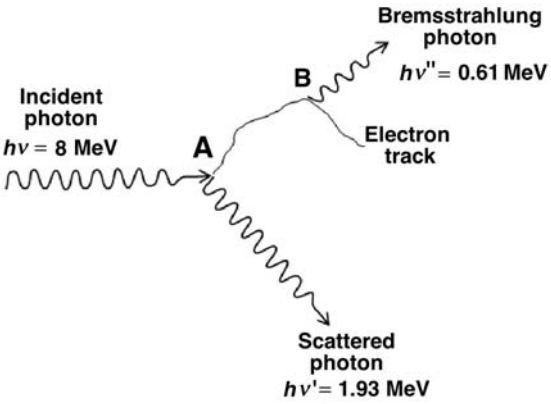

Fig. 7.37. Schematic diagram for general photon interactions with an atom. In this example an 8 MeV photon $h\nu$ interacts with a copper atom. An individual 8 MeV photon, as it encounters a copper atom at point A, may interact with the atom through photoelectric effect, Rayleigh scattering, Compton effect or pair production, or it may not interact at all. However, for a large number of 8 MeV photons striking copper, we may state that on the average:

- 6.07 MeV will be transferred at point A to charged particles (mainly to fast energetic electrons, but possibly also to positrons if the interaction is pair production);
- 1.93 MeV will be scattered through Rayleigh and Compton scattering ($h\nu'$)

Of the 6.07 MeV transferred to charged particles:

- 5.46 MeV will be absorbed in copper over the fast charged particle tracks,
- 0.61 MeV will be emitted in the form of bremsstrahlung photons ($h\nu''$)
- The average energies transferred to charged particles in a photoelectric process, Rayleigh scattering, Compton scattering, and pair production are $\sim$8 MeV, 0, 5.36 MeV, and $\sim$7 MeV.